SMITHSONIAN CONTRIBUTIONS TO THE EARTH SCIENCES • NUMBER 21

Schreibersite Growth and Its Influence on the Metallography of Coarse-Structured Iron Meteorites

Roy S. Clarke, Jr.
and Joseph I. Goldstein

SMITHSONIAN INSTITUTION PRESS
City of Washington
1978

ABSTRACT

Clarke, Roy S., Jr., and Joseph I. Goldstein. Schreibersite Growth and Its Influence on the Metallography of Coarse-Structured Iron Meteorites. *Smithsonian Contributions to the Earth Sciences,* number 21, 80 pages, 28 figures, 20 tables, 1978.—The role that schreibersite growth played in the structural development process in coarse-structured iron meteorites has been examined. The availability of many large meteorite surfaces and an extensive collection of metallographic sections made it possible to undertake a comprehensive survey of schreibersite petrography. This study was the basis for the selection of samples for detailed electron microprobe analysis. Samples containing representative structures from eight chemical Groups I and IIAB meteorites were selected.

Electron microprobe traverses were made across structures representative of the observed range of schreibersite associations. Particular emphasis was placed on schreibersite-kamacite interface compositions. An analysis of these data has led to a comprehensive description of the structural development process.

Massive schreibersite, one of the four major types of schreibersite encountered, may be accounted for by equilibrium considerations. Subsolidus nucleation and growth with slow cooling from temperatures at least as high as 850° C, and probably much higher, explain the phase relationships that one sees in meteorite specimens. The retention of taenite in the octahedrites establishes that bulk equilibrium did not extend as low as 550° C. Schreibersite undoubtedly continued in equilibrium with its enclosing kamacite to lower temperatures.

A second type of schreibersite to form is homogeneously nucleated rhabdite. It nucleated in kamacite in the 600° C temperature range, either as a consequence of low initial P level or after local P supersaturation developed following massive schreibersite growth.

A third type of schreibersite is grain boundary and taenite border schreibersite. It formed at kamacite-taenite interfaces, absorbing residual taenite. Nucleation took place successively along grain boundaries over a range of temperatures starting as high as 500° C or perhaps slightly higher. Grain boundary diffusion probably became an increasingly important factor in the growth of these schreibersites with decreasing temperature.

The fourth type of schreibersite is microrhabdite. These schreibersites nucleated homogeneously in supersatuated kamacite at temperatures in the 400° C range or below.

P diffusion controlled the growth rate of schreibersite. The Ni flux to a growing interface had to produce a growth rate equal to that established by the P flux. This was accomplished by tie line shifts that permitted a broad range of Ni growth rates, and these shifts account for the observed range of Ni concentrations in schreibersite. Equilibrium conditions pertained at growth interfaces to temperatures far below those available experimentally. Kinetic factors, however, restricted mass transfer to increasingly small volumes of material with decreasing temperature.

OFFICIAL PUBLICATION DATE is handstamped in a limited number of initial copies and is recorded in the Institution's annual report, *Smithsonian Year*. SERIES COVER DESIGN: Aerial view of Ulawun Volcano, New Britain.

Library of Congress Cataloging in Publication Data
Clarke, Roy S., Jr.
Schreibersite growth and its influence on the metallography of coarse-structured iron meteorites.
(Smithsonian contributions to the earth sciences; no. 21)
Bibliography: p.
1. Schreibersite. 2. Metallography. 3. Meteorites, Iron. I. Goldstein, Joseph I., joint author. II. Title. III. Series: Smithsonian Institution. Smithsonian contributions to the earth sciences; no. 21.
QE1.S227 no. 21 [QE395] 550'.8s [552] 77-10840

Contents

	Page
Introduction	1
Acknowledgments	2
Historical Background	2
Introduction	2
19th-Century Studies of Schreibersite	3
Early 20th-Century Studies of Iron Meteorites	4
Modern Work on Metallic Phases of Iron Meteorites	5
Related Materials	8
Experimental	9
Results	11
Coahuila	13
Bellsbank	16
Ballinger	18
Santa Luzia	21
Lexington County	25
Bahjoi	29
Goose Lake	30
Balfour Downs	31
Discussion	37
Equilibrium Considerations of Phase Growth	37
Coahuila	40
Ballinger	42
Santa Luzia	43
Lexington County and Bahjoi	44
Goose Lake and Balfour Downs	45
Bellsbank	46
Low Temperature Phase Growth and the Equilibrium Diagram	48
Diffusion-Controlled Schreibersite Growth	54
Cooling Rate Variations	58
Interface Data and Schreibersite Distribution	59
Interface Data and the α/α + Ph Boundary	66
Schreibersite with Cohenite Borders	70
Summary and Conclusions	73
Appendix	75
Literature Cited	77

Schreibersite Growth and Its Influence on the Metallography of Coarse-Structured Iron Meteorites

Roy S. Clarke, Jr. and Joseph I. Goldstein

Introduction

Meteorites are currently understood to be the oldest rocks available for scientific study, containing components and structures that span the period from the final stages of solar nebula condensation to the present (Anders, 1962, 1971; Grossman and Larimer, 1974; Wasson, 1974). They are fragments of parent bodies that accreted from preexisting aggregations of material during the period of planetary system formation some 4.6 billion years ago. These parent bodies were subsequently disrupted into smaller objects that then had independent existences in space. Individual fragments eventually intercepted the earth and landed as recoverable meteorites. Meteorite structures and compositions have undergone varying degrees of modification while resident in their parent bodies, as small bodies in space, on their passage through the atmosphere, and on landing on the earth's surface. Further changes result from long residence time on the ground and may continue during storage in collections. Bearing evidences of these complex histories, meteorites are samples not only from a far distant place but also from a far distant time, having been preserved in a remarkably gentle environment when compared to terrestrial or lunar rocks. As a consequence, meteorites have a unique place in the study of the development of the planetary system, yielding information that is available from no other source.

Iron meteorites represent only a small fraction of the meteorites that have been observed to fall, about five percent. Fortunately, many specimens from ancient falls have been preserved under such conditions that deterioration has not been severe and are available for study (Buchwald, 1976). If this were not the case, our view of iron meteorite compositions and structures would be much narrower than it is. Only one of the meteorites used in this study is an observed fall.

The spectacular metallographic structures revealed on prepared surfaces of iron meteorites have fascinated scientist and dilettante alike for more than 160 years (Perry, 1944). The Widmanstätten pattern is the historical distinguishing characteristic of the populous octahedrite classes of iron meteorites (Goldstein and Axon, 1973). At an early date this structure was understood to result from very slow cooling at relatively low temperatures in the meteorite parent body. The temperature range through which this structure develops is now believed to be from 700° to 350° C, temperatures well below those where silicate systems undergo change. Interpretation of metallographic structures, therefore, gives information on a late, low temperature period in the history of a parent

Roy S. Clarke, Jr., Department of Mineral Sciences, National Museum of Natural History, Smithsonian Institution, Washington, D. C. 20560. Joseph I. Goldstein, Department of Metallurgy and Materials Sciences, Lehigh University, Bethlehem, Pennsylvania 18015.

body, information that is not readily available from other types of meteorite studies.

Modern interpretations of iron meteorite structures have been based on the Fe-Ni equilibrium diagram (Goldstein and Olgivie, 1965a), as it was the only applicable system known with sufficient accuracy in the low temperature range required. The Widmanstätten pattern, therefore, resulted simply from taenite transforming to kamacite with decreasing temperature as a solid state, diffusion controlled reaction. Recently the iron-rich corner of the Fe-Ni-P equilibrium system has been determined experimentally down to 550° C, leading to new possibilities for investigating meteorite structures (Doan and Goldstein, 1970). In this study the metallography of a group of schreibersite-containing coarse-structured iron meteorites has been examined using this low temperature Fe-Ni-P diagram. It will be shown that equilibrium growth at higher temperatures combines with diffusion-controlled growth at lower temperatures to explain observed structure more comprehensively than was possible using the simpler system. Schreibersite growth becomes an integral part of the overall structural development process, and schreibersite may no longer be considered an "inclusion" that can be safely ignored when structural development is discussed.

Acknowledgments

A number of colleagues and associates have contributed invaluable assistance throughout the course of this study. The support and encouragement of departmental chairman William G. Melson and his predecessor Brian Mason are acknowledged with sincere thanks. Erik Randich provided penetrating discussion of many of the problems studied here, and his analysis of ternary diffusion as applied to schreiberate growth and meteorite cooling rates was made available to us prior to publication. A. D. Romig, Jr., of Lehigh University made available to us data on the low temperature Fe-Ni-C system prior to publication. Eugene Jarosewich and Charles R. Obermeyer III furnished unstinting help with the electron microprobe work. Grover C. Moreland and Richard Johnson prepared many excellent polished sections. Ann Garlington and Kathy P. Porter were scrupulous in their attention to the details of manuscript preparation. Dante Piacesi, Jr., of the Office of Computer Services was responsible for the preparation of data reduction programs. A grant from the Secretary's Fluid Research Fund supported a brief visit to Cambridge University, Cambridge, England, in the fall of 1974, where a serious beginning was made on the interpretation of the data. The support of the Geochemistry Program, Division of Earth Sciences, National Science Foundation, through Grant No. DES 74-22518 is also acknowledged. The acronym USNM (for the former United States National Museum) is used for catalog numbers in the National Museum of Natural History, Smithsonian Institution.

This paper was presented to the George Washington University, Washington, D.C., by R. S. Clarke, Jr. in partial fulfillment of the requirements for the Ph.D. degree.

Historical Background

Introduction

Meteorites, with their dramatic arrivals on earth, exotic origins, and unusual structures, have attracted much more than routine scientific interest ever since they became respectable objects of study at the end of the 18th century. Many of the leaders in the development of 19th-century physical science made significant contributions to their study, and several of them will be mentioned below. The older literature is extensive, but it is mainly obsolete for other than descriptive and historical purposes. A critical review of this material was not attempted, but a survey of selected early developments will be given. Scientific interest in schreibersite dates from near the beginning of meteorite studies, and it is interesting to place modern work in this perspective.

The first major development in the metallography of meteorites was the discovery of the phenomenon that has become known as the Widmanstätten pattern. This structure was first discovered by William Thomson, an Englishman living in exile in Naples. He published a French version of his findings along with a good illustration in a Swiss journal in 1804. What appears to be an identical paper, only in Italian, dated 6 February 1804, was published in Siena four years later (G. Thomson, 1804, 1808). Modern writers on meteoritics have been unaware of the earlier paper by

Thomson, and this has led to confusion as to whether Thomson or Von Widmanstätten really had priority. The record seems to be unambiguously in favor of Thomson. Marjorie Hooker of the U.S. Geological Survey retrieved this 1804 paper, and its existence was mentioned in a footnote in a biographic study of Thomson by C. D. Waterston (1965: 133). The writer ran across Waterston's paper among unindexed material in the F. A. Paneth meteorite literature collection that was deposited in the Smithsonian Institution in 1974.

Alois von Widmanstätten, Director of the Imperial "Fabrik-Produkten-Cabinett" (Industrial Products Collection), Vienna, discovered the phenomenon that now bears his name independently in 1808. He devoted many years to its study and circulated his observations privately, drawing the phenomenon to the attention of students of meteorites. Von Widmanstätten's observations were finally published in 1820 by his co-worker, Carl von Schreibers (1820). The history of the discovery of the Widmanstätten pattern has been reviewed by Paneth (1960) and Smith (1960, 1962). Smith's review contains excellent reproductions of early prints and a lengthy translation of Schreibers' description of Widmanstätten's work. These early reproductions of iron meteorite structures by Widmanstätten not only represent an advance in the science of meteoritics but also one in the art of printing.

During the 19th century descriptive studies of meteorites advanced with the broadening base of understanding in mineral chemistry and related physical science. Many of the iron meteorites known today were already represented in collections, and a number of them had been carefully described in the literature. The major phases of iron meteorites had been characterized and given mineral names: kamacite (low-nickel Ni-Fe, ferrite, α-iron, b.c.c.), taenite (high-nickel Ni-Fe, austenite, γ-iron, f.c.c.), plessite (fine-grained intergrowth of kamacite and taenite), troilite (FeS), cohenite (Fe_3C), and schreibersite ($(Fe,Ni)_3P$) were all known and their bulk compositions understood. Accessory minerals such as daubreelite ($FeCr_2S_4$), chromite ($FeCr_2O_4$), and graphite (C) were also known. The Widmanstätten pattern was understood to have formed by slow cooling under crystallographicly controlled conditions, kamacite plates forming parallel to the faces of an octahedron, giving the name octahedrite to those meteorites that displayed this pattern on polished and etched surfaces.

19TH-CENTURY STUDIES OF SCHREIBERSITE

Schreibersite was first characterized in 1832 by the great Swedish chemist J. J. Berzelius (1832a,b, 1833, 1834). He isolated brittle, silver-white grains of a magnetic material from an acid insoluble residue of the Bohumilitz, Bohemia, coarse octahedrite. Berzelius' elaborate analytical procedure yielded a surprisingly good analysis for the time, demonstrating that his material was an iron-nickel-phosphorus compound containing about 14 percent phosphorus and considerably more nickel than the bulk of the meteorite. In 1834 he reported similar analyses for schreibersite from the Elbogen, Bohemia, medium octahedrite and the Krasnojarsk, Siberia, pallasite (the historic Pallas Iron). It is also interesting to note that Berzelius' concept of the Widmanstätten pattern included the element phosphorus, as is indicated by the following quotation:

> Es möchte wahrscheinlich seyn, dass die sogenannten *Widmanstädtschen* Figuren einer, der hier analysirten Schuppen analogen, Verbindung zwischen Eisen, Nickel und Phosphor, zuzuschreiben seyen, welches zu erforschen ich aus Mengel an Material verhindert bin.
>
> Berzelius (1832b:297)

Early descriptions of schreibersite occurrences were confounded by inadequate separation techniques, poor analytical methods, and complications arising from both the varied morphology and the wide range in composition that is typical of this mineral. C. U. Shepard (1846, 1853) analysed schreibersite and attempted to assign a mineral name to it. His suggestion, however, was supported by inadequate data. Credit for naming schreibersite belongs to A. Patera, whose recommendation was reported by Haidinger (1847). The name honors Professor Karl von Schreibers (1775–1852), director of the Imperial Cabinet, Vienna, a pioneer worker on meteorites and colleague of Von Widmanstätten.

The writings of J. Lawrence Smith, a distinguished chemist of the middle part of the last century (Silliman, 1886; Phillips, 1965), include numerous examples of early work on meteorites.

His description of the Tazewell, Tennessee, finest octahedrite contains a lengthy discussion of his observations (Smith, 1855). At this early date he recognized the name schreibersite and applied it to the correct mineral. He reports having identified schreibersite by visual inspection in a number of iron meteorites from "the Yale College Cabinet," where it had previously been thought to be pyrite. Smith's low nickel value for Tazewell schreibersite is suspect and his attempt at a formula was unsuccessful, but he clearly recognized the species and understood which elements were its major constituents. This work was undoubtedly done, at least in part, in the chemical laboratory of the Smithsonian Institution. This laboratory was organized by Professor Smith in 1854, and Secretary Joseph Henry reported that during the year "he also made a series of analyses of meteorites, among which were fourteen specimens from the cabinet of James Smithson, the founder of the Institution" (Goode, 1897:614).

Confusion in nomenclature, however, persisted in the literature for many years. Von Reichenbach (1861) discussed schreibersite under the descriptive term "Ganzeisen" and also used the name lamperite. Both of these names are now part of the synonymy of schreibersite. Rose (1865) introduced the synonym rhabdite into the literature, a name derived from the Greek word for "rod." This term is still in common use by meteoriticists, but only when morphological distinctions are of interest. Rhabdite is the term used for the small schreibersite crystals occurring in the kamacite of iron meteorites. In polished sections these small schreibersite crystals have rhombohedral cross sections that in some cases are elongated, suggesting rods or needles.

The early literature on meteoritic phosphides, schreibersite and rhabdite, was reviewed in detail by Cohen (1894). Included were a number of analyses of schreibersite and rhabdite isolated from various meteorites by Cohen and his coworkers, as well as selected analyses from the literature. This work established that schreibersite and rhabdite are morphological variations of the same mineral species, the rhabdite form having a somewhat higher nickel concentration than that observed in large schreibersite inclusions. A similar review was given a few years later by Farrington (1915), using much of the same data Cohen used but with several later analyses.

The 19th-century work on meteoritic phosphides that culminated with Cohen's and Farrington's reviews was limited by the capabilities of classical descriptive mineralogy and classical analytical chemistry. A plateau had been reached in descriptive iron meteorite studies in general that became an accepted norm that was exceeded by few workers during the first half of the 20th century. Most iron meteorite descriptions published during this period employed neither concepts nor techniques beyond those available to Cohen. The descriptive literature grew in volume and in quality, but new interpretations lagged. Powerful petrographic techniques were being developed and used by metallurgists and ore microscopists, but they were not much used by students of iron meteorites. The availability of good transmitted light microscopes in the hands of petrographers who were accustomed to working with silicate minerals resulted in stony meteorites being preferred subjects of investigation.

Early 20th-Century Studies of Iron Meteorites

The emergence of modern physical chemistry and physical metallurgy during the decades adjacent to the turn of the century had a marked effect on the future course of iron meteorite investigations. Descriptive studies following the 19th-century pattern continued to comprise the bulk of the published literature and, indeed, continue to be published today as essential documentation. More modern experimental approaches, however, became significant, resulting in a body of knowledge more readily interpretable in terms of origins and developmental histories of meteorites than was previously possible.

Actually, the roots of this work go back to a much earlier period. Pioneering synthetic experiments were made by Michael Faraday as early as 1820. He prepared metals of meteoritic compositions in the course of an investigation to improve steel (Stodart and Faraday, 1820). At a later period, Daubrée (1868) described synthetic experiments related to meteorites. Sorby (1877, 1887), the father of metallography, made astute observations, some of which were based on artificial alloys of meteoritic compositions. Unfortunately, Sorby's pioneering efforts in the metallography of meteorites were not pursued. The following quotation

from his 1877 paper reflects his perceptive understanding of the structures he observed:

> These facts clearly indicate that the Widmanstatt's figuring is the result of such a complete separation of the constituents and perfect crystallisation as can occur only when the process takes place slowly and gradually. . . . Difference in the rate of cooling would serve well to explain the difference in the structure of some meteoritic iron which do not differ in chemical composition; . . . we are quite at liberty to conclude that they may have been melted . . . .

During the same period the well-known French mineralogist, Meunier (1880), reported the results of his synthetic work on meteoritic systems. A paper by Brezina (1906) is an excellent summarizing statement of this early period. It contains a number of good photomicrographs of iron meteorites, an unusual feature for papers of the time, and it discusses the development of these structures in terms of exsolution phenomena (solid state transformation). He also gave a succession for the formation of the constituents of iron meteorites, starting with olivine in pallasites: olivine, daubreelite, troilite, graphite, schreibersite, cohenite, chromite, swathing kamacite, kamacite bands, taenite, and plessite. This is a remarkably informative listing for the time, demonstrating careful petrographic observation and keen insight.

One of the perennial problems of meteorite research has been that of drawing the attention of those with the knowledge and facilities to make significant contributions to the meteorite specimens and the important and interesting scientific problems they represent. Despite Sorby's enthusiasm for meteorite studies, metallurgists showed little interest and had to be attracted into the field. An example of this process is an invited paper read before the Vienna meeting of the Iron and Steel Institute in 1907. Professor Frederick Berwerth's (1907) paper, "Steel and Meteoritic Iron," was based on his knowledge of the meteorite collection of the Imperial Natural History Museum, Vienna. It was an open invitation to metallurgists to become involved in this field of study.

During the early decades of this century, synthetic studies were combined with analyses based on equilibrium phase diagrams. The work of Osmond and Cartaud (1904), Benedicks (1910), and Belaiew (1924) are examples. Unfortunately, the tools were not available at the time to determine sufficiently accurate equilibrium diagrams. As a result, many of the conclusions drawn were seriously flawed. These studies, however, pointed the way for future workers.

The introduction of X-ray diffraction analysis into metallurgical and mineralogical research in the 1920s had an important influence on meteorite studies. Young (1926) published an early study establishing that kamacite precipitates from taenite, not the converse as many had previously thought. X-ray examination of the Widmanstätten pattern continued for over a decade with deepening understanding and some controversy (Mehl and Derge, 1937; Derge and Komnel, 1937; Owen, 1938; Smith and Young, 1938, 1939).

Rudolf Vogel's contributions to metallurgical studies in meteorites deserves special mention, his published papers having covered the period 1925 to 1967. They treated a broad range of topics related to meteoritics, eight of them being of particular interest in this context (Vogel, 1927, 1928, 1932, 1951, 1952, 1957, 1964; Vogel and Baur, 1931). These papers deal with the role of phosphorus in the development of meteoritic structures. His 1928 paper discusses schreibersite and rhabdite precipitation in terms of a hypothetical ternary Fe-Ni-P system. His 1932 and 1952 papers discuss the same material in terms of experimentally derived ternary diagrams.

A watershed publication that represents the culmination of this earlier period of iron meteorite research is Perry's (1944) monograph on the metallography of meteoritic iron. Although many photographs of iron meteorites had been published in the older literature, most of these were external views of complete specimens or macrophotographs of meteorite slices prepared for exhibit purposes. Perry's publication was the first comprehensive and systematic collection of iron meteorite photomicrographs. The variety of metallic structures in iron meteorites was presented to the scientific public in a way that has had significant impact up to the present. Sorby had pointed out the power of the metallographic approach in 1877, but it was not seriously pursued until E. P. Henderson drew the publisher and meteorite collector S. H. Perry into this field in the 1930s (Henderson and Perry, 1958: ii).

Modern Work on Metallic Phases of Iron Meteorites

Modern work on the metallic phases of iron meteorites includes studies that may be grouped

into the following categories for convenience: (1) interpretations of the Widmanstätten pattern in terms of cooling histories of meteoritic parent bodies, (2) compositional studies utilizing trace elements and structure as a means of identifying parent bodies, (3) schreibersite growth as a key to structure development and cooling history, (4) descriptive studies and literature reviews. These studies are interrelated and provide essential background for the work to be discussed below. Brief mention of major contributions in these areas will be given here.

Progress in developing accurate low temperature phase diagrams has played an essential role in modern iron meteorite studies. The Fe-Ni diagram of Goldstein and Ogilvie (1965a) has been used by meteoriticists for over 10 years (Figure 1). Electron microprobe techniques were employed by these workers to improve upon earlier equilibrium diagrams (Owen and Sully, 1939; Owen and Lui, 1949) and to reconcile the Fe-Ni diagram with observations on meteorites (Agrell et al., 1963). Buchwald (1966) studied the Fe-Ni-P system at low temperature using X-ray techniques and proposed a diagram that he used to discuss meteorite structure development. More extensive work on the Fe-Ni-P system based on longer cooling periods and electron microprobe measurements was reported by Doan and Goldstein (1970), and their diagram is basic to the interpretation of the experimental observations discussed below.

The modern literature on the growth of the Widmanstätten pattern is extensive. Massalski and Park (1962) used the Fe-Ni equilibrium diagram to calculate initial temperatures of kamacite precipitation and final equilibrium temperatures, using areal distribution of kamacite and taenite and a lever rule calculation. Wood (1964) and Goldstein and Ogilvie (1965b) considered the nonequilibrium nature of iron meteorite structures, and combined phase diagram and kinetic considerations to derive cooling rates and to estimate parent body sizes. Both papers recognize Widmanstätten pattern growth as diffusion controlled and not subject to bulk equilibrium consideration. Wood (1964) uses the relationship between Ni buildup at the centers of taenite bands and kamacite band widths to calculate cooling rates. The Goldstein and Ogilvie (1965b) approach used a detailed analysis of diffusion gradients within taenite at taenite-kamacite interfaces. Both approaches gave comparable cooling rates within reasonable limits of error. A number of other papers were published during this period that contributed significantly to our knowledge of the structural detail of meteoritic iron (Short and Anderson, 1965; Goldstein, 1965; Reed, 1965b; Axon and Boustead, 1967). Cooling rate and thermal history studies were pursued by Goldstein and co-workers (Short and Goldstein, 1967; Goldstein and Short, 1967a, b; Fricker et al., 1970). Goldstein and Doan (1972) discussed the effect of phosphorus on the formation of the Widmanstätten pattern and reported the first laboratory production of an artificial Widmanstätten pattern. They conclude that cooling rate calculations are not seriously affected by phosphorus. A comprehensive review of Widmanstätten pattern studies has been published by Goldstein and Axon (1973).

Compositional studies of iron meteorites have traditionally gone hand-in-hand with classification, bulk Ni values and metallographic structure being the primary considerations in assigning classification categories. Modern versions of this type of classification have been given by Buchwald and Munck (1965) and Goldstein (1969). The grouping of iron meteorites on the basis of trace element content was introduced by Goldberg et al. (1951) and Lovering et al. (1957). Wasson and co-workers in a series of papers (Wasson, 1974; Scott and Wasson, 1975, 1976) have extended this approach to define genetic groups in a large number of iron meteorites, based on Ni, Ga, Ge, and Ir contents and structural considerations. Sixteen iron meteorite groups have been characterized, representing 12 genetically related meteorite groups and a number of individual meteorite parent bodies.

Recent work on schreibersite growth in iron meteorites may be dated from the observations of Henderson and Perry (1958). Using conventional chemical analysis, they observed unusually low Ni concentrations in swathing kamacite bordering the large low-Ni (12%) schreibersite in the Tombigbee River meteorite, a meteorite they also showed to contain low-Ni (20%) rhabdite. They explained their observations in part on the migration of Fe and Ni atoms in the solid state and suggested that much of the phosphide may have separated from the liquid. Somewhat later, the first electron microprobe measurements of schreibersite composi-

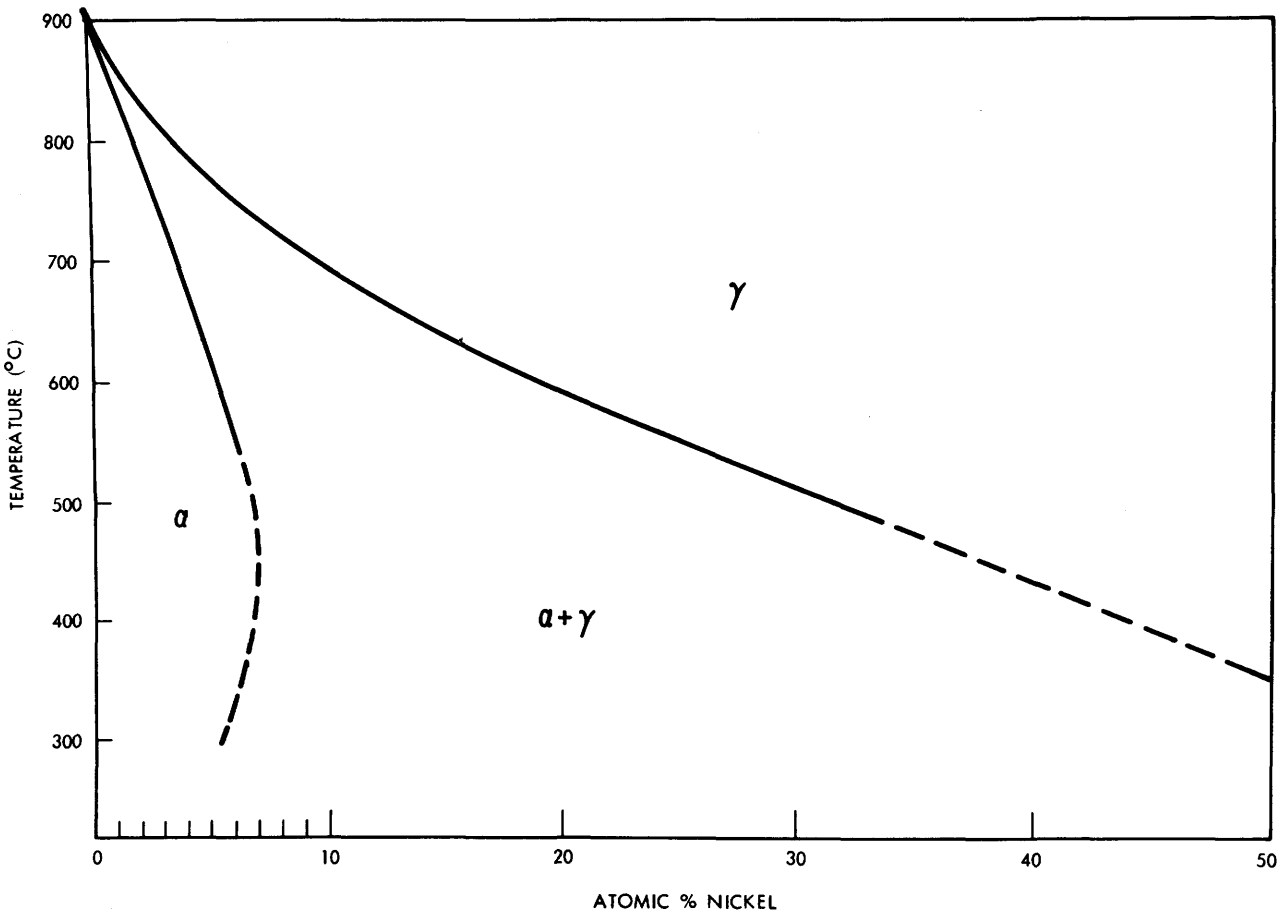

FIGURE 1.—Low temperature Fe-Ni phase diagram of Goldstein and Ogilvie (1965).

tions were reported by Adler and Dwornik (1961) on schreibersite and individual rhabdite crystals from the Canyon Diablo meteorite.

Goldstein and Ogilvie (1963) reported electron microprobe analyses of the composition of various-sized schreibersites in the Canyon Diablo, Breece and Grant meteorites. They observed a size-composition correlation, the smaller the schreibersite the higher the Ni content, and showed the presence of a zone of Ni depletion (swathing zone) even around very small schreibersites (rhabdites). They suggested that most schreibersite grew by solid state precipitation; although massive schreibersites showing no relation to the Widmanstätten pattern probably formed directly from the liquid state. Size and composition of the schreibersites were explained as dependent upon nucleation temperature and time available for growth of the precipitate. A growth analysis based on diffusion kinetics demonstrated that larger schreibersites nucleated between 700° and 500° C, and that small schreibersites (rhabdites) formed between 500° and 400° C. They also demonstrated that P solubility was greater in kamacite than in taenite.

Reed (1965a) emphasized the important role P plays in the formation of iron meteorite structures. He determined the range of Ni values in schreibersites and rhabdites in a large number of meteorites, finding Ni values as low as 14% in large schreibersites and as high as 50% in small taenite-border schreibersites. Ni depletion at kamacite-schreibersite interfaces was also demonstrated. The precipitate size and Ni content relationships were confirmed, and Reed pointed out that size-for-size rhabdite grains in the Canyon Diablo meteorite are 7% higher in Ni than those in the Coahuila meteorite. The author recognized the approximate nature of chemical analysis values

for total P, suggesting that in most cases the actual values are higher than the measured values. He discussed the sequence of phase formation in meteorites based on Vogel and Baur's (1931) phase diagram and stressed the need for more precise information on phase equilibria.

In a subsequent paper, Reed (1967) measured P distribution in the Mount Edith meteorite, demonstrating the practicality of measuring Ni and P distribution profiles in kamacite, taenite, and schreibersite. Later Reed (1969) discussed the role of P in relation to Widmanstätten pattern formation and cooling rate calculations, and reported measurements of P content in the kamacite of 61 meteorites.

Doan and Goldstein (1969) discussed the formation of phosphides in the various meteorite classification groups on the basis of their newly determined Fe-Ni-P phase diagram. They estimated total P values from examination of the largest available polished sections of a number of meteorites, and used them as the basis of a discussion of schreibersite precipitation reactions in various meteorite composition ranges. They inferred thermal equilibrium in iron meteorites down to 650° C, with schreibersites forming at higher temperatures while rhabdites form from kamacite at low temperatures when Ni and P diffusion are severely limited.

Comerford (1969) discussed schreibersite and cohenite occurrences in iron meteorites and pointed out that rhabdites, schreibersites that nucleated within kamacite, may be more reliable for diffusion analysis than grain boundary schreibersites. Axon and co-workers have discussed schreibersite occurrences in a broad range of meteorites (Axon and Faulkner, 1970; Axon and Waine, 1971, 1972; Axon and Smith, 1972). The papers of Axon and Waine (1971, 1972) discuss schreibersite morphology, mode of occurrence, and relationship to other minerals in great detail. Hornbogen and Kreye (1970) have reported detailed metallographic studies on the Coahuila and Gibeon meteorites and have discussed Ni and P solid state reactions in some detail. Reed (1972) has reported analyses of schreibersite in the Oktibbeha County meteorite, the highest Ni schreibersite known in meteorites (65.1%), and De Laeter et al. (1973) have reported on schreibersite in the Redfields meteorites, the lowest Ni schreibersite on record (7.0%).

Modern reviews that are particularly important to the investigations at hand have been mentioned previously. The paper by Goldstein and Axon (1973) is a comprehensive review of the development of the Widmanstätten pattern. The recent book by Wasson (1974) is a broad treatment of meteorites and includes an excellent summary of the work on chemical groupings of iron meteorites with extensive listings of individual iron meteorite analyses and classification. The treatise on iron meteorites by Buchwald (1976) has been of great help. Much of the descriptive material on individual meteorites had been available to us in manuscript, and Dr. Buchwald spent many hours teaching the senior author the rudiments of iron meteorite metallography during his two-year stay (1968–1970) at the Division of Meteorites, Smithsonian Institution.

Related Materials

Schreibersite occurrences are not restricted solely to iron meteorites. It is an accessory mineral in pallasites, mesosiderites, and enstatite chondrites, and has been reported in several ordinary chondrites, and a few carbonaceous chondrites and achondrites (Ramdohr, 1973; Powell, 1971; Malissa, 1974). Schreibersite is also known as a product of combustion in the coal mines of Commentry and Cranzac, France (Palache et al., 1944: 125), as a cavity mineral in iron slags (Spencer, 1916), and associated with metallic iron in the Disko Island, Greenland, basalts (Pauly, 1969).

Schreibersite has been observed by a number of workers in metal particles in lunar soil and rocks. Individual particles have been described in great detail, and Ni/Co ratios have been used to identify metal of meteoritic origin (Goldstein et al., 1970; Goldstein and Yakowitz, 1971; Axon and Goldstein, 1972; Goldstein et al., 1972). Nickel concentration in metal and schreibersite in contact with each other have also been used to suggest final equilibrium temperatures and to imply cooling histories. As lunar studies have continued, it has become apparent that a greater proportion of schreibersite-containing lunar metal than had previously been thought has been derived from processes other than simple disruption of impacting meteorites (Axon and Goldstein, 1973; El Goresy et al., 1973; Brown et al., 1973; Carter and Padovani, 1973; McKay et al., 1973; Goldstein and Axon, 1973; Gooley et al., 1973).

A second phosphide mineral, barringerite $(Fe,Ni,Co)_2P$, has been reported from the Ollague pallasite (Buseck, 1969). This material is probably a secondary product of some type and not an endogenous meteoritic mineral (Buchwald, 1976: 105).

The phosphide mineral, schreibersite, is the only phosphorus mineral that is observed as a minor phase in most iron meteorites, and it is the only phosphorus-containing mineral that will be considered in this paper. There are, however, nine phosphate minerals known in meteorites, and seven of these have been identified as trace constituents in iron meteorites (Fuchs, 1969; Bild, 1974). They are chlorapatite, $Ca_5(PO_4)_3Cl$; graftonite, $(Fe,Mn)_3(PO_4)_2$; sarcopside, $(Fe,Mn)_3(PO_4)_2$; whitlockite, $Ca_3(PO_4)_2$; brianite, $Na_2MgCa(PO_4)_2$; panethite, $Na_2Mg_2(PO_4)_2$; and farringtonite, $Mg_3(PO_4)_2$. These minerals are observed in a variety of associations: as inclusions in graphite-troilite-silicate nodules, in simple troilite nodules or in troilite-chromite nodules, as inclusions in or in contact with schreibersite, and associated with other minor minerals or isolated in metal. The phosphate-phosphide association has been used to calculate equilibrium oxygen fugacity in iron meteorites and pallasites (Olsen and Fredriksson, 1966; Olsen and Fuchs, 1967). In the iron meteorites considered in this paper, phosphate minerals are either absent or isolated within inclusions that represent a higher temperature stage in the development of the meteorite structure. No evidence has been developed in this work to indicate that the observed phosphide-metal equilibria have been affected by the presence of phosphates.

Experimental

Two types of data are needed in order to interpret iron meteorite structural development as a consequence of cooling through the subsolidus Fe-Ni-P system. Accurate bulk compositions are the first requirement, and good bulk Ni values are available from the literature. The problem of obtaining good bulk P values has not been solved satisfactorily, and estimated values were found to be useful. This aspect of the problem will be discussed in detail below. The second type of data required are P and Ni gradients within kamacite and schreibersite, and particularly P and Ni values at kamacite-schreibersite interfaces. Experimental procedures for obtaining these values were developed in the electron microprobe laboratory of the Department of Mineral Sciences, National Museum of Natural History, Smithsonian Institution. Reed (1967, 1969) had reported traverse data on the Mount Edith meteorite and had demonstrated the practicality of measuring the low P levels in kamacite with the microprobe. Doan and Goldstein's (1970) experience in their phase diagram studies was also encouraging. Ideally, one required step-by-step traverses over many meteorite structures, each traverse consisting of a large number of individual analyses for P and Ni. Ni concentrations were in a range that presented no unusual analytical problems, but the expected low levels of P required special care.

An A.R.L. EMX electron microprobe (Applied Research Laboratory, Sunland, California) was used in this work. Simultaneous measurements were made for Ni K_α (LiF crystal) and P K_α (ADP crystal) radiation at an X-ray takeoff angle of 52.5°. The instrument was operated at an accelerating voltage of 20 KV, with an approximately 0.1 μa sample current on 100% Fe and a beam size of approximately 1 μm. Average count rates measured on 50% Ni and calculated to 100% Ni were 30,000 cts/sec, with a peak to background ratio of 230. Count rates for 100% P measured on schreibersite were 25,000 cts/sec with a peak to background ratio of 915. Standard statistical assumptions suggest that for the 20 second counting periods employed, a detectability limit for P of 150 ppm for a single determination would be achieved, within a satisfactory range for the problem at hand (Ziebold, 1967). Neighboring P determinations within a given traverse generally agreed within ±50 ppm.

The standards used were 100% Fe, 100% Ni, a series of Fe-Ni alloys of known composition, and a fragment of a large schreibersite from the Canyon Diablo meteorite. The 100% Fe was used for determining both Ni and P background counts. The Fe-Ni standards were prepared by R. E. Ogilvie and obtained from J. I. Goldstein. They were used to derive an empirical curve that was incorporated into a data reduction program to correct Ni determinations. The schreibersite standard contained 12.9% Ni, 0.26% Co, and was assumed to contain 15.5% P. A linear relationship between P counts in schreibersite and concentration in an unknown was assumed. This was thought to cause

no serious error in low level P measurements, but it does introduce errors in P determination in schreibersite. In this study, P values for schreibersite were only used to identify the mineral, and for this purpose corrections seemed unnecessary.

Sections were prepared for study by standard metallographic procedures. Pieces of meteorite were mounted in one-inch diameter Bakelite, ground on a graded series of sandpapers, and polished with 3 μm diamond paste and finally Linde B alumina compound. The sections were then lightly etched with 0.5% nital (0.5 ml nitric acid in 100 ml of 95% ethanol). Light etching was essential to reveal structures that were examined and to permit their being relocated and analyzed in the microprobe. It would have been impossible to obtain the mass of data required using unetched sections. While deep etching is known to cause errors in microprobe measurements at phase interfaces, the light etching used here did not seem to cause a problem. A schreibersite-kamacite-taenite structure in the Carleton meteorite was selected to test this point. As nearly identical traverses as possible, considering that the section had to be removed from the microprobe, were made before and after etching. The results were identical within reasonable experimental error. Areas selected for microprobe analysis were photographed in detail, permitting the recording of the exact location of microprobe traverses.

The electron microprobe data was accumulated using a step-scan procedure. Ni and P counts were measured simultaneously and recorded on punch cards along with step length. The data were computer processed, resulting in a second set of cards containing calculated P values, empirically corrected Ni values, and step length. These cards in turn were used to obtain computer generated plots. Photographs of the data plots as received from the computer are given in Figures 2 and 3. The only additions to these diagrams are the vertical lines that have been added to help identify the structural elements. Figure 2 is a traverse across a structure in the Ballinger, Texas, meteorite, catalog number USNM 824. The labeling indicates that this is the fifth traverse made over structures in that meteorite, the data having been taken on 8 September 1972. Two symbols are used to indicate P concentration, the ordinate scale being zero to 0.7% P for low values and zero to 70% P for high values. The traverse started in kamacite and crossed a very thin, elongated phosphide (4 μm wide) at the edge of a taenite lamella. It passed into kamacite and after traveling 275 μm entered a rhombohedral phosphide (rhabdite) 30 μm across and then passed into kamacite again. The two unusually high P values in the kamacite are undoubtedly due to unseen phosphides that were included in the excitation volume of the microprobe beam. Figure 3 is a similar plot for the Lexington County Meteorite. In this case only a portion of the complete traverse is reproduced (700 out of 1600 μm). The traverse started in kamacite, entered a phosphide at a taenite border, passed into kamacite, a second phosphide, and a second taenite lamella. Interface concentration values and concentration gradient shapes and lengths were read from these plots.

Data obtained in this way are subject to several sources of error beyond those that apply to an individual point analysis in a homogeneous material. Stability of the microprobe over the long periods required to obtain lengthy traverses was a problem. Due to the survey nature of this investigation, compromises were made in favor of large numbers of traverses and for lengthy traverses. The microprobe beam current was monitored and kept within narrow limits, but this does not necessarily prevent all instrumental drift. Data were rejected when drift became an obvious problem, but normally measurements on standards or repeated measurements on the same structures gave identical results within reasonable limits of error ($\pm$ 0.005% P, $\pm$ 0.1% Ni).

The schreibersite-kamacite interface measurements are subject to errors due to both finite beam size and to interface geometry. The finite beam produces measured interface profiles that are less sharp than the actual profile. It is unlikely that this is a serious error in determining the interface value of P in kamacite, as this is only read to the nearest 0.01%. The interface value of Ni in kamacite is probably increased slightly by the proximity of high Ni in the adjoining schreibersite. More serious errors may result from interface geometry, as there is no reason to assume that the interfaces measured were perpendicular to the surface of the section. The small size of most of the structures measured, combined with their large number, made it impractical to attempt measuring slopes and applying corrections. Reproducibility of measurements on the same structure

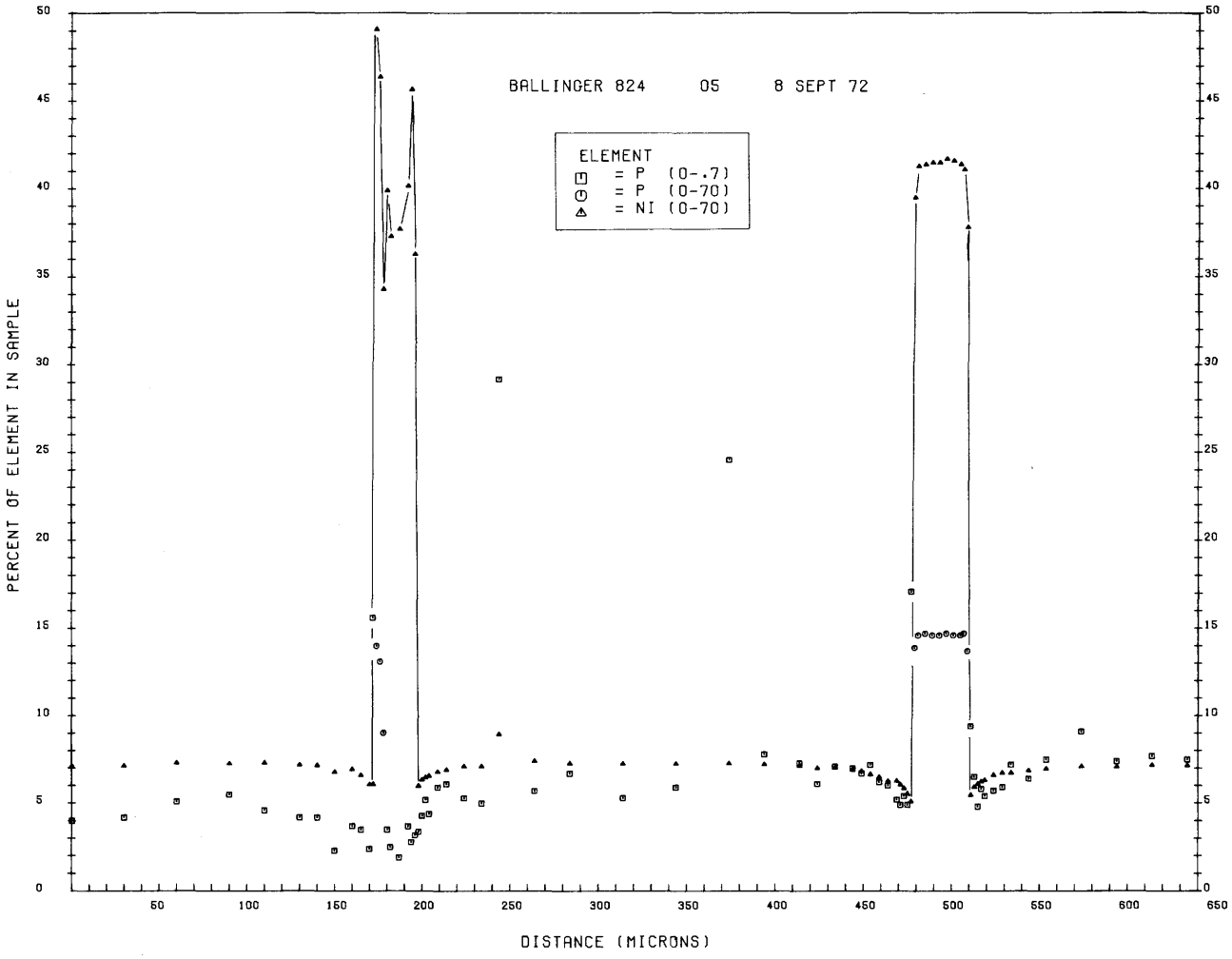

FIGURE 2.—Computer plotted Ni-P traverse across structure in Ballinger meteorite.

and on similar structures within the same meteorite indicated that this is not too serious a problem for the study at hand.

Results

Eight coarse-structured iron meteorites covering a range of bulk Ni and bulk P contents were selected for Ni and P measurements at kamacite-schreibersite interfaces (Table 1). Four structural and five chemical classification categories are represented in the group. The Bellsbank meteorite contains very low total Ni, while Balfour Downs is one of the highest Ni members of Group IA. Coahuila contains only about 0.3 wt. %P, while Bellsbank contains exceptionally high P. The other meteorites in the group range between these limits in Ni and P contents. The data in Table 1 were taken from Wasson (1974) and Buchwald (1976). Buchwald's values combine, where appropriate, chemical analytical values with the results of planometric analyses of large surfaces. Contributions of Ni and P due to large schreibersite inclusions are included in this approach, resulting in estimates more representative of the meteorite as a whole than uncorrected chemical values. Wasson's Ni values are chemical values determined on small samples taken for trace element analysis. A complete review of the literature of each of these meteorites and a discussion of their detailed metallography has been given by Buchwald (1976).

Microscopic examination of metallographic sections of these eight meteorites led to the selection of representative schreibersite-containing struc-

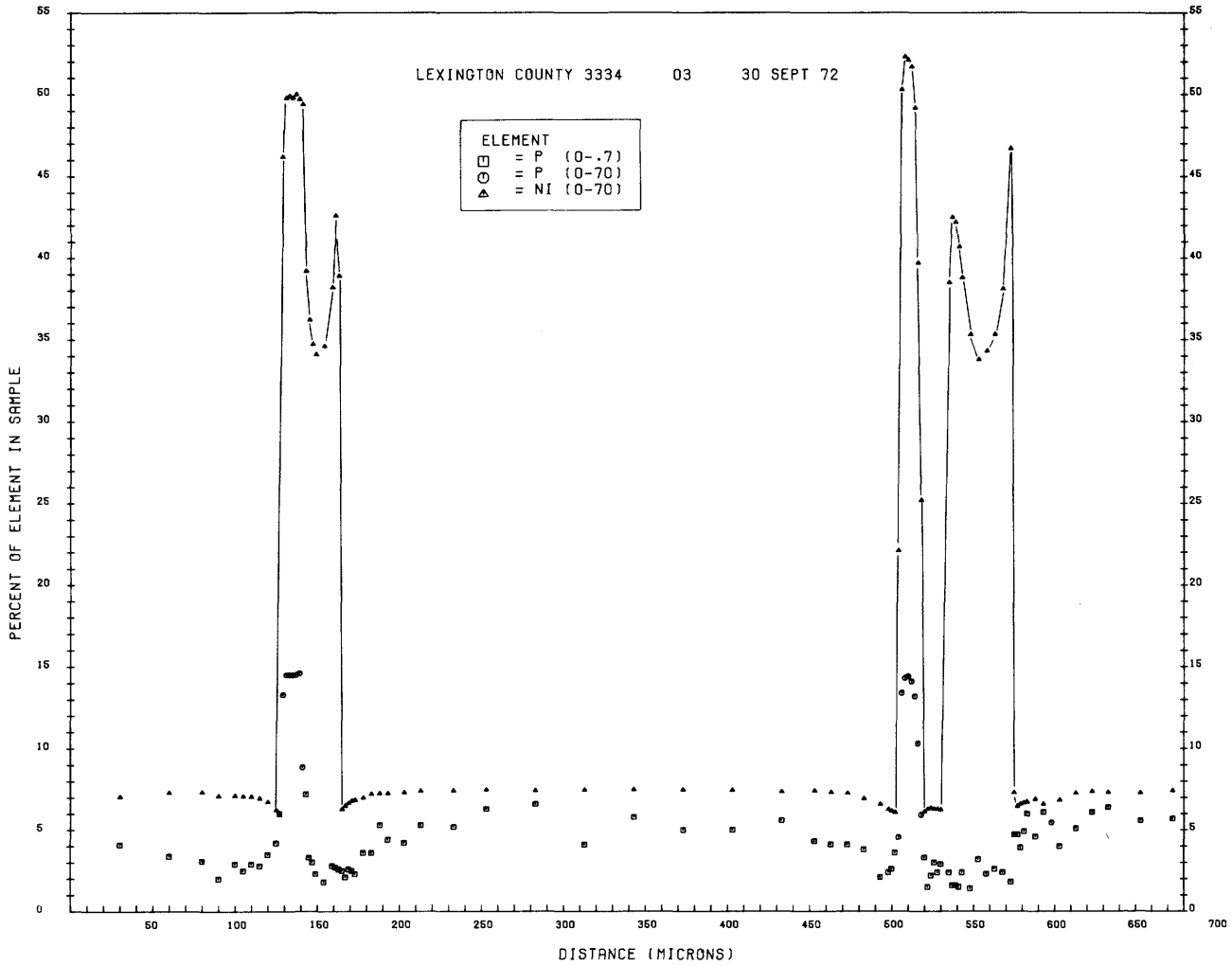

FIGURE 3.—Computer plotted Ni-P traverse across structure in Lexington County meteorite.

tures for detailed study by the electron microprobe step-scan procedure described above. Several microprobe traverses were made for each meteorite, and the data obtained on Ni and P values at kamacite-schreibersite interfaces and on Ni and P gradients in kamacite are summarized below. A separate table accompanies the description of traverses for a given meteorite, the format used being the same in each case (Tables 2–9). The first two columns give the specimen number, which includes the USNM catalog number, and the traverse number. Column three contains two types of information. The first entry for each traverse is enclosed in square brackets and gives the sequence of phases traversed and the length of the traverse. The abbreviations used here are Ph for the various morphologies of schreibersite, α for kamacite and γ for taenite. The following entries for a given traverse identify the specific schreibersites measured and give the length of schreibersite traversed. The next column, headed $\%Ni_{Sch}$, gives the weight percent Ni in schreibersite either at a kamacite-schreibersite interface or within a large schreibersite. Where an interface measurement has been made, the schreibersite Ni value will be followed in the next two columns by the weight percent Ni in kamacite at the interface ($\%Ni_{\alpha}$) and the weight percent P at the interface ($\%P_{\alpha}$). The next two sets of two columns each indicate the length of observed Ni and P gradients away from the interface and the Ni and P values at which a gradient was no longer distinguishable. Factors

TABLE 1.—Composition and classification of selected meteorites

Meteorite	Weight Percent %P*	%Ni*	%Ni**	Chemical Classification**	Structural Classification*
Coahuila	0.3	5.6	5.49	IIA	H
Bellsbank	2	5.3	4.13	IRANOM	H
Ballinger	0.4	6.5	6.19	IA-AN	Og
Santa Luzia	0.9	6.6	6.3	IIB	Ogg
Lexington County	0.3	~7.0	6.69	IA	Og
Bahjoi	---	7.7	7.95	IA-AN	Og
Goose Lake	0.4	8.3	8.00	IA-AN	Om
Balfour Downs	0.3	8.4	8.39	IA	Og

*Buchwald (1976)
**Wasson (1974)

such as impingement and termination of a particular traverse influence these final observed Ni and P values. In the final three columns the Ni and P values from columns three through six have been converted to atomic percent for use later.

COAHUILA

The Coahuila, Mexico, meteorite is an example of an ordinary hexahedrite (IIA), similar in composition and structure to a number of other hexahedrites. It consists of single crystal kamacite containing profuse small schreibersites generally of rhabdite morphology, and occasional larger schreibersites. The larger schreibersites sometimes border troilite or troilite-daubreelite inclusions, and in rare instances are associated with cohenite.

Section 3298 is dominated by six troilite-daubreelite inclusions, ranging in size from 5 to 0.3 mm in diameter. Half to three-quarters of the length of the borders of these sulfides are rimmed with schreibersite. One small sulfide is bordered for most of its circumference with schreibersite, the remaining border being rimmed with cohenite. Kamacite in the vicinity of these inclusions contains many subgrain boundaries and is free of schreibersite. Microrhabdites measuring less than a few microns in maximum length and generally considerably smaller are present in profusion away from these inclusions. Somewhat larger rhabdites are present in several areas aligned along Neumann bands. Several lamellar schreibersites, 5 to 10 μm wide and extending to lengths that are a major part of a millimeter or more, are also present. A summary of the traverses of this section is given below and specific measurements are listed in Table 2.

3298, traverse 1: crossed a 150 μm wide schreibersite bordering a 2 × 2 mm troilite-daubreelite inclusion and then extended into the surrounding kamacite for nearly 1 mm.

3298, traverse 2: crossed a 40 μm wide schreibersite bordering a 0.5 × 0.5 mm troilite-daubreelite inclusion and then extended 350 μm into the surrounding kamacite.

3298, traverse 3: crossed a 100 μm wide schreibersite bordering the 5 × 5 mm troilite-daubreelite inclusion and then extended for 350 μm into surrounding kamacite. This traverse is reproduced at the upper left in Figure 4.

Section 1641(1) primarily contains regions of kamacite with evenly distributed rhabdite, the individual rhabdites averaging 200 μm^2 in cross-sectional area. Also present in areas of clear kamacite are several large schreibersite inclusions and schreibersite-cohenite inclusions. The largest schreibersite inclusion has an area of 0.25 mm^2. A 0.1 × 0.6 mm schreibersite is bordered by cohenite, and an adjacent, slightly smaller schreibersite is partially surrounded by cohenite. One cohenite area, 0.2 × 0.3 mm, contains six small schreibersites. A 0.4 × 1.4 mm cohenite area contains a number of small schreibersites and surrounds a central schreibersite measuring 0.04 × 0.6 mm. An 80 × 150 μm daubreelite is surrounded by schreibersite. Two lamellar schreibersites, each approximately 0.02 × 1.0 mm, are present, and one of these is partially bordered with cohenite.

1641(1), traverse 4: crossed a large skeletal schreibersite enclosing a kamacite area. The traverse first crossed 450 μm of kamacite, then 120 μm of schreibersite, 70 μm of included kamacite, a second 70 μm schreibersite crossing, and terminated after passing through 360 μm of kamacite. The schreibersite was of uniform composition, and the measurements

TABLE 2.—Coahuila schreibersite-kamacite interface measurements

Specimen No.	Traverse No.	Structure traversed & schreibersites measured	Weight Percent			Ni Gradient		P Gradient		Atomic Percent		
			%Ni_{Sch}	%Ni_{α}	%P_{α}	Length (μm)	Wt.%Ni	Length (μm)	Wt.%P	%Ni_{Sch}	%Ni_{α}	%P_{α}
3298	1	[Ph border of troilite-daubreelite inclusion-α, 1.1 mm]										
		Schreibersite, 150 μm wide	23.5	3.4	0.07	600	5.5	800	0.16	20.1	3.2	0.13
3298	2	[Ph border of troilite-daubreelite inclusion-α, 400 μm]										
		Schreibersite, 40 μm wide	25.0	3.6	0.07	250	5.3	350	0.15	21.4	3.4	0.13
3298	3	[Ph border of troilite-daubreelite inclusion-α, 450 μm]										
		Schreibersite, 100 μm wide	25.0	3.7	0.08	250	5.3	300	0.15	21.4	3.5	0.14
1641(1)	4	[α-Ph-α-Ph-α, 1 mm]										
		Schreibersite 260x500 μm with 60x170 μm included kamacite										
		120 μm traverse	23.5	3.5	0.08	200	5.3	50	0.10	20.1	3.3	0.14
		70 μm traverse	23.5	3.5	0.08	250	5.3	200	0.10	20.1	3.3	0.14
1641(1)	5	[α-Ph-α, 350 μm]										
		Rhabdite, 25 μm traverse										
		Enter	34.5	4.9	0.06	50	5.3	Flat	0.06	29.7	4.7	0.11
		Exit	34.5	4.9	0.06	50	5.3	100	0.07	29.7	4.7	0.11
1641	6	[α-Ph-α, 750 μm]										
		Rhabdite (45x75 μm), 45 μm traverse	27.5	3.7	0.07	175	5.3	100	0.08	23.6	3.5	0.13
1641	7	[α-Ph-α, 800 μm]										
		Rhabdite (50x70 μm), 70 μm traverse										
		Exit	27.0	4.0	0.07	100	5.3	Flat	0.07	23.1	3.8	0.13
1641	8	[α-Ph-α-Ph-α, 850 μm]										
		Rhabdite (50x70 μm), 50 μm traverse	27.0	4.1	0.07	150	5.3	Flat	0.07	23.1	3.9	0.13
		Rhabdite (25x30 μm), 25 μm traverse	29.0	3.7	0.06	200	5.3	100	0.08	24.9	3.5	0.11
1641	9	[α-Ph-α, 200 μm]										
		Rhabdite (20x40 μm), 25 μm traverse	33.0	4.5	0.05	50	5.3	Flat	0.05	28.4	4.3	0.09

in Table 2 are for the initial and final schreibersite-kamacite interfaces.

1641(1), traverse 5: crossed 100 μm of kamacite, a 25 μm wide rhabdite and terminated after another 200 μm of kamacite. This traverse is reproduced at the lower left in Figure 4.

Section 1641 is a neighboring specimen to 1641(1) and is similar in metallography. Evenly distributed rhabdites averaging about 200 μm^2 in area are the primary feature. Random larger schreibersites, schreibersite-daubreelite, and schreibersite-cohenite inclusions similar to those described above are present, although they are neither as numerous nor as large as the largest mentioned above. Two unusually large rhabdites and two smaller ones were selected for measurement.

1641, traverse 6: crossed 400 μm of kamacite, a 45 μm wide rhabdite, and 300 μm of kamacite. Values reported in Table 2 are an average of the two similar interface measurements. This traverse is reproduced upper right in Figure 4.

1641, traverse 7: crossed 230 μm of kamacite, entered the rhabdite from an area of disturbed kamacite, traversed 70 μm of rhabdite and then 0.5 mm of kamacite. Only the measurements on leaving the rhabdite were usable.

1641, traverse 8: crossed 370 μm of kamacite, 50 μm of rhabdite, 25 μm of kamacite, 25 μm of rhabdite, and 350 μm of kamacite. The large rhabdite traversed here is the same one traversed in number 7 but from a near perpendicular direction. Values reported in Table 2 are averages of two similar interface measurements.

1641, traverse 9: crossed a smaller rhabdite approximately 1 mm from traverses 6 through 8. 90 μm of kamacite were crossed, followed by 25 μm of rhabdite and 80 μm of kamacite. Average interface values are listed in Table 2. This traverse is reproduced at the lower right in Figure 4.

Ni and P concentration-distance profiles typical of the Coahuila data outlined above are given in Figure 4. These diagrams were prepared from tracings of the computer plotted step-scan data. Ni concentrations are indicated by the solid lines, and P concentrations multiplied by 100 by dashed lines. The Ni profiles are normally readily reproduced from the data charts without ambiguity. The low level P data contains more scatter; drawing the appropriate line, and particularly selecting

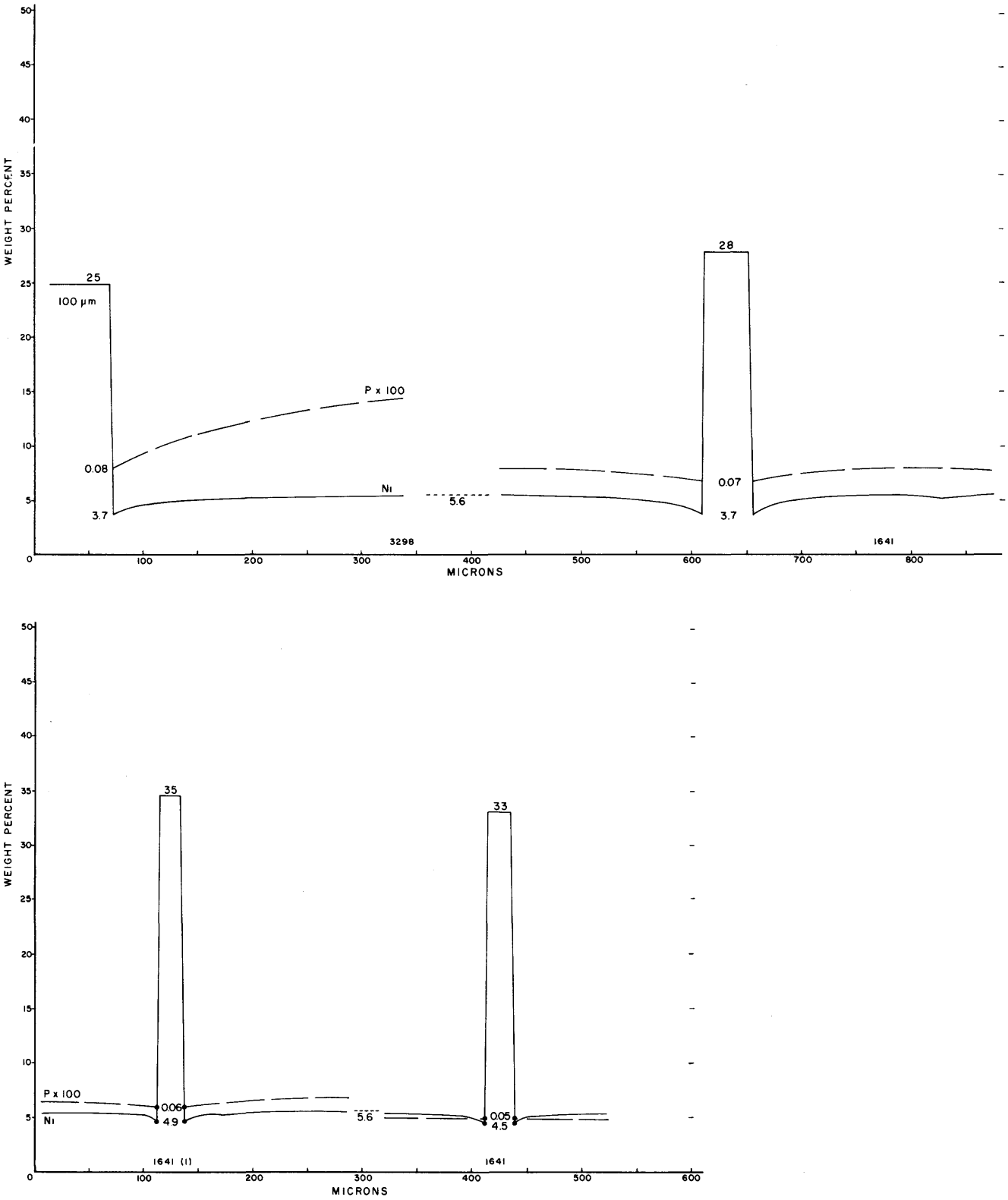

FIGURE 4.—Ni and P profiles at kamacite-schreibersite interfaces in Coahuila: upper left, traverse 3; upper right, 6; lower left, 5; lower right, 9.

the kamacite interface P level, is more subjective. A smoothing procedure relying on eyeball examination was used. Ni values for schreibersite and Ni and P concentrations in kamacite at the kamacite-schreibersite interface are indicated at an appropriate place on the diagrams. The bulk Ni content of the meteorite is also given and indicated by a short dashed line.

The four profiles (Figure 4) illustrate the observed range of Ni in Coahuila schreibersite and the shape and level of the Ni and P gradients in the surrounding kamacite. They are given from upper left to lower right in order of decreasing P concentration at the kamacite-schreibersite interface. Three of the profiles are of large rhabdites (traverses 6, 5, 9, Table 2), while the one at the upper left is of a 100 μm wide schreibersite bordering a large troilite-daubreelite inclusion (traverse 3, Table 2). The high P interface value and the high level in the surrounding kamacite are of particular interest. The three rhabdites appear to increase in Ni, both with decreasing cross-sectional area and with increasing interface Ni in kamacite value. The interface P values do not seem to correlate with either Ni in schreibersite or with interface Ni in kamacite values. Ni and P gradients extend for several hundred microns around the larger schreibersites but appear to be much more restricted in extent around the smaller ones. The 33% Ni schreibersite has an essentially flat P concentration at 0.05%. For these four cases, the length and steepness of the P gradient decreases with decreasing P at the interface.

Bellsbank

The Bellsbank, South Africa, meteorite is a phorphorus-rich hexahedrite. Massive and large skeletal schreibersite crystals, with individual faces over a centimeter in length and areas larger than 2 cm^2, dominate polished surfaces and appear to be distributed throughout this meteorite (photograph in Henderson, 1965). The kamacite matrix contains a network of lamellar schreibersite. These rarely intersecting planar crystals may exceed a centimeter in length, but are normally only 5 to 10 μm thick. Occasional large rhabdites and subgrain boundary schreibersites are present. Microrhabdites are present in profusion in kamacite areas away from the other forms of schreibersite. The Bellsbank meteorite has experienced severe terrestrial weathering. Many of the lamellar schreibersites have been replaced with corrosion products, and corrosion along kamacite-schreibersite interfaces is common.

Section 2162 contains parts of two massive schreibersites surrounded by schreibersite-free kamacite areas. Two lengthy subgrain boundaries

TABLE 3.—Bellsbank schreibersite-kamacite interface measurements

Specimen No.	Traverse No.	Structure traversed & schreibersites measured	Weight Percent			Ni Gradient		P Gradient		Atomic Percent		
			%Ni$_{Sch}$	%Ni$_{\alpha}$	%P$_{\alpha}$	Length (μm)	Wt.%Ni	Length (μm)	Wt.%P	%Ni$_{Sch}$	%Ni$_{\alpha}$	%P$_{\alpha}$
2162	1	[α-Ph, 3.6 mm]										
		Massive schreibersite (7x2 mm), 1 mm traverse	12.4	1.6	0.09	900	3.9	1000	0.20	10.6	1.5	0.16
2162	2	[α-Ph-α, 900 μm]										
		Large rhabdite along sub-grain boundary, 40x50 μm, diagonally across body.	22.0	3.2	0.09	20	4.5	50	0.18	18.8	3.1	0.16
2162	3	[α-Ph-α, 200 μm]										
		Same rhabdite as traverse 2, parallel to 50 μm direction										
		Enter	22.0	3.3	0.09	40	4.2	Flat	0.09	18.8	3.1	0.16
		Exit	22.0	2.7	0.05	40	4.2	60	0.12	18.8	2.5	0.09
2162	4	[α-Ph-α, 300 μm]										
		Rhabdite along sub-grain boundary, 15x120 μm	22.6	2.6	0.05	80	4.3	100	0.20	19.3	2.5	0.09
2162	5	[α-Ph-α, 300 μm]										
		Rhabdite along sub-grain boundary, 15x120 μm, repeat of traverse 2162-4	22.8	2.6	0.05	90	4.3	100	0.18	19.5	2.5	0.09
2162	6	[α-Ph-α, 130 μm]										
		Large rhabdite isolated in micro-rhabdite area of α, 30x60 μm	18.6	2.8	0.09	40	4.2	30	0.20	15.9	2.7	0.16

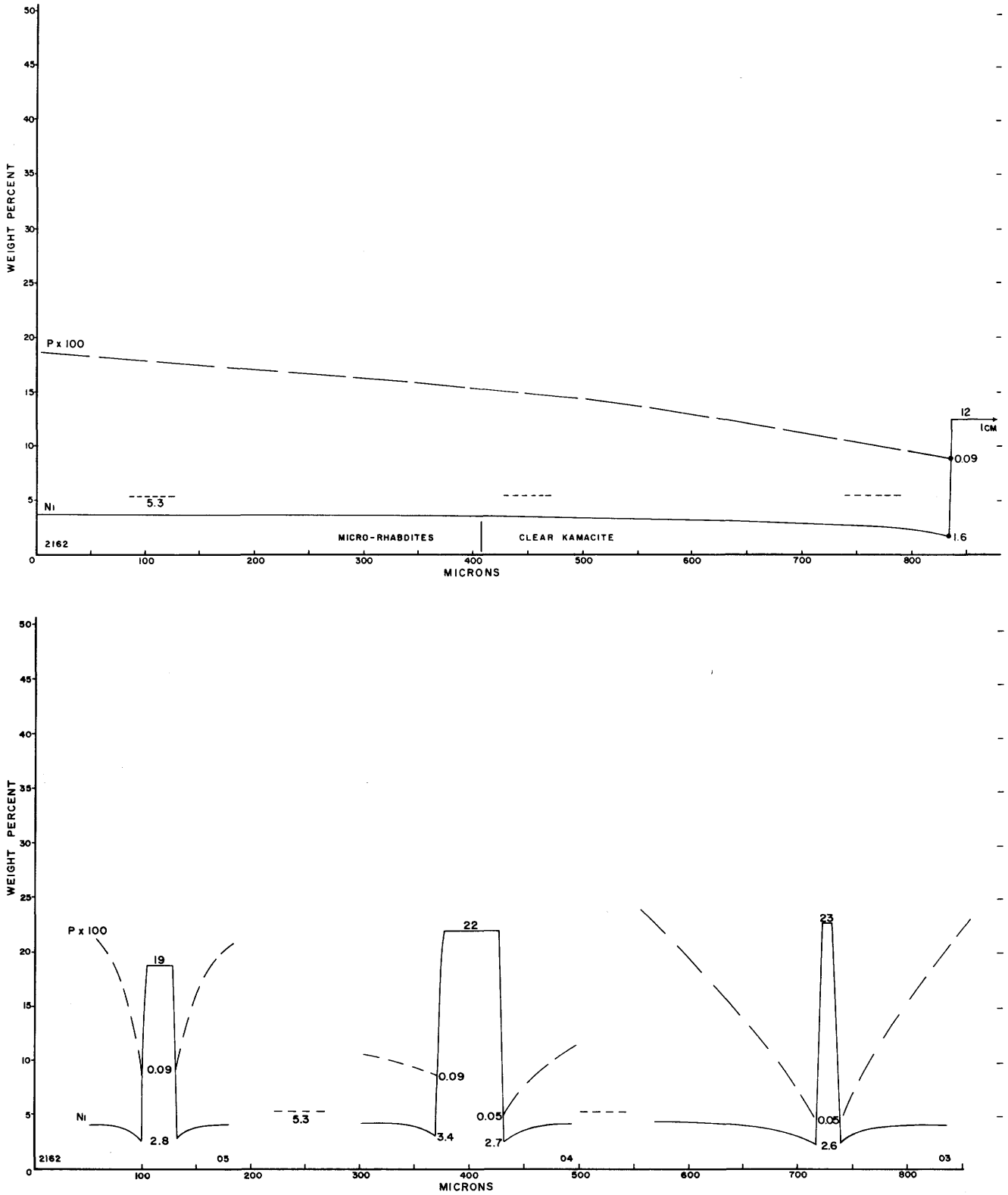

FIGURE 5.—Ni and P profiles at kamacite-schreibersite interfaces in Bellsbank: top, traverse 1; lower left, 6; lower middle, 3; lower right, 4 and 5. (Dashed line indicates bulk Ni value.)

cross the kamacite and are sites of small lamellar, irregular-shaped, and rhabdite-shaped schreibersites. The kamacite matrix contains profuse microrhabdites. Oxidation products are present at sites previously occupied by lamellar schreibersite, and along some Neumann bands and possibly cleavage planes.

2162, traverse 1: crossed 2.6 mm of kamacite and entered a large schreibersite and continued for 1 mm. The traverse was perpendicular to a straight kamacite-schreibersite interface, and the Ni content of the schreibersite was uniform for the length of the measurement (reproduced at top of Figure 5). Numerical data for this and succeeding Bellsbank traverses are given in Table 3.

2162, traverse 2: crossed 650 μm of kamacite, a rhabdite at a subgrain boundary and continued into surrounding kamacite for 200 μm. Average values for the two interface values are given in Table 3.

2162, traverse 3: crossed 70 μm of kamacite, the same rhabdite measured above, and passed into 70 μm of kamacite. Traverse 2 crossed diagonally, while this one passed through the middle parallel to the 50 μm edge. Two different interface values for Ni and P in kamacite were obtained, perhaps influenced by the presence of the subgrain boundary (Table 3 and lower middle of Figure 5).

2162, traverse 4: crossed 170 μm of kamacite, the narrow direction of an elongated rhabdite situated along a subgrain boundary, and 100 μm of kamacite (lower right in Figure 5).

2162, traverse 5: a remeasurement of traverse 4.

2162, traverse 6: crossed a large rhabdite surrounded by a region of clear kamacite within a microrhabdite area (lower left in Figure 5).

An attempt was made to determine Ni in other small schreibersites in Bellsbank. A number of measurements were made on schreibersites ranging down to a minimum of a few microns in width. Twelve measurements were obtained where the P value indicated that the microprobe beam had been completely within a schreibersite. The Ni values ranged from 22% to a maximum of 32%. Interface measurements were not attempted on these small bodies.

The four profiles in Figure 5 represent the traverses described above and illustrate the shapes and levels of the Ni and P gradients in the surrounding kamacite. The profile at the top is the interface portion of traverse 1. The low value for Ni in the schreibersite combines with an unusually low interface value for Ni and a high interface value for P in kamacite. The rhabdite profile at the lower left has the same P interface value, but higher Ni in both kamacite and schreibersite. The P gradient in this case is particularly severe. The rhabdite at the lower right has similar Ni values to the one on the left, but the P interface value is considerably lower. The middle profile has uniform Ni in the schreibersite but has two different sets of P and Ni kamacite interface values, the only such observation made in this study.

Ballinger

The Ballinger, Texas, meteorite is a low-Ni coarse octahedrite. Figure 6 is a photograph of the slice studied, USNM 824. The area marked PS shows where material was taken for section preparation. Section 824 is from the back of this surface and contains a large schreibersite similar in size and shape to the one at the lower right in Figure 6. Section 824(1) is the outlined surface after repolishing. The overall structure consists of large kamacite grains and three areas of heiroglyphic schreibersite. A Widmanstätten pattern is suggested in some areas of the structure, but it is certainly not well developed. The large schreibersite on the left is completely surrounded by rims of partially decomposed cohenite. The center group of schreibersite crystals is partly bordered by partially decomposed cohenite, while the schreibersite on the right is completely free of cohenite. Areas of this surface containing the best Widmanstätten pattern development are well away from the large schreibersite inclusions. It is interesting to note that the lower left-hand edge of this slice contains a rim of kamacite heat altered to α_2, a remnant from ablation heating. This structure has not been previously observed in the Ballinger meteorite.

Section 824 contains a large schreibersite 0.8 mm long and averaging 1 to 2 mm in width, surrounded by a narrow area of schreibersite-free kamacite. The kamacite matrix contains a profusion of both Neumann bands and rhabdites. Neumann band bending, particularly at the interfaces with the large schreibersite, suggests mild mechanical distortion in Ballinger. The kamacite contains numerous grain boundaries that are the sites of grain boundary schreibersites. Terrestrial oxidation has penetrated areas of this section.

824, traverse 1: crossed three areas of the large schreibersite. 500 μm of kamacite were crossed, followed by 350 μm of schreibersite, 800 μm of kamacite, 400 μm of schreibersite, 450 μm of kamacite, 670 μm of schreibersite, and finally 500 μm of kamacite. The three schreibersite areas traversed are essentially free of Ni gradients and they all have approxi-

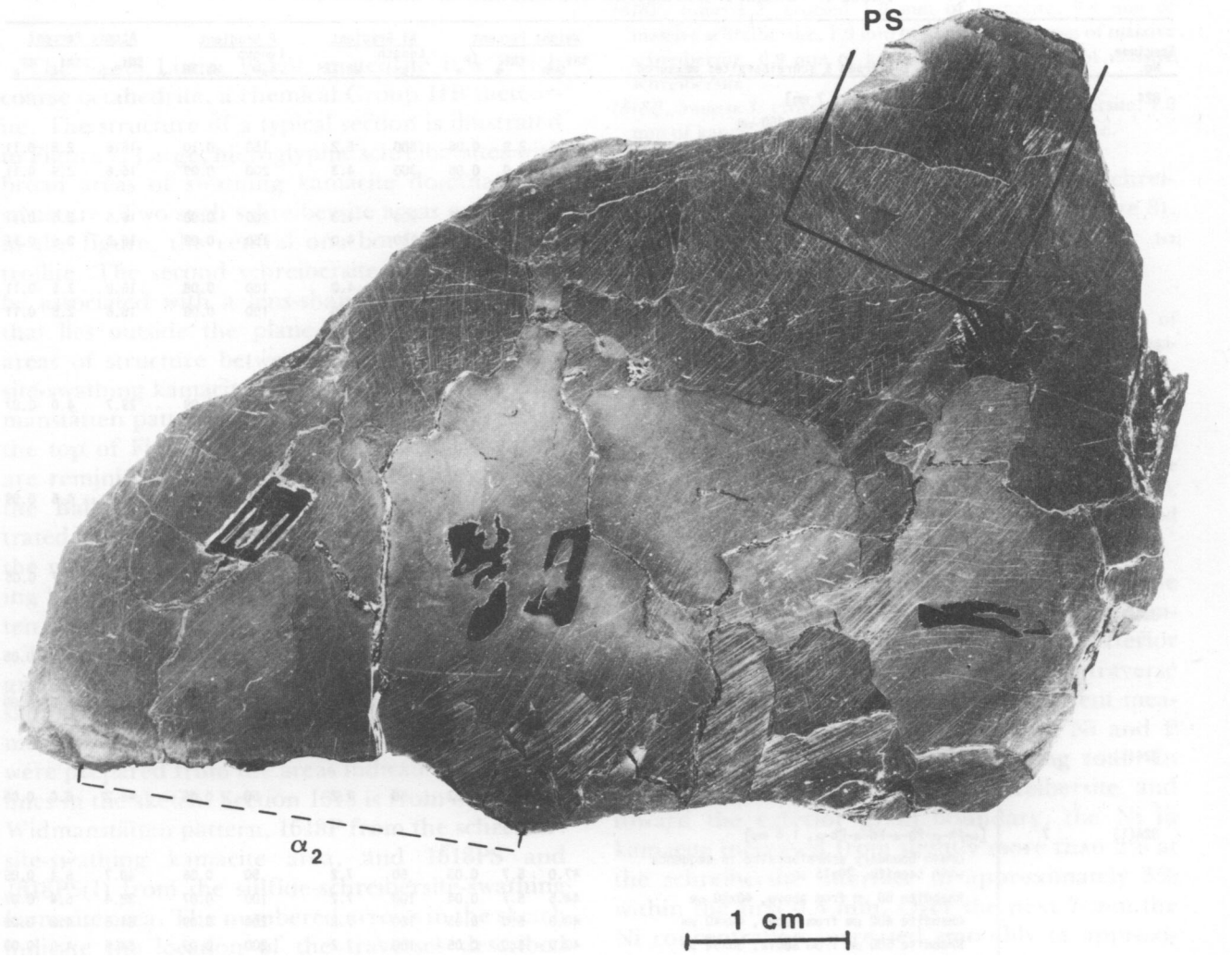

FIGURE 6.—Macrostructure of a slice of Ballinger meteorite (large dark inclusions are schreibersite, the one on the left enclosed in partially decomposed cohenite; area marked PS was used for microstructure examination [824(1)]; and edge marked α_2 contains a rim of ablation recrystallized kamacite).

mately the same Ni value. Numerical data for this and succeeding Ballinger traverses are given in Table 4.

824, traverse 2: crossed two rhabdites along a grain boundary 2 mm away from the massive schreibersite. 400 μm of kamacite were crossed, followed by two 40 μm rhabdites separated by 25 μm of kamacite, and finally 300 μm of kamacite. Because of impingement effects, the interface values in Table 4 are an average of the two similar external measurements.

824, traverse 3: crossed two areas of a 1 × 0.4 mm skeletal schreibersite 3.5 mm from the massive schreibersite. The values given in Table 4 are averages of the two external interface values.

Section 824(1) is from a typical Widmanstätten area of the Ballinger meteorite, the area outlined in Figure 6. The kamacite matrix contains Neumann bands and rhabdites in a wide range of sizes. Kamacite lamellae are separated by grain boundaries that are alternately sites of grain boundary schreibersites and taenite-plessite bands.

824(1), traverse 4: crossed 230 μm of kamacite and entered a small schreibersite embedded in a taenite border, passed through a narrow band of taenite, and then 220 μm of kamacite.

824(1), traverse 5: crossed 150 μm of kamacite, a schreibersite embedded in taenite, 20 μm of taenite, 270 μm of kamacite, a large rhabdite, and finally 120 μm of kamacite (see Figure 2 in experimental section).

TABLE 4.—Ballinger schreibersite-kamacite interface measurements

Specimen No.	Traverse No.	Structure traversed & schreibersites measured	Weight Percent %Ni$_{Sch}$	%Ni$_{\alpha}$	%P$_{\alpha}$	Ni Gradient Length (μm)	Wt.%Ni	P Gradient Length (μm)	Wt.%P	Atomic Percent %Ni$_{Sch}$	%Ni$_{\alpha}$	%P$_{\alpha}$
824	1	[α-Ph-α-Ph-α-Ph-α, 3.7 mm]										
		Massive schreibersite, 350 μm										
		Enter	19.5	2.9	0.06	500	5.2	150	0.10	16.6	2.8	0.11
		Exit	19.5	3.0	0.06	300	4.3	200	0.09	16.6	2.9	0.11
		Massive schreibersite, 400 μm										
		Enter	19.5	2.6	0.06	200	4.3	200	0.08	16.6	2.5	0.11
		Exit	19.3	2.6	0.06	150	4.0	150	0.08	16.5	2.5	0.11
		Massive schreibersite, 670 μm										
		Enter	19.7	---	0.06	150	4.0	100	0.08	16.8	2.5	0.11
		Exit	19.5	2.6	0.06	500	5.0	150	0.08	16.6	2.5	0.11
824	2	[α-Ph-α-Ph-α, 850 μm]										
		Two large rhabdites, 40x40 μm each, separated by 25 μm. Values recorded are averages of similar values.	34.5	4.2	0.04	200	6.0	100	0.09	29.7	4.0	0.07
824	3	[α-Ph-α-Ph-α, 700 μm]										
		Skeletal schreibersite 1x0.4 mm. Values recorded are average of similar values from the two exterior interfaces.	35.8	4.8	0.05	150	6.8	200	0.08	30.8	4.6	0.09
824(1)	4	[α-Ph-γ-α, 480 μm]										
		Rhabdite embedded in taenite border, 15x20 μm	49.8	6.0	0.03	50	7.2	50	0.05	43.1	5.7	0.05
824(1)	5	[α-Ph-γ-α-Ph-α, 650 μm]										
		Rhabdite embedded in taenite border, 5 μm wide	49.5	6.0	0.03	50	7.2	50	0.05	42.9	5.7	0.05
		Large rhabdite (35x25 μm), 250 μm into α from above	41.5	5.2	0.05	50	7.2	50	0.07	35.8	5.0	0.09
824(1)	6	[α-Ph-γ-α, 300 μm]										
		Rhabdite embedded in taenite border, 10x15 μm	51.0	6.3	0.03	50	7.2	50	0.06	44.2	6.0	0.05
824(1)	7	[α-Ph-α-Ph-α-Ph-α-Ph-α, 1.4 mm]										
		Grain boundary schreibersite in sequence with taenite, 20x15 μm	47.0	5.7	0.03	50	7.2	50	0.06	40.7	5.4	0.05
		Rhabdite 50 μm from above, 40x50 μm	44.5	5.7	0.04	100	7.2	100	0.07	38.4	5.4	0.07
		Rhabdite 400 μm from above, 40x40 μm	40.0	5.0	0.05	100	7.2	200	0.09	34.5	4.8	0.09
		Rhabdite 600 μm from above, 30x50 μm	40.0	5.0	0.05	100	7.2	200	0.09	34.5	4.8	0.09
824(1)	8	[α-Ph-α, 1.0 mm]										
		Grain boundary schreibersite in sequence with taenite, 15x140 μm	48.8	6.0	0.03	100	7.0	300	0.08	42.3	5.7	0.05

824(1), traverse 6: crossed 80 μm of kamacite, a taenite border schreibersite, 15 μm of taenite, and 150 μm of kamacite.

824(1), traverse 7: crossed 140 μm of kamacite, a grain boundary schreibersite in sequence with taenite, 50 μm of kamacite, a large rhabdite, 300 μm of kamacite, a large rhabdite, 620 μm of kamacite, a large rhabdite, and finally 80 μm of kamacite.

824(1), traverse 8: crossed 90 μm of kamacite, a grain boundary schreibersite in sequence with taenite, and 1 mm of kamacite.

The massive schreibersite in Ballinger contains higher Ni than similar sized schreibersite in Bellsbank, and the Ni in kamacite interface values are higher while the P interface values are lower. Large rhabdites in Ballinger contain more Ni than similar ones in Coahuila or Bellsbank, and their interface values are generally higher in Ni and lower in P. Grain boundary schreibersite tends to contain more Ni than kamacite matrix rhabdites, and taenite border schreibersite contains the highest Ni values observed. As the Ni values in the schreibersite go up, interface values in kamacite tend to go up for Ni and down for P. Ni and P gradients extend over relatively large distances around the massive schreibersite and over much shorter distances in the higher Ni forms of schreibersite.

Santa Luzia

The Santa Luzia, Brazil, meteorite is a P-rich coarse octahedrite, a chemical Group IIB meteorite. The structure of a typical section is illustrated in Figure 7. Large, hieroglyphic schreibersites with broad areas of swathing kamacite dominate the structure. Two such schreibersite areas are shown in the figure, the central one bordering a large troilite. The second schreibersite area could also be associated with a lens-shaped troilite nucleus that lies outside the plane of this section. The areas of structure between the troilite-schreibersite-swathing kamacite areas contain a coarse Widmanstätten pattern, particularly well developed in the top of Figure 7. These Widmanstätten areas are reminiscent of the schreibersite-free areas of the Ballinger meteroite. Weathering has penetrated deeply into Santa Luzia, particularly along the major grain boundaries separating the swathing kamacite areas from the areas of Widmanstätten pattern.

Figure 8 is a sketch of the section of the photograph (Figure 7), indicating how this slice was sampled for detailed metallographic and electron microprobe analysis. Four metallographic sections were prepared from the areas indicated by dashed lines in the sketch. Section 1618 is from an area of Widmanstätten pattern, 1618P from the schreibersite-swathing kamacite area, and 1618PS and 1618PS(1) from the sulfide-schreibersite-swathing kamacite area. The numbered arrows in the sketch indicate the location of the traverses described below. Lengthy traverses were made in each of the two hieroglyphic phosphide areas, with short ones being made in the Widmanstätten pattern area.

Section 1618P contains massive schreibersite and swathing kamacite (Figure 8). Clear kamacite surrounds the large schreibersite, grading into kamacite containing a profusion of microrhabdites. Neumann bands are most obvious in the transition areas between clear kamacite and microrhabdite areas. Occasional subgrain boundaries are present within the kamacite, and small schreibersites of various morphologies are associated with them.

1618P, traverse 1: crossed 1.3 mm of massive schreibersite, 2.0 mm of kamacite, 0.7 mm of massive schreibersite, 0.5 mm of kamacite, 0.2 mm of massive schreibersite, and 2.6 mm of kamacite. Numerical data for this and succeeding Santa Luzia traverses are given in Table 5.

1618P, traverse 2: crossed 1.0 mm of kamacite, 0.4 mm of massive schreibersite, 1.9 mm of kamacite, 0.8 mm of massive schreibersite, 0.9 mm of kamacite, and 0.2 mm of massive schreibersite.

1618P, traverse 3: crossed 0.2 mm of massive schreibersite, 1.0 mm of kamacite, and 0.2 mm of massive schreibersite.

Section 1618PS contains troilite, massive schreibersite and areas of swathing kamacite (Figure 8). Its metallographic characteristics are similar to those of section 1618P.

1618PS, traverse 4: crossed 0.2 mm of troilite, 2.9 mm of kamacite, 140 μm of massive schreibersite, 0.6 mm of kamacite, 2.9 mm of massive schreibersite, and 0.5 mm of kamacite.

1618PS, traverse 5: crossed 0.4 mm of troilite, 0.7 mm of massive schreibersite, 4.6 mm of kamacite, 2.5 mm of massive schreibersite, and 1.8 mm of kamacite. A representative interface profile for this traverse is reproduced in Figure 9.

1618PS, traverse 6: crossed 0.6 mm of massive schreibersite and 1.9 mm of kamacite.

Section 1618PS(1) contains an outer edge of the massive schreibersite and spans the swathing kamacite zone, containing a segment of its exterior boundary. A detailed electron microprobe traverse was not made on this sample, but sufficient measurements were taken to establish the Ni and P concentration patterns for the swathing zone. In the direction away from the schreibersite and toward the exterior grain boundary, the Ni in kamacite increased from slightly more than 2% at the schreibersite interface to approximately 5% within the first 0.5 mm. Over the next 7 mm the Ni concentration increased smoothly to approximately 7%. It is in the first 0.2 mm of kamacite surrounding the schreibersite that the Ni concentration increases most rapidly, and it is this zone that is free of microrhabdites. The P concentration increases to approximately 0.1% within this same region of approximately 0.2 mm bordering the interface. Upon entering the zone of microrhabdite precipitation, P concentration falls off in kamacite to a uniform level of approximately 0.05% for the remainder of the swathing zone. Late-stage microrhabdite precipitation seems to have effectively removed the P gradient that must have been produced within the swathing zone during the massive schreibersite growth, while apparently only slightly modifying the Ni gradient.

The clear kamacite surrounding the central schreibersite within the swathing zone is 100 to

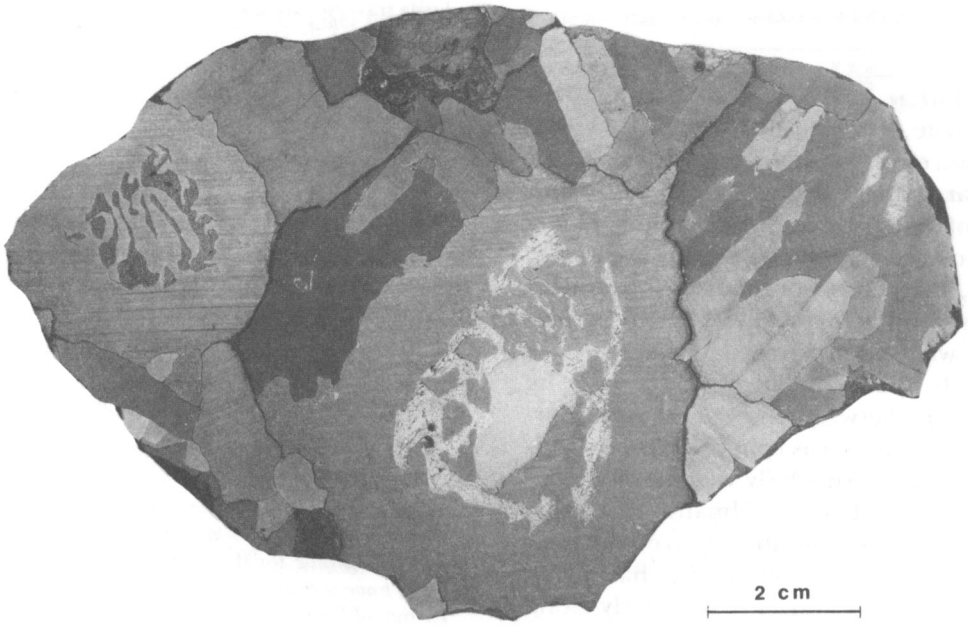

FIGURE 7.—Etched surface of Santa Luzia meteorite, USNM 1618: center, troilite surrounded by schreibersite and swathing kamacite; left, schreibersite area in swathing kamacite.

FIGURE 8.—Sketch of Santa Luzia meteorite slice in Figure 7, (coarse pattern, troilite; fine pattern, schreibersite; lines enclose areas of swathing kamacite; broken lines, locations of metallographic sections; numbered arrows, positions of electron microprobe traverses; stars, positions of residual taenite areas).

200 μm wide. This clear kamacite grades into kamacite containing profusion of microrhabdites, and it is in this transitional area that Neumann bands are frequently best developed. Microrhab-

TABLE 5. – Santa Luzia schreibersite-kamacite interface measurements

Specimen No.	Traverse No.	Structure traversed & schreibersites measured	Weight Percent			Ni Gradient		P Gradient		Atomic Percent		
			$\%Ni_{Sch}$	$\%Ni_{\alpha}$	$\%P_{\alpha}$	Length (μm)	Wt.%Ni	Length (μm)	Wt.%P	$\%Ni_{Sch}$	$\%Ni_{\alpha}$	$\%P_{\alpha}$
1618P	1	[Ph-α-Ph-α-Ph-α, 7.3 mm]										
		Massive schreibersite, 1.3 mm traverse										
		Start	16.0							13.6		
		Exit	16.5	2.4	0.07	500	4.9	500	0.15	14.1	2.3	0.13
		Massive schreibersite, 0.7 mm traverse										
		Enter	16.5	2.3	0.06	600	4.9	400	0.15	14.1	2.2	0.11
		Exit	16.5	2.4	0.07	200	3.8	100	0.08	14.1	2.3	0.13
		Massive schreibersite, 250 μm traverse										
		Enter	17.9	2.4	0.07	200	3.8	Flat	0.07	15.3	2.3	0.13
		Exit	17.9	2.4	0.07	1000	5.3	800	0.16	15.3	2.3	0.13
1618P	2	[α-Ph-α-Ph-α-Ph, 5.3 mm]										
		Massive schreibersite, 430 μm traverse										
		Enter	16.0	2.3	0.07	900	4.0	500	0.09	13.6	2.2	0.13
		Exit	16.0	2.3	0.07	1000	3.7	300	0.09	13.6	2.2	0.13
		Massive schreibersite, 800 μm traverse										
		Enter	16.2	2.2	0.07	600	3.8	400	0.09	13.8	2.1	0.13
		Exit	16.2	2.4	0.07	400	4.2	300	0.09	13.8	2.3	0.13
		Massive schreibersite, 200 μm traverse										
		Enter	16.1	2.3	0.07	400	4.2	200	0.09	13.7	2.2	0.13
		Stop	16.1							13.7		
1618P	3	[Ph-α-Ph, 1.4 mm]										
		Massive schreibersite, 220 μm traverse										
		Start	16.0							13.6		
		Exit	16.0	2.3	0.07	200	4.0	300	0.11	13.6	2.2	0.13
		Massive schreibersite, 200 μm traverse										
		Enter	16.2	2.3	0.07	300	4.0	300	0.11	13.8	2.2	0.13
		Stop	16.2							13.8		
1618PS	4	[Troilite-α-Ph-α-Ph-α, 7.4 mm]										
		Massive schreibersite, 140 μm traverse										
		Enter	17.3	2.6	0.08	600	4.8	800	0.16	14.8	2.5	0.14
		Exit	17.3	2.3	0.06	300	3.5	300	0.08	14.8	2.2	0.11
		Massive schreibersite, 2.9 mm traverse										
		Enter	16.6	2.4	0.07	300	3.5	200	0.08	14.4	2.3	0.13
		Exit	17.1	2.5	0.08	500	5.0	250	0.14	14.6	2.4	0.14
1618PS	5	[Troilite-Ph-α-Ph-α, 1 cm]										
		Massive schreibersite, 0.7 mm traverse										
		Start	16.6							14.2		
		Exit	16.6	2.5	0.07	900	4.6	700	0.14	14.2	2.4	0.13
		Massive schreibersite, 2.5 mm traverse										
		Enter	16.4	2.5	0.07	500	4.6	800	0.14	14.0	2.4	0.13
		Exit	16.6	2.5	0.07	600	5.2	800	0.18	14.2	2.4	0.13
1618PS	6	[Ph-α, 2.5 mm]										
		Massive schreibersite, 0.6 mm traverse										
		Start	16.6							14.2		
		Exit	16.6	2.3	0.07	600	4.8	500	0.13	14.2	2.2	0.13
1618	7	[α-Ph-α, 350 μm]										
		Traverses across grain boundary schreibersite, 12x170 μm										
		Tip	45.5	5.8	0.03	50	7.3	100	0.10	39.4	5.5	0.05
		Center	44.7	6.0	0.04	100	7.4	100	0.10	38.6	5.7	0.07
		Tip	45.7	6.2	0.04	50	7.4	100	0.10	39.6	5.9	0.07
1618	8	[α-γ-Ph-α, 400 μm]										
		Taenite border schreibersite, 10x20 μm	48.0	6.4	0.03	100	7.4	150	0.10	41.5	6.1	0.05
1618	9	[α-γ-Ph-α, 350 μm]										
		Taenite border schreibersite, 15x40 μm	48.5	6.5	0.03	70	7.5	150	0.10	42.0	6.2	0.05

TABLE 5—*continued*

Specimen No.	Traverse No.	Structure traversed & schreibersites measured	Weight Percent			Ni Gradient		P Gradient		Atomic Percent		
			$\%Ni_{Sch}$	$\%Ni_{\alpha}$	$\%P_{\alpha}$	Length (μm)	Wt.%Ni	Length (μm)	Wt.%P	$\%Ni_{Sch}$	$\%Ni_{\alpha}$	$\%P_{\alpha}$
772	10	[α-Ph-α-Ph-α, 3.6 mm]										
		Massive schreibersite, 650 μm traverse										
		Enter	19.3	2.8	0.07	800	5.8	500	0.14	16.5	2.7	0.13
		Exit	19.3	2.8	0.07	250	4.7	250	0.10	16.5	2.7	0.13
		Massive schreibersite, 600 μm traverse										
		Enter	19.7	2.8	0.07	250	4.7	250	0.10	16.8	2.7	0.13
		Exit	19.7	2.8	0.07	80	5.8	600	0.15	16.8	2.7	0.13
772	11	[α-Ph-α, 2.3 mm]										
		Grain boundary schreibersite, 400x450 μm										
		Enter	28.0	3.7	0.06	1400	6.9	1000	0.11	24.0	3.5	0.11
		Exit	28.0	3.9	0.06	500	6.3	300	0.12	24.0	3.7	0.11
772	12	[α-Ph, 750 μm]										
		Grain boundary schreibersite, 70 μm traverse										
		Enter	36.2	4.6	0.05	500	7.2	500	0.09	31.2	4.4	0.09
		Stop	36.2							31.2		
772	13	[α-Ph-γ-α, 1.4 mm]										
		Taenite border schreibersite, 15x20 μm										
		α-border	47.0	6.0	0.03	200	7.4	200	0.07	40.7	5.7	0.05
		γ-border	47.5							41.1		

dites appear to increase in number per unit area for the first few hundred microns away from the clear kamacite. As distance increases further, there appears to be a slight increase in both concentration and coarseness of microrhabdites. Coarser microrhabdites are occasionally associated with subgrain boundaries within the kamacite. There are also occasional aligned microrhabdites, as if they had precipitated along Neumann bands that are no longer present. Rare lamellar schreibersites 2 μm or less in width and as long as 200 μm are present. Near the outer edge of the swathing zone occasional segments of grain boundary type schreibersite protrude into the swathing kamacite or are observed enclosed within it. Four areas that contain residual taenite as well as associated schreibersite were observed within the two swathing zones (Figure 8), and close to their exterior borders.

The swathing zone boundary has suffered severe terrestrial weathering and now contains secondary iron oxides that have penetrated into the adjoining kamacite. Remnant grain boundary schreibersite is present, but it is encased in oxides precluding interface measurements. The amount of remnant schreibersite suggests that originally as much as 50% of the length of the grain boundary may have been occupied by schreibersite. A Ni determination on one of these schreibersites gave a value of 29%.

Section 1618 is from an area of the large section containing coarse-structured Widmanstätten pattern (Figure 8). Parts of four kamacite grains 4 to 5 mm wide are present. The general metallography of the section is similar to that described for Ballinger, with the exception that only microrhabdites are present within kamacite areas. Measurements described below were made along a 1.5 mm grain boundary containing taenite and taenite-plessite areas in sequence with grain boundary schreibersite.

1618, traverse 7: combines data from three short (350 μm) traverses perpendicular to the long direction of a single grain boundary schreibersite. It measured 170 μm in length and was separated from taenite by 10 to 20 μm at either end. Measurements were made near the two ends and in the middle of the schreibersite. The interface profile for the center traverse is given in Figure 9.

1618, traverse 8: crossed 200 μm of kamacite, 10 μm of schreibersite, 15 μm of taenite, and 170 μm of kamacite. This taenite border schreibersite was embedded in the taenite lamella at one end of the schreibersite in traverse 7, approximately 200 μm away. The schreibersite interface profile is given in Figure 9.

1618, traverse 9: crossed 200 μm of kamacite, 15 μm of schreibersite, 25 μm of taenite, and 120 μm of kamacite. The location was 200 μm farther along the same taenite measured in traverse 8.

Section 772 is from a separate small specimen of the Santa Luzia meteorite. It combines both the swathing kamacite and Widmanstätten pattern

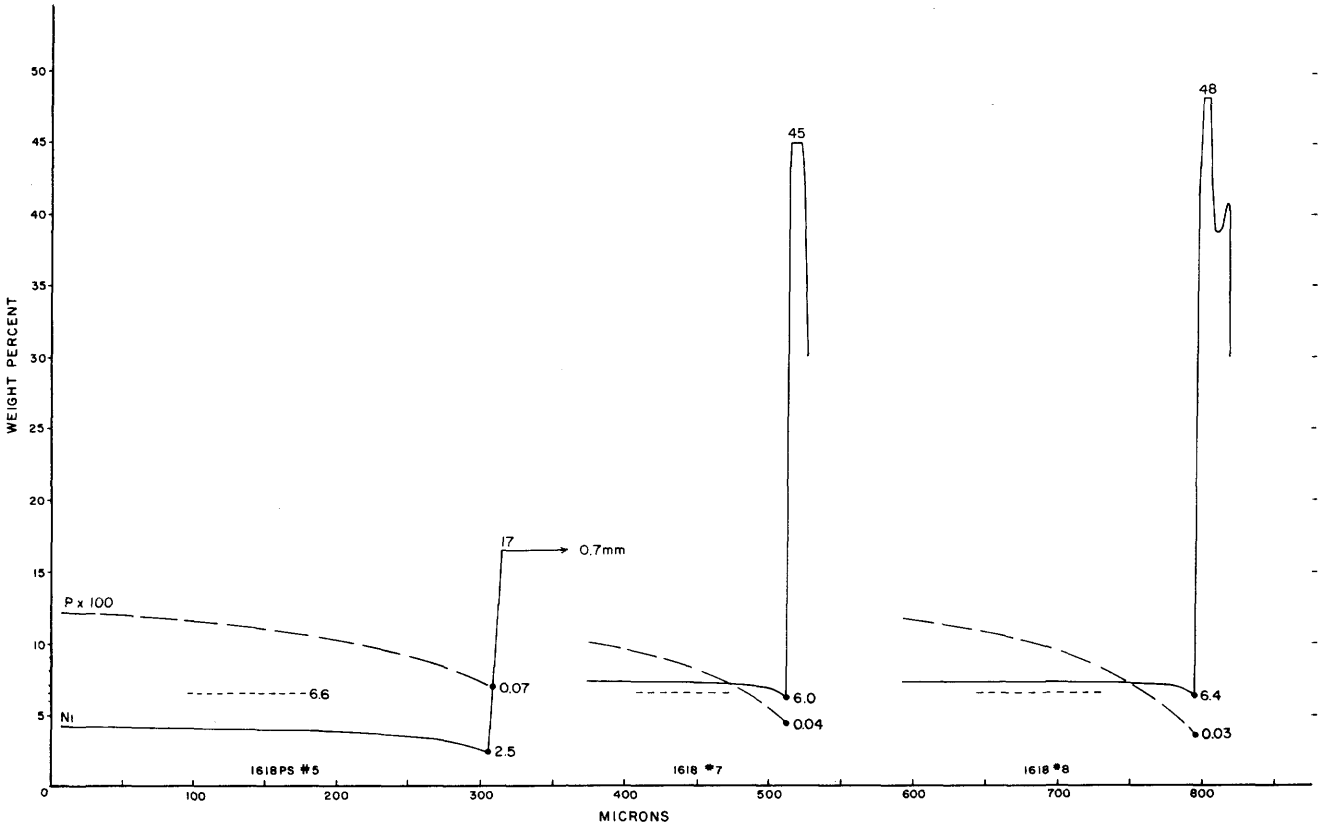

FIGURE 9.—Ni and P profiles at kamacite-schreibersite interfaces in Santa Luzia meteorite, USNM 1618: traverses 5, 7, and 8 as indicated.

areas measured above on separate sections in one microprobe section of 2 cm^2. Figure 10 is a scale drawing indicating the areas of interest. A massive schreibersite approximately 7 mm in length is surrounded by clear kamacite that in turn is enclosed in microrhabdite-containing kamacite. A major grain boundary containing grain boundary schreibersite is within 3 mm of one end of the massive schreibersite. Leading off of that grain boundary is another that contains taenite as well as grain boundary schreibersite, within 6 mm of the massive schreibersite. Measurements have been made in these areas as indicated in Figure 10.

772, traverse 10: crossed 0.9 mm of kamacite, 0.6 mm of massive schreibersite, 0.6 mm of kamacite, 0.6 mm of massive schreibersite, and 0.9 mm of kamacite. Part of this traverse including the first kamacite-schreibersite interface is given in Figure 11.

772, traverse 11: crossed 1.4 mm of kamacite, 0.4 mm of grain boundary schreibersite, and 0.5 mm of kamacite. The kamacite-schreibersite interface on leaving the schreibersite is given in Figure 11.

772, traverse 12: crossed 0.7 mm of kamacite and 50 μm of schreibersite. The Ni and P profiles are reproduced in Figure 11.

772, traverse 13: crossed a taenite boundary schreibersite (see inset in Figure 10). The major features of this traverse are given in Figure 11.

The data on the Santa Luzia meteorite may be of particular significance from the standpoint of classification considerations. The schreibersite relationships observed for the large swathing zones and their included schreibersite are in many ways similar to the Bellsbank meteorite. The schreibersite relationships in the Widmanstätten areas of Santa Luzia are similar to those observed in Ballinger. Could the differences in these two structures (Figures 6, 7) be due primarily to differences in initial P concentration?

LEXINGTON COUNTY

The Lexington County, South Carolina, meteorite is a coarse octahedrite of intermediate Ni

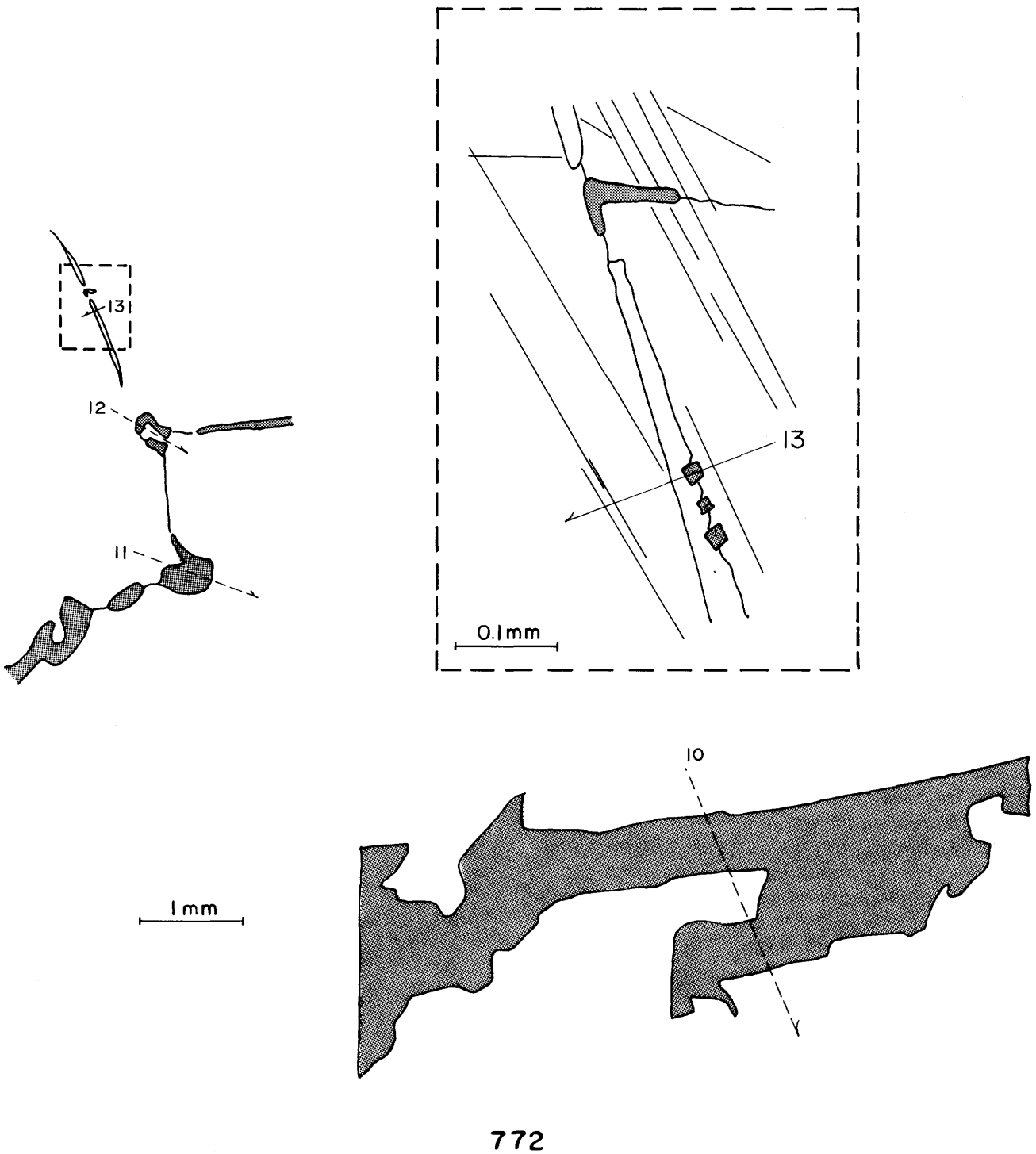

FIGURE 10.—Scale drawing of schreibersites in an area of Santa Luzia meteorite section, USNM 772 (location of electron microprobe traverses indicated; traverse 13 is of a taenite border schreibersite, indicated in more detail in the inset).

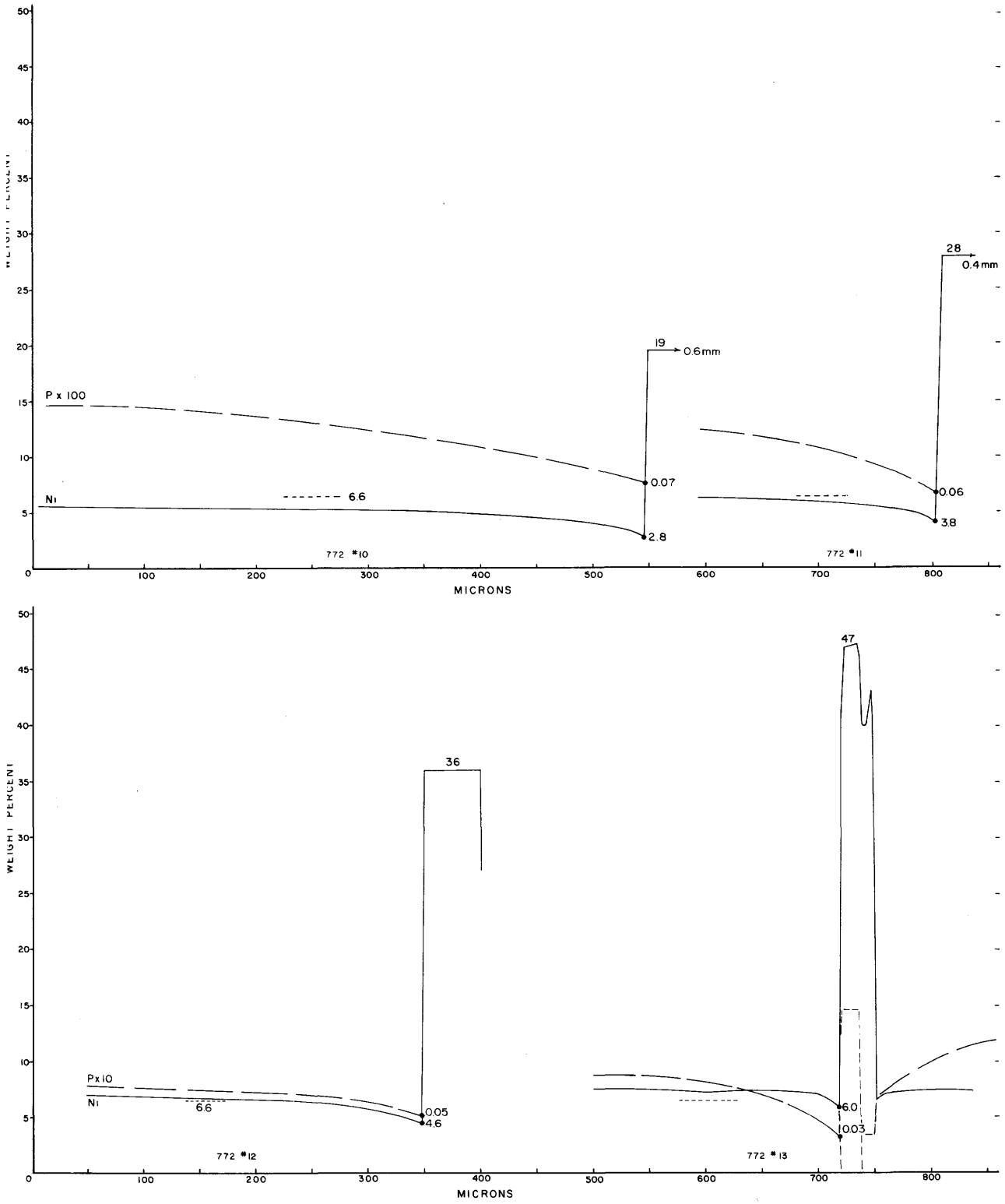

FIGURE 11.—Ni and P profiles at kamacite-schreibersite interfaces in Santa Luzia meteorite, USNM 772: traverses 10 through 13 as indicated. (Dashed line indicates bulk Ni value.)

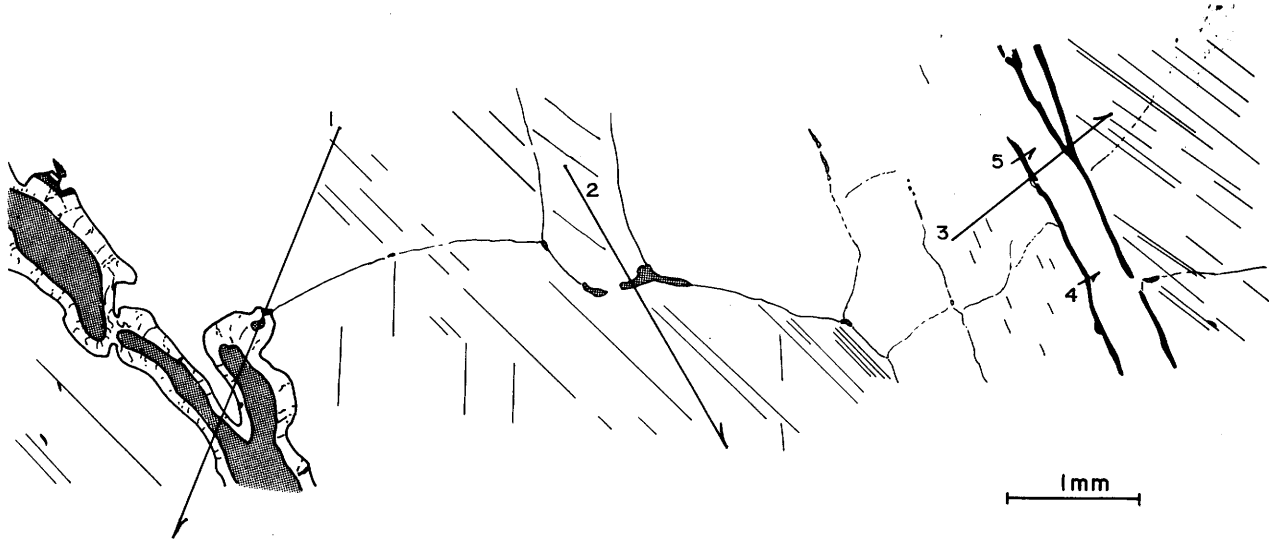

FIGURE 12.—Sketch of Lexington County section, USNM 3334, prepared from photomosaic of area studied (arrows, electron microprobe traverses; large structure at left, massive schreibersite surrounded by cohenite; subgrain boundaries, grain boundary schreibersites, taenite, and taenite border schreibersite are indicated).

content. Polished and etched surfaces reveal large areas of well-developed Widmanstätten pattern. The kamacite of these areas contains rhabdites of various sizes, grain boundary schreibersites, grain boundary and residual taenite and plessite, and Neumann bands. Oxidation has severely penetrated the exterior surface of the specimen and invaded the interior of the meteorite along major grain boundaries. Occasional skeletal schreibersites in the millimeter size range are present, normally completely surrounded by cohenite. These large schreibersites tend to be surrounded by areas of swathing kamacite that interrupt the regularity of the Widmanstätten pattern. Isolated patches of cohenite are also present.

Section 3334 contains a typical Lexington County Widmanstätten pattern area and a large schreibersite surrounded by cohenite (6 × 0.3 mm). Edges of the section and major grain boundaries have been invaded by oxidation, but the areas selected for microprobe analysis appear fresh. The paths of the traverses listed below are indicated in Figure 12 and numerical data are given in Table 6.

3334, traverse 1: crossed 1.4 mm of kamacite, a 30 μm schreibersite partially embedded in cohenite at a cohenite-kamacite interface, 60 μm of cohenite, 90 μm of schreibersite embedded in cohenite, 0.3 mm of cohenite, 0.2 mm of massive schreibersite, 0.1 mm of cohenite, 0.2 mm of kamacite, 50 μm of cohenite, 0.2 mm of massive schreibersite, 80 μm of cohenite, and 0.8 mm of kamacite.

3334, traverse 2: crossed 1.0 mm of kamacite, 50 μm of a large grain boundary schreibersite, and 1.5 mm of kamacite.

3334, traverse 3: crossed 0.8 mm of kamacite, a 15 μm wide taenite border schreibersite, 25 μm of taenite, 0.3 mm of kamacite, a 15 μm wide schreibersite in sequence with taenite, 10 μm of kamacite, a 40 μm taenite, and 0.4 mm of kamacite. The data for an abbreviated section of this traverse are given in Figure 3.

3334, traverse 4: crossed 0.1 mm of kamacite, a 10 μm wide taenite border schreibersite, 25 μm of taenite, and 50 μm of kamacite.

3334, traverse 5: crossed 50 μm of kamacite, a 5 μm wide taenite-border schreibersite, 20 μm of taenite, and 60 μm of kamacite.

Figure 12 is a tracing of a photomosaic of the studied area in Lexington County, section 3334. The path of the traverses, the phases crossed, and the nature of the structure are indicated diagrammatically. This section illustrates a general problem encountered in obtaining kamacite-schreibersite interface data in the more carbon-rich coarse-structured octahedrites. The large, low-Ni schreibersites in these meteorites are frequently completely surrounded by cohenite. Their Ni values may be determined, but kamacite interfaces are not present. Traverse 1, however, illustrates an interesting schreibersite-cohenite relationship that will be observed later in other meteorites. Cohenite borders around large schreibersites occasionally include small schreibersites, and more frequently have small schreibersites at cohenite-kamacite in-

TABLE 6.—Lexington County schreibersite-kamacite interface measurements

Specimen No.	Traverse No.	Structure traversed & schreibersites measured	Weight Percent			Ni Gradient		P Gradient		Atomic Percent		
			$\%Ni_{Sch}$	$\%Ni_{\alpha}$	$\%P_{\alpha}$	Length (μm)	Wt.%Ni	Length (μm)	Wt.%P	$\%Ni_{Sch}$	$\%Ni_{\alpha}$	$\%P_{\alpha}$
3334	1	[α-Ph-cohenite-Ph-cohenite-Ph-cohenite-α-cohenite-Ph-cohenite-α, 3.5 mm]										
		Schreibersite embedded in cohenite at α-interface, 25x120 μm	34.8	4.4	0.04	150	6.0	200	0.07	29.9	4.2	0.07
		Schreibersite embedded in cohenite, 140x280 μm										
		Enter	33.0							28.3		
		Exit	32.5							27.9		
		Massive schreibersite surrounded by cohenite (6x0.3 mm), 200 μm traverse										
		Enter	25.0							21.4		
		Exit	24.6							21.1		
		Massive schreibersite surrounded by cohenite (6x0.3 mm), 170 μm traverse										
		Enter	24.1							20.6		
		Exit	24.1							20.6		
3334	2	[α-Ph-α, 2.5 mm]										
		Grain boundary schreibersite, 500x40 μm	39.3	5.0	0.04	300	7.0	200	0.06	33.9	4.8	0.07
3334	3	[α-Ph-γ-α-Ph-α-γ-α, 1.6 mm]										
		Taenite border schreibersite, 15x40 μm	50.0	6.0	0.03	50	7.2	150	0.06	43.3	5.7	0.05
		Schreibersite near taenite, 10x20 μm	52.5	6.2	0.03	50	7.4	100	0.05	45.6	5.9	0.05
3334	4	[α-Ph-γ-α, 200 μm]										
		Taenite border schreibersite, 5x10 μm	50.5	6.2	0.03	50	7.3	50	0.05	43.6	5.9	0.05
3334	5	[α-Ph-γ-α, 140 μm]										
		Taenite border schreibersite, 5x10 μm	51.0	6.3	0.03	30	7.4	30	0.05	44.2	6.0	0.05

terfaces. The Ni values in these schreibersites increase away from the large schreibersite. In this case, the large schreibersite contains approximately 25% Ni, the small one completely embedded in cohenite has an apparent Ni gradient from 32.5% to 33.0% increasing in the direction toward kamacite, and the kamacite interface schreibersite contains 35% Ni. The measurements in Table 6 are otherwise comparable to those reported above for similar structures.

BAHJOI

The Bahjoi, India, meteorite is an observed fall of 1934, the only one included in this study. It is a typical Group I meteorite of above average Ni content. Bahjoi contains complex silicate-troilite-graphite-chromite nodules surrounded by rims of schreibersite, and, in turn, cohenite. Grain boundary schreibersites, rhabdites of various sizes, and taenite border schreibersites are present. Taenite and plessite are present in greater abundance than in the previously examined meteorites, and pearlitic and martensitic forms are common. An area of the carbide haxonite was observed within a pearlitic plessite area.

Section 1807(Sil) contains part of a complex silicate-containing inclusion surrounded by schreibersite and cohenite, and small areas of kamacite.

1807(Sil), traverse 1: started within the complex inclusion, crossing first an island of kamacite surrounded by cohenite. The phases in sequence were: 0.1 mm of cohenite, 0.2 mm of kamacite, 0.1 mm of cohenite, 1.5 mm of schreibersite, 0.5 mm of cohenite, 0.1 mm of schreibersite containing a slight Ni gradient, and finally 1.0 mm of kamacite. The central part of this traverse is illustrated in Figure 13 and the data is given in Table 7.

Section 1807 is of a typical Widmanstätten area of Bahjoi, free of large inclusions. Rhabdites, grain boundary schreibersites, and taenite border schreibersites are present in abundance. Many taenite-plessite areas are present in a variety of morphologies. One of these martensitic areas contains a 0.1 × 0.1 mm area of haxonite.

1807, traverse 2: crossed 30 μm of grain boundary schreibersite, 0.7 mm of kamacite, a 15 μm wide taenite border schreibersite, 20 μm of taenite, and 10 μm of kamacite.

The observations made on the Bahjoi meteorite

TABLE 7.—Bahjoi schreibersite-kamacite interface measurements

Specimen No.	Traverse No.	Structure traversed & schreibersites measured	Weight Percent			Ni Gradient		P Gradient		Atomic Percent		
			$\%Ni_{Sch}$	$\%Ni_{\alpha}$	$\%P_{\alpha}$	Length (μm)	Wt.%Ni	Length (μm)	Wt.%P	$\%Ni_{Sch}$	$\%Ni_{\alpha}$	$\%P_{\alpha}$
1807(Si1)	1	[Cohenite-α-cohenite-Ph-cohenite-Ph-α, 3.5 mm]										
		Massive schreibersite, 10x4 mm, surrounded by cohenite and containing ~30% silicate										
		Enter	18.8							16.0		
		Exit	18.9							16.1		
		Schreibersite 100 μm wide embedded in cohenite at α-border										
		Enter	32.3							27.7		
		Exit	33.5	4.2	0.04	600	6.5	200	0.06	28.8		
1807	2	[Ph-α-Ph-α, 750 μm]										
		Grain-boundary schreibersite, 35x250 μm	38.8	5.2	0.04	150	7.2	150	0.06	33.4	5.0	0.07
		Taenite-border schreibersite, 20x60 μm	49.0	6.2	0.03	30	6.2	100	0.06	42.4	5.9	0.05

are mainly similar in character to examples previously described. Figure 13 is a composition profile based on data from a part of traverse 1. Part of the massive schreibersite and its cohenite border are included. Ni values are low in cohenite and increase slightly upon moving away from the large schreibersite. The small exterior schreibersite is enclosed on three sides by cohenite and contains a measurable Ni gradient. This type of association is common in high C Group I meteorites.

GOOSE LAKE

The Goose Lake, California, meteorite is a high Ni member of Group I with a medium octahedrite structure. Polished and etched surfaces reveal many large cohenite bordered, skeletal schreibersite inclusions, and occasional complex silicate-troilite-graphite-schreibersite-cohenite associations. The cohenite has undergone partial decomposition to kamacite and graphite. Grain boundary schreibersites, rhabdites in a range of sizes, and taenite border schreibersites are present. Taenite-plessite areas are more abundant than in the meteorites examined previously and are present in a variety of forms. Weathering has invaded the structure along grain boundaries and is present in cracks within the large schreibersites.

Section 1332 is dominated by two areas of cohenite bordered schreibersite of approximately 5 × 10 mm each (photograph in Doan and Goldstein, 1969:765). One smaller cohenite-schreibersite inclusion is also present. Kamacite areas around these inclusions are comparatively free of other structures for distances up to 2 mm. Beyond this, normal Widmanstätten areas are present.

1332, traverse 1: began at the border of a taenite area, crossed 2.4 mm of kamacite, and entered a 30 μm wide grain boundary schreibersite near its contact with a taenite border of a plessite area. Numerical data for this and succeeding Goose Lake traverses are given in Table 8.

1332, traverse 2: crossed 430 μm of kamacite, 50 μm of schreibersite embedded in a cohenite rim of a large schreibersite, 90 μm of cohenite, 0.2 mm of schreibersite, 50 μm of cohenite, and 0.9 mm of kamacite.

1332, traverse 3: began by crossing a 40 μm wide schreibersite associated with a taenite-plessite area, crossed 2.5 mm of kamacite, entered a 40 μm wide schreibersite embayed in cohenite, 150 μm of cohenite, and 0.3 mm of massive schreibersite.

1332, traverse 4: started near the initial point of traverse 3 within the taenite border, crossed 0.2 mm of kamacite, a 50 μm wide grain boundary schreibersite, and 0.7 mm of kamacite.

Section 1332(2) is similar to number 1332 in that it also contains a 5 × 10 mm skeletal schreibersite-cohenite area. This section contains an unusually large schreibersite that is only partially surrounded by cohenite, thus permitting kamacite-schreibersite interface measurements. Its longest dimension is 1.4 mm and has a maximum thickness of 0.6 mm. Morphology suggests that it is an unusually large grain boundary schreibersite rather than a massive schreibersite of the skeletal variety. The areas away from these inclusions contained normal Widmanstätten pattern.

1332(2), traverse 5: crossed 0.1 mm of kamacite, 0.1 mm cohenite, 1.8 mm of massive schreibersite, 170 μm cohenite, 2.1 mm of kamacite, 20 μm of cohenite, 0.1 mm of large grain boundary schreibersite, and 0.8 mm kamacite.

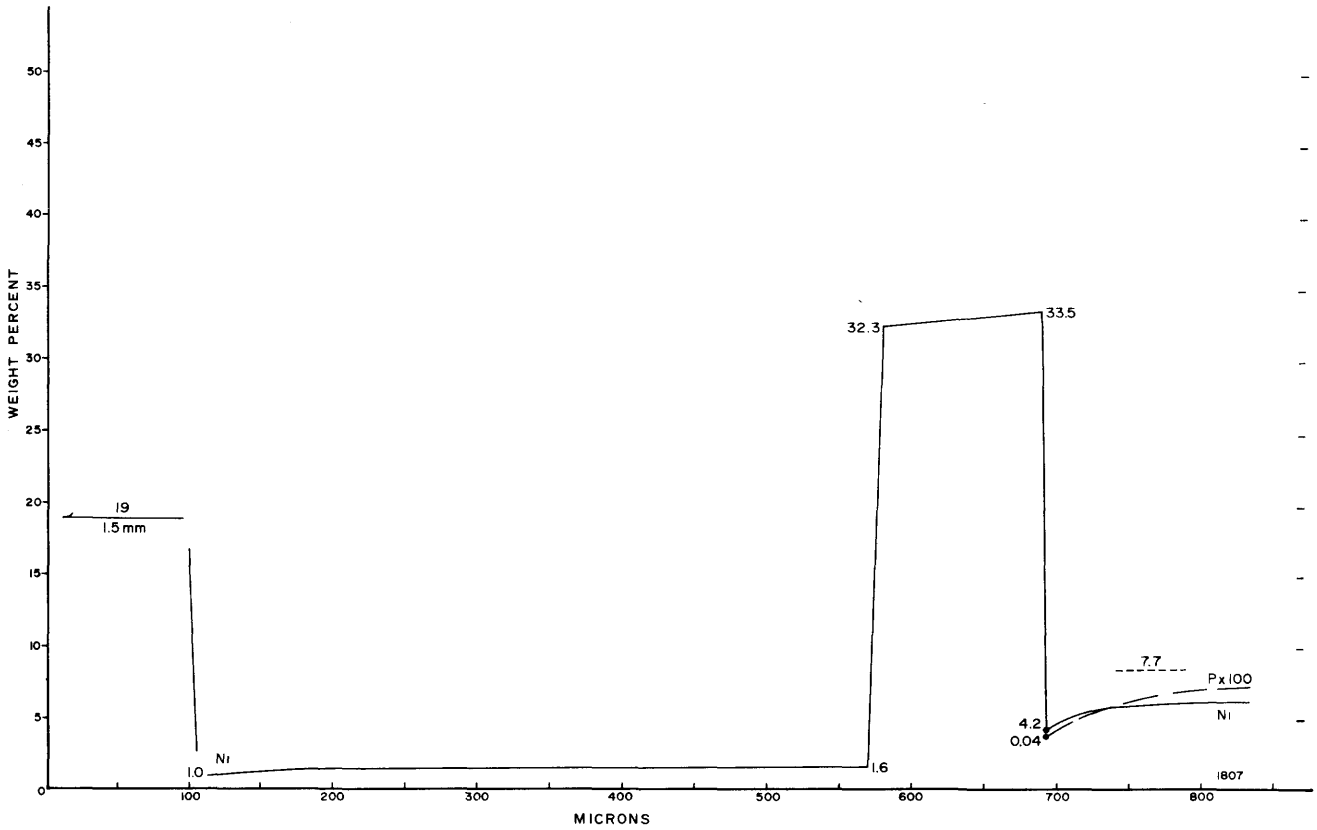

FIGURE 13.—Ni and P profile for Bahjoi meteorite, USNM 1807: left, massive schreibersite bordered by cohenite; right, small schreibersite partially enclosed in cohenite, but also with an edge in contact with kamacite.

1332(2), traverse 6: crossed 0.4 mm of kamacite, 25 μm of cohenite, 1.2 mm of schreibersite containing a small Ni gradient over part of its distance, and 0.5 mm of kamacite. This traverse crosses the length of the large schreibersite in number 5.

1332(2), traverse 7: crossed 40 μm tip of large schreibersite, 1.2 mm of kamacite, 0.2 mm of second tip of same schreibersite, and 0.4 mm of kamacite. This is the same large schreibersite traversed in numbers 5 and 6.

1332(2), traverse 8: crossed 0.5 mm of kamacite, 150 μm of the third tip of the large schreibersite measured in traverses 5 through 7, and 0.5 mm of kamacite.

1332(2), traverse 9: crossed 0.4 mm of kamacite, 150 μm of a small schreibersite near the large schreibersite in traverses 5 through 8, and 0.3 mm of schreibersite.

1332(2), traverse 10: crossed 0.2 mm of kamacite, 30μm of a grain boundary schreibersite, and 0.2 mm of kamacite.

1332(2), traverse 11: crossed 0.3 mm of massive schreibersite close to traverse number 5, 0.1 mm of cohenite, a 20 μm wide schreibersite embedded in cohenite, 0.1 mm of kamacite, and 50 μm of cohenite.

The associations measured in Goose Lake are similar in character to those described above for other meteorites. The schreibersite precipitates in this case, however, exist in an environment that is more Ni-rich.

BALFOUR DOWNS

The Balfour Downs, Western Australia, meteorite is one of the highest Ni members of Group I. The first prepared surface of this specimen was perpendicular to the one shown in Figure 14, along its bottom edge. This area of approximately 12 cm^2 was free of large inclusions, having the regular structure of the upper right-hand area in Figure 14. On the basis of this casual observation, Balfour Downs was assumed to be a low P medium octahedrite. Actually, it contains localized massive schreibersite enclosing significant quantities of silicates. These schreibersites are normally enclosed in cohenite and surrounded by swathing kamacite areas that interrupt the regular Widmanstätten

TABLE 8.—Goose Lake schreibersite-kamacite interface measurements

Specimen No.	Traverse No.	Structure traversed & schreibersites measured	Weight Percent			Ni Gradient		P Gradient		Atomic Percent		
			$\%Ni_{Sch}$	$\%Ni_{\alpha}$	$\%P_{\alpha}$	Length (μm)	Wt.%Ni	Length (μm)	Wt.%P	$\%Ni_{Sch}$	$\%Ni_{\alpha}$	$\%P_{\alpha}$
1332	1	[γ-α-Ph-γ, 2.4 mm]										
		Schreibersite at γ-border, 25 μm wide	52.0	6.0	0.03	25	7.2	100	0.07	45.1	5.7	0.05
1332	2	[α-Ph-cohenite-Ph-cohenite-α, 1.6 mm]										
		Schreibersite embaying cohenite, 55 μm traverse										
		Enter	35.0	4.1	0.05	100	6.4	50	0.06	30.1	3.9	0.09
		Exit	34.0							29.2		
		Massive schreibersite enclosed in cohenite (3.4x0.2 mm), 260 μm traverse	25.0							21.4		
1332	3	[Ph-α-Ph-cohenite-Ph, 3.1 mm]										
		Schreibersite near taenite, 40x70 μm	46.5	6.0	0.04	50	7.0	100	0.07	40.2	5.7	0.07
		Schreibersite embaying cohenite, 30x50 μm	36.5	4.3	0.05	150	5.7	200	0.08	31.4	4.1	0.09
		Massive schreibersite (6x2 mm), 300 μm traverse	18.5							15.8		
1332	4	[γ-α-Ph-α, 950 μm]										
		Grain boundary schreibersite (60x250 μm), 60 μm traverse	41.0	5.1	0.05	100	7.2	Flat	0.05	35.4	4.9	0.09
1332(2)	5	[α-cohenite-Ph-cohenite-α-cohenite-Ph-α, 5.3 mm]										
		Cohenite bordered massive schreibersite (2x6 mm), 1.8 mm traverse										
		Enter	18.7							15.9		
		Middle	18.2							15.5		
		Exit	18.5							15.8		
		Large schreibersite with partial cohenite border (1.4x0.6 mm), 100 μm traverse	31.3	3.8	0.06	200	5.7	100	0.08	26.9	3.6	0.11
1332(2)	6	[α-cohenite-Ph-α, 2.2 mm]										
		Large schreibersite with partial cohenite border (1.4x0.6 mm), 1.2 mm traverse										
		Enter	29.3							25.1		
		Middle	27.3							23.4		
		Exit	27.3	3.6	0.07	500	5.8	250	0.09	23.4	3.4	0.13
1332(2)	7	[Ph-α-Ph-α, 1.8 mm]										
		Large schreibersite of traverses 5 and 6										
		40 μm traverse	31.0	3.9	0.06	400	6.0	200	0.08	26.6	3.7	0.11
		200 μm traverse										
		Enter	27.0	3.3	0.06	600	6.2	150	0.08	23.1	3.1	0.11
		Exit	27.0	3.5	0.06	300	6.8	150	0.09	23.1	3.3	0.11
1332(2)	8	[α-Ph-α, 1.2 mm]										
		Large schreibersite of traverses 5-7, 150 μm traverse										
		Enter	29.1	3.7	0.06	500	6.5	150	0.09	25.0	3.5	0.11
		Exit	29.1	3.8	0.06	400	6.5	150	0.08	25.0	3.6	0.11
1332(2)	9	[α-Ph-α, 0.9 mm]										
		Small schreibersite near traverses 5-8 (250x400 μm), 150 μm										
		Enter	27.2	3.1	0.06	300	6.0	100	0.07	23.3	3.0	0.13
		Exit	27.2	3.6	0.06	250	5.5	100	0.07	23.3	3.4	0.13
1332(2)	10	[α-Ph-α, 0.5 mm]										
		Grain boundary schreibersite (0.03x1.6 mm) associated with plessite, 30 μm traverse	44.0	5.8	0.05	100	7.4	200	0.06	38.0	5.5	0.09
1332(2)	11	[Ph-cohenite-Ph-α-cohenite, 0.7 mm]										
		Massive schreibersite (same as traverse 5), 0.4 mm traverse										
		Start	18.3							15.6		
		Exit	18.3							15.6		
		Schreibersite (20x60 μm) embedded in cohenite-α border	37.3	4.5	0.06	150	6.0	100	0.09	32.1	4.3	0.11

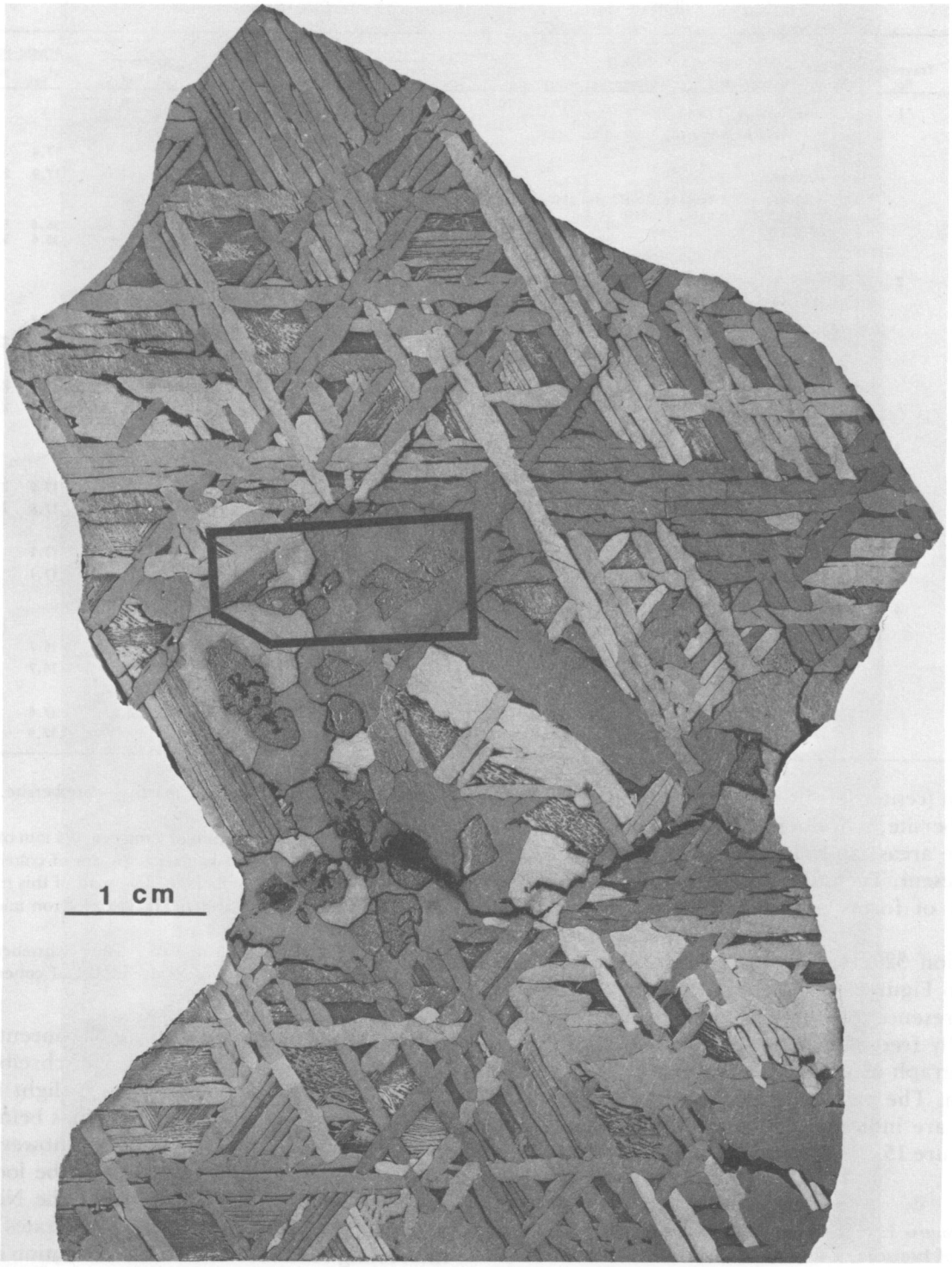

FIGURE 14.—Etched surface of Balfour Downs meteorite, USNM 3202: left-hand side of the slice, large schreibersites, several containing silicates; (outlined area indicates polished section that was prepared for detailed study).

TABLE 9.—Balfour Downs schreibersite-kamacite interface measurements

Specimen No.	Traverse No.	Structure traversed & schreibersites measured	Weight Percent			Ni Gradient		P Gradient		Atomic Percent		
			$\%Ni_{Sch}$	$\%Ni_{\alpha}$	$\%P_{\alpha}$	Length (μm)	Wt.%Ni	Length (μm)	Wt.%P	$\%Ni_{Sch}$	$\%Ni_{\alpha}$	$\%P_{\alpha}$
3202	1	[Ph-α-Ph-α-Ph-γ, 3.3mm]										
		Massive schreibersite, 1550 μm traverse										
		Start	20.5							17.5		
		Exit	21.0	2.9	0.05	1150	6.7	200	0.09	17.9	2.8	0.09
		Residual schreibersite 30x800 μm, associated with taenite, crossed at two locations	41.0	5.3	0.04	100	6.8	100	0.09	35.4	5.1	0.07
			41.0	5.5	0.03	50	6.8	--	--	35.4	5.2	0.05
3202	2	[Ph-α-Ph-α, 3.1 mm]										
		Massive schreibersite, 600 μm traverse										
		Start	21.3							18.2		
		Exit	21.5	2.6	0.05	300	4.8	300	0.09	18.4	2.5	0.09
		Massive schreibersite, 500 μm traverse										
		Enter	21.5	2.8	0.05	250	4.8	200	0.09	18.4	2.7	0.09
		Exit	21.5	3.0	0.05	1500	7.0	300	0.11	18.4	2.9	0.09
3202	3	[α-Ph-α-cohenite-Ph, 2.3 mm]										
		Massive schreibersite, 400 μm traverse										
		Enter	21.0	2.9	0.05	250	5.3	200	0.10	17.9	2.7	0.09
		Exit	21.0	2.8	0.05	150	4.8	150	0.08	17.9	2.7	0.09
		Massive schreibersite, 1350 μm traverse										
		Enter	20.0							17.1		
		End	20.0							17.1		
3202	4	[Ph-cohenite-α-cohenite-Ph, 2.1 mm]										
		Massive schreibersite, 800 μm traverse										
		Start	19.5							16.7		
		Exit	19.5							16.7		
		Massive schreibersite, 250 μm traverse										
		Enter	20.5							17.5		
		Stop	21.0							17.9		

pattern (center left in Figure 14). Grain boundary schreibersite, schreibersite associated with taenite-plessite areas, and rhabdites in a variety of sizes are present. Taenite-plessite areas are present in a variety of forms and Neumann bands are common.

Section 3202 was prepared from the outlined area in Figure 14. It was selected particularly for the presence of massive schreibersite that was partially free of cohenite borders. Figure 15 is a photograph of a photomosaic of a portion of this section. The paths of the four traverses described below are indicated in Figure 16, a sketch based on Figure 15.

3202, traverse 1: crossed 1.5 mm of massive schreibersite, 4.5 mm of kamacite, a 40 μm wide schreibersite surrounding a taenite area, 0.1 mm of kamacite, recrossed a 30 μm width of the same schreibersite previously crossed, 50 μm of kamacite, and 50 μm of taenite. Numerical data for this and succeeding Balfour Downs traverses are given in Table 9.

3202, traverse 2: crossed 0.6 mm of massive schreibersite, 0.6 mm of kamacite, 0.5 mm of massive schreibersite, and 1.5 mm of kamacite.

3202, traverse 3: crossed 0.3 mm of kamacite, 0.4 mm of massive schreibersite, 0.2 mm of kamacite, 80 μm of cohenite, and 1.3 mm of massive schreibersite. The path of this traverse is indicated in Figures 15 and 16 and the electron microprobe profile is shown in Figure 17.

3202, traverse 4: crossed 0.8 mm of massive schreibersite, 0.1 mm of cohenite, 0.8 mm of kamacite, 0.1 of cohenite, and 0.2 mm of massive schreibersite.

Also indicated in Figure 16 are Ni concentrations in various areas of the two massive schreibersites. One is tempted to conclude that a slight Ni gradient exists, with the lowest Ni values being adjacent to cohenite. The differences, however, are small, and this should undoubtedly be looked at more systematically in the future. The Ni and P profile reproduced in Figure 17 illustrates several interesting features. The Ni concentration in kamacite is low close to these large schreibersites, as are the Ni interface values. There also appears to be a Ni gradient in cohenite, with Ni increasing away from the massive schreibersite.

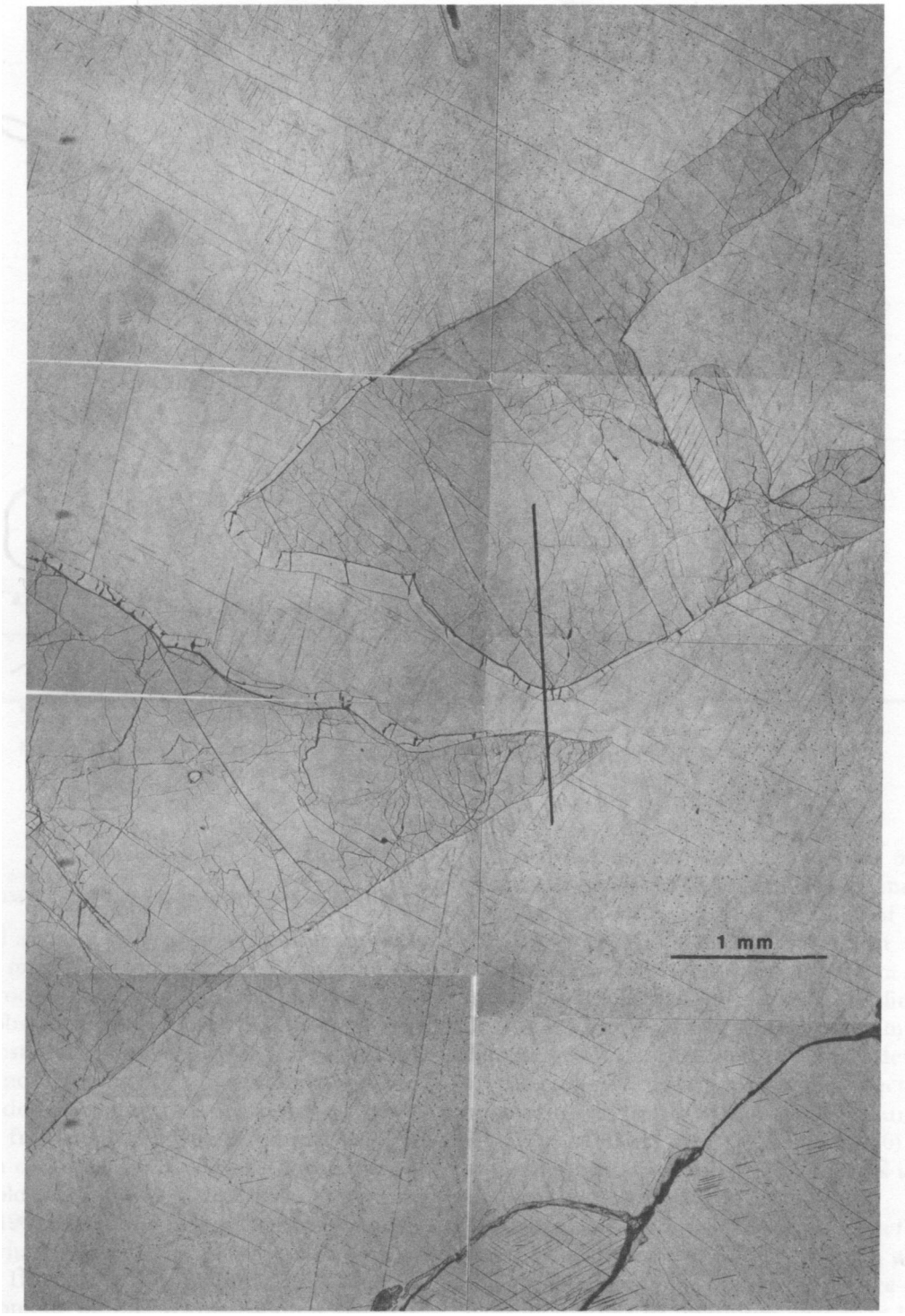

FIGURE 15.—Photograph of photomosaic of area of Balfour Downs meteorite examined, USNM 3202: large schreibersite inclusions in kamacite, partially bordered by cohenite. (Line indicates position of traverse 3; see Figure 17.)

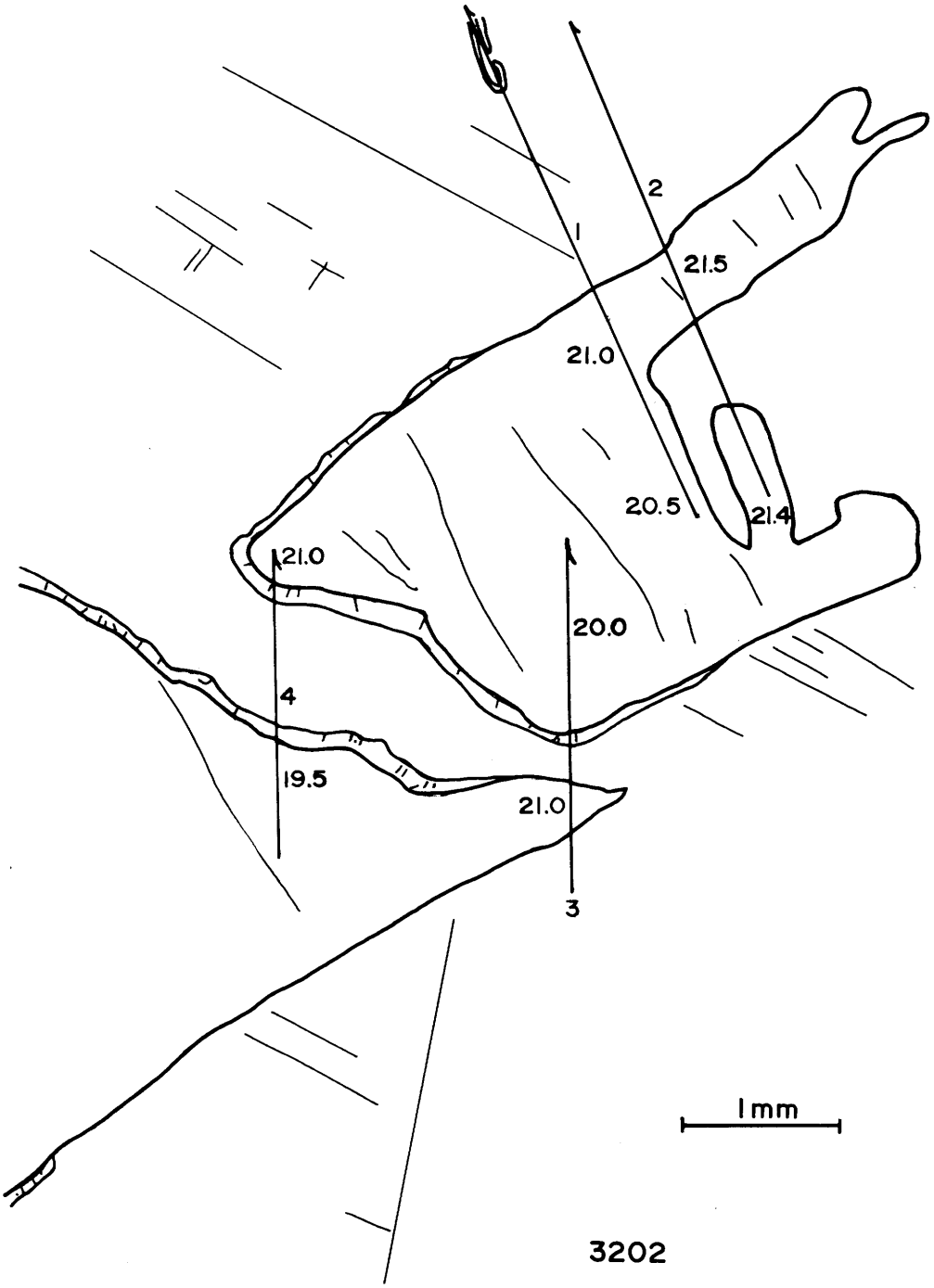

FIGURE 16.—Sketch based on Balfour Downs section illustrated in Figure 15 (arrrows indicate location of traverses; numbers give schreibersite Ni concentrations in weight percent)

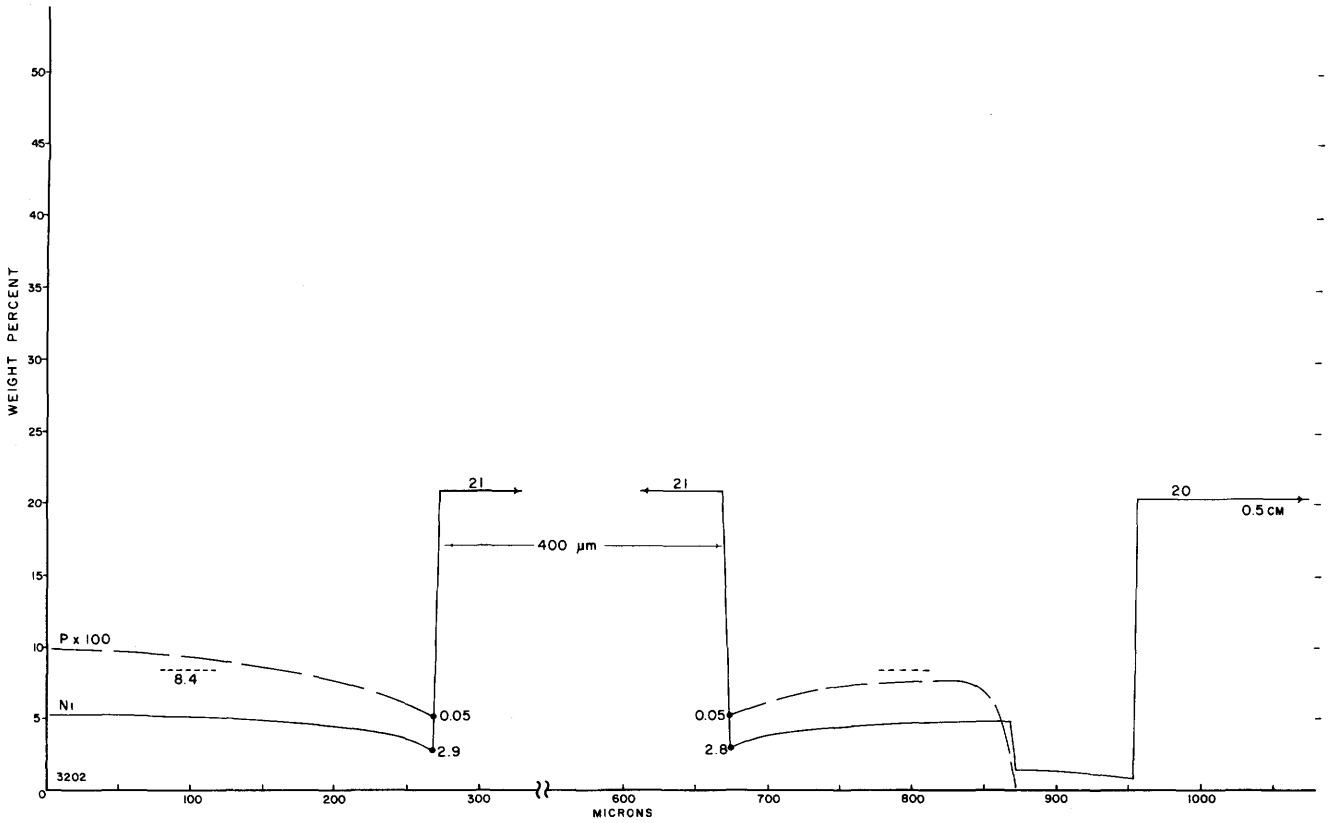

FIGURE 17.—Ni and P profiles in Balfour Downs meteorite, USNM 3202, traverse 3 in Figure 16 (schreibersite inclusion at the right enclosed in cohenite).

Discussion

Equilibrium Considerations of Phase Growth

The total amount of P present in an iron meteorite has a marked effect on the structural development process, and consequently on the final structure observed in prepared sections. Studies of Widmanstätten pattern growth (Wood, 1964; Goldstein and Ogilvie, 1965b; Goldstein and Axon, 1973) have demonstrated that octahedrite meteorites cooled from high temperatures and were in equilibrium down to 700° C. Schreibersite growth studies (Goldstein and Ogilvie, 1963; Doan and Goldstein, 1969) led to similar conclusions concerning equilibrium temperatures for iron meteorites in general. In a discussion of the effects of P on the development of the Widmanstätten pattern, Goldstein and Doan (1972) estimate that equilibrium in iron meteorites was maintained down to 650° C, and probably to 600° C. Recent work by Randich (1975) suggests the schreibersite-kamacite equilibrium is maintained down to 500° C for diffusion distances as great as 1000 μm. Previous work, therefore, suggests that many of the schreibersite precipitates observed in iron meteorites nucleated and grew under equilibrium conditions during a significant part of their cooling history. It is the purpose of this section to examine schreibersite growth and related structural development in the selected group of coarse-structured iron meteorites in terms of the equilibrium Fe-Ni-P diagram of Doan and Goldstein (1970). How far can equilibrium considerations take us in explaining observed structures?

Before proceeding, however, brief mention must be made of the effects of S, C, and Co on the Fe-Ni-P system. These elements are present in iron meteorites in quantities that may be comparable to or in excess of P. The role of S has been discussed recently by Goldstein and Axon (1973) and Wai (1974). Goldstein and Axon (1973) point out that S may be important in lowering the

temperature of metal melts, thereby mobilizing metal without melting silicates. This effect, however, would only extend down to temperatures in the range of 1000° C. At lower temperatures, material of Fe-FeS eutectic composition becomes enclosed in solidifying metal, and the solubility of S in the metallic phases becomes negligibly small. Sulfur is removed from the metal by this process, becoming isolated in complex sulfide nodules (El Goresy, 1965).

The situation with respect to carbon is much more complex. Graphite or graphite-troilite nodules present in many meteorites represent high temperature segregations of C as well as S. The petrography of these complex associations has been described by El Goresy (1965). Comparatively large amounts of C, however, remain soluble in the metal to lower temperatures, temperatures within the schreibersite growth range. Brett (1967) has discussed the occurrence of cohenite ($(Fe,Ni)_3C$) in meteorites and described its formation in terms of phase equilibria using an extrapolated Fe-Ni-C diagram. He proposed that cohenite formed within a narrow range of bulk Ni values in the temperature range of 650° to 610° C. Scott (1971a) has discussed carbides in iron meteorites in great detail from a petrographic point of view. He has also reported two new carbides, haxonite ($(Fe,Ni,Co)_{23}C_6$) (Scott, 1971b), and a phase designated W-carbide ($(Fe,Ni,Co)_{2.5}C$), both of which contain considerably more Ni and Co in their structure than is observed in cohenite. Scott (1971a) suggests that cohenite may have formed at somewhat lower temperatures than those suggested by Brett (1967). Both Scott (1971a) and Buchwald (1976) point out that cohenite is much more widely distributed in meteorites than previously realized. Cohenite and schreibersite are frequently observed in intimate association (Drake, 1970; Clarke, 1969; Buchwald, 1976), with cohenite normally encapsulating large schreibersite inclusions in the high C Group I meteorites. These schreibersite-bordering cohenites normally enclose occasional small later-formed schreibersites as has been illustrated above (Figure 13). This morphology suggests the possibility of concurrent schreibersite-cohenite growth after major amounts of schreibersite have formed. Carbon, therefore, is seen to be a component of the system of direct concern here. Experimental data on carbon's effect on the Fe-Ni-P system at low temperatures is not available, and it has been assumed that it can be ignored here except in cases where its physical presence in the form of cohenite or other carbides is important. This assumption may well require reevaluation when appropriate experimental data becomes available.

Another simplifying assumption made in this study is to ignore the presence of Co, an element present in iron meteorites in the range of 0.3% to 0.7% (Moore et al., 1969). Co distributes itself between the three phases of interest, following Fe and seemingly having little effect on the equilibria involved.

In the following sections, individual meteorites will be discussed in terms of structural development on equilibrium cooling through the low temperature portion (995° to 550° C) of the Fe-Ni-P system. The Doan and Goldstein (1970) isothermal sections were recalculated on an atom percent basis, and four of these sections plotted on a triangular coordinate system are given in Figure 18.

Equilibrium in the system at hand may be defined as (1) the phases present are homogeneous, that is to say, free of measurable concentration gradients, and (2) the compositions of individual phases are related to the bulk composition by the phase diagram. In the case at hand, this means that (a) the bulk composition is the composition of the single phase present when it lies within the kamacite (α) or taenite (γ) field of the diagram; (b) the bulk composition is on a tie line joining the compositions of the two phases present in the kamacite + schreibersite (α + Ph), the kamacite + taenite (α + γ), and the taenite + schreibersite (γ + Ph) fields of the diagram; and (c) the bulk composition is related to the three phases present by the compositions at the corners of the triangular kamacite + taenite + schreibersite (α + γ + Ph) field of the diagram. The proportions of the phases present in the two- and three-phase fields may be calculated using lever rule principles. Calculations of this type were carried out for each of the meteorite compositions considered and are presented in a series of tables to follow (Tables 10–15). Temperatures, the proportion of phases present, and their Ni contents are given. These data will be discussed for each meteorite in terms of observed structures. Selected compositions representing these meteorites are plotted on a series of isothermal sections of the iron-rich corner of

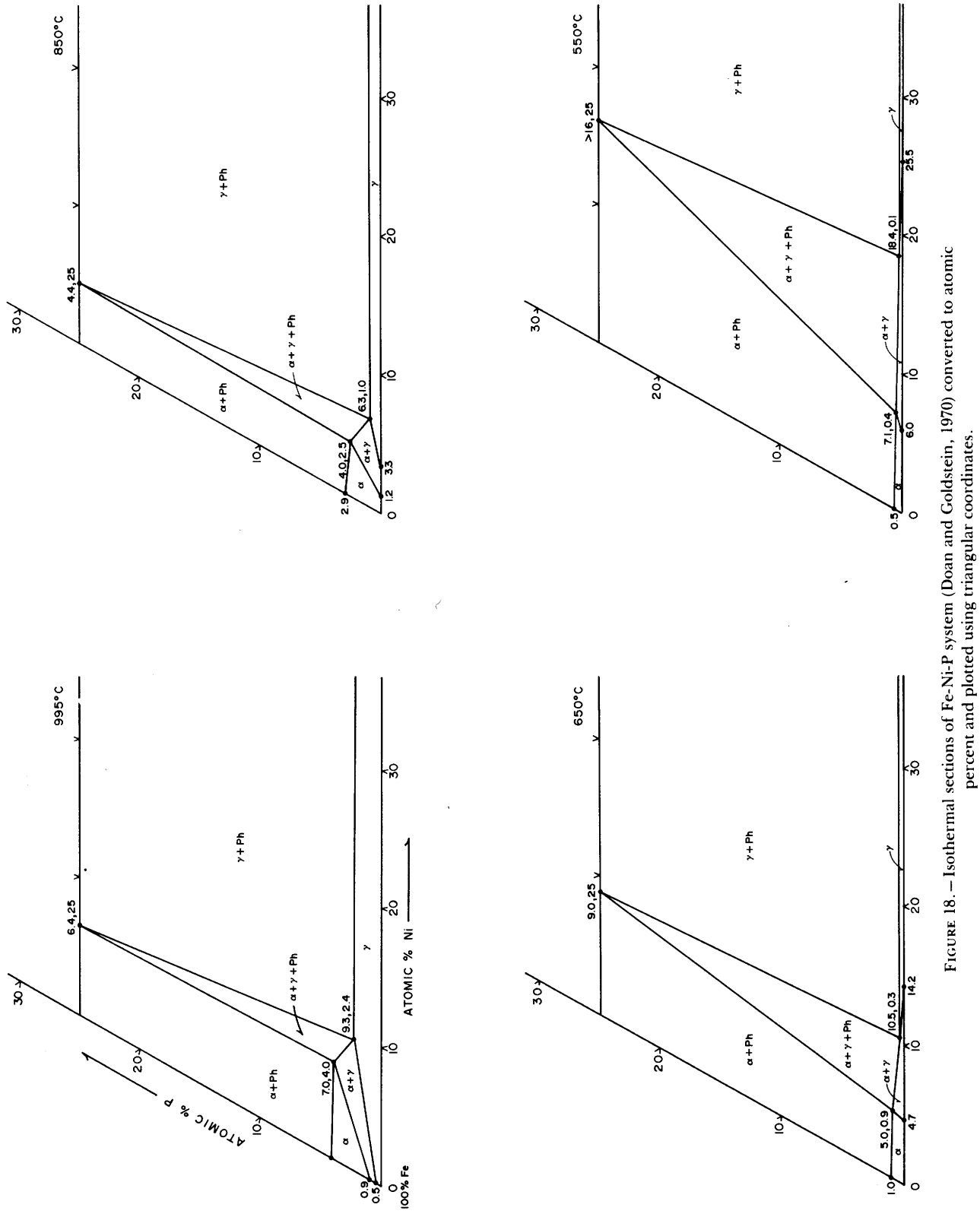

FIGURE 18.—Isothermal sections of Fe-Ni-P system (Doan and Goldstein, 1970) converted to atomic percent and plotted using triangular coordinates.

TABLE 10.—Equilibrium cooling of compositions appropriate to the Coahuila meteorite (percentage of phases present at indicated temperatures with their Ni contents)

	0.5 Atomic % P, 5.3 Atomic % Ni					
°C	%α	%γ	%Ph	%Ni_α	%Ni_γ	%Ni_{Ph}
995		100			5.3	
975		100			5.3	
925		100			5.3	
875		100			5.3	
850		100			5.3	
750	60	40		3.3	6.5	
700	75	25		4.0	9.2	
650	93	7		4.4	12	
600	99	1		5.2	14	
550	99.7		0.3	5.2		14

	1.1 Atomic % P, 5.3 Atomic % Ni					
°C	%α	%γ	%Ph	%Ni_α	%Ni_γ	%Ni_{Ph}
995		100			5.3	
975		100			5.3	
925		100			5.3	
875		100			5.3	
850	12	88		3.5	5.6	
750	50	50		3.8	6.9	
700	82	18		4.5	9.1	
650	94	5	1	5.0	11	9.0
600	98		2	5.2		13
550	98		2	5.2		13

the Fe-Ni-P system from 850° to 550° C in Figure 19.

COAHUILA.—The Coahuila hexahedrite is a meteorite of both low Ni (5.6 weight %, 5.3 atomic %) and low P (0.3 weight %, 0.5 atomic %). These bulk composition values are well established in the literature and are generally consistent with the major features of the observed structure. The presence of occasional large schreibersites as described above suggests, however, that the P value may be somewhat low. For this reason the calculations given in Table 10 were made using two P values, the literature value (0.5 atomic %) and one approximately twice as high (1.1 atomic %). The equilibrium phases present, their amounts in mole percent, and their Ni contents in atomic percent are listed in Table 10 for 10 temperatures between 995° to 550° C.

Due to Caohuila's low P (0.5 atomic %), the predicted structural development sequence using the Fe-Ni-P diagram is essentially the same as that derived using the Fe-Ni diagram. At 995° C (Table 10), taenite of the bulk meteorite composition is the only phase present, and this situation continues until the meteorite cools to below 850° C. As the temperature drops an additional 200° C, taenite transforms almost completely to massive single crystal kamacite. The last of the taenite transforms to kamacite below 600° C, in the temperature range where schreibersite first nucleates. This sequence accounts for kamacite containing homogeneously nucleated rhabdite, the most prominent feature of Caohuila. This low temperature of initial schreibersite nucleation and the small amount formed, however, make it difficult to understand the presence of the occasional larger schreibersites mentioned above.

If a somewhat higher P content is assumed, significant differences are revealed. With an assumed content of 1.1 atomic % P (Table 10), transformation of taenite to kamacite starts more than 50° C higher, extends over a slightly larger temperature range, and is complete at a higher temperature than in the previous case. Schreibersite precipitates, while more than 5% taenite remains in the structure, and a total of 2% schreibersite is present at 600° C. In this case, one would expect schreibersite to nucleate at taenite-kamacite boundaries, but no direct evidence for this has been developed. The actual equilibrium P value may well lie between the two selected values, perhaps 0.8 atomic %. This amount of P would produce upon cooling a somewhat smaller quantity of schreibersite, initially nucleating at a temperature below 650° C, and consuming any remaining residual taenite. Both sufficient P and adequate time at higher temperatures would be available to permit growth of the isolated larger schreibersites observed, and the bulk of the meteorite would appear to have formed under conditions of lower total P.

The 5.3 atomic % Ni and 0.8 atomic % P compositions are plotted on a series of isothermal sections in Figure 19. At 850° C, Coahuila's composition is just inside the kamacite-taenite field of the diagram, yielding a structure containing a small amount of kamacite within a taenite matrix. The field moves in relation to this composition with decreasing temperature, until at 650° C only a small amount of taenite remains in equilibrium with a kamacite matrix. At 600° C, the composition is within the kamacite-schreibersite field, perhaps having passed through the corner of the kamacite-taenite-schreibersite field. By 550° C, the composition lies well within the kamacite-schreibersite field of the diagram, with approximately 98% kamacite

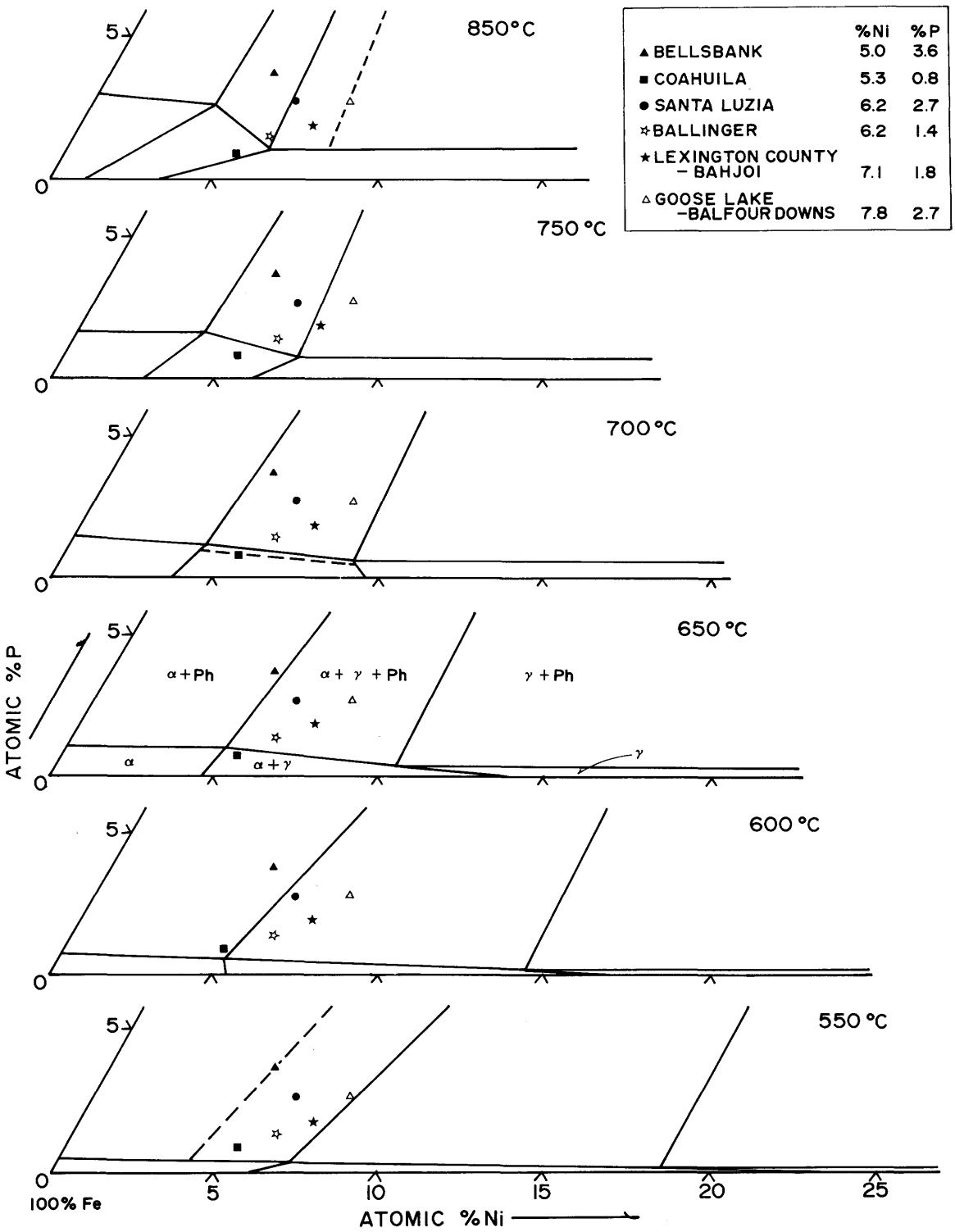

FIGURE 19.—Meteorite bulk compositions plotted on series of isothermal sections of Fe-Ni-P system.

containing 5.1 atomic % Ni and 0.5 atomic % P, being in equilibrium with 2% schreibersite containing 13 atomic % Ni and 25 atomic % P.

The development sequence described above accounts for the major features of Coahuila structure. Equilibrium cooling of this bulk composition produced large single crystals of kamacite containing minor inclusions. The earliest-formed schreibersite nucleated and grew on preexisting sulfide inclusions where available, or perhaps at kamacite-taenite interfaces. The great majority of the individual schreibersite crystals, however, may be assumed to have nucleated homogeneously within kamacite. If this process had stopped at 550° C, the meteorite would contain kamacite of 5.1 atomic % Ni and 0.5 atomic % P, and schreibersite of 13 atomic % Ni. Phase composition measurements from the literature and those reported above indicate that diffusion controlled growth continued to lower temperatures, modifying phase compositions significantly, while producing only subtle changes in the gross structural features. These changes in phase compositions and subtle differences in structure will be discussed in some detail later in this paper.

BALLINGER.—The Ballinger meteorite is a low Ni octahedrite probably containing more P than the analytical value given in Table 1 (0.4 weight % P, 0.7 atomic % P). The Ballinger photograph (Figure 6) shows three areas containing large schreibersite inclusions, perhaps suggesting that the amount of P should be doubled. The calculations given in Table 11, therefore, were made using 6.2 atomic % Ni (6.5 weight %) and both 0.7 atomic % and 1.4 atomic % P.

During equilibrium cooling in the low P case (Table 11), taenite is the only phase present until kamacite appears around 800° C. At 600° C, the equilibrium structure contains 89% kamacite, 10% taenite, and only 1% schreibersite. Upon cooling to 500° C, all of the taenite would be expected to transform, producing an equilibrium structure of 99% kamacite and 1% schreibersite. Both the presence of the massive schreibersites and residual taenite in the actual structure argue against this interpretation. The growth of such large schreibersites requires more P, and the presence of taenite demonstrates that equilibrium cooling was not maintained down to 550° C.

The 1.4 atomic % P calculation for Ballinger (Table 11) leads to a more reasonable interpretation of the structure. Small amounts of kamacite form in taenite around 900° C, and by 850° C the taenite matrix contains 4% kamacite and 1% schreibersite, a situation that might be expected to lead to the growth of several rather large schreibersites on subsequent cooling rather than a number of small ones. By 750° C, one-third of the meteorite is kamacite, undoubtedly the swathing kamacite surrounding the large schreibersites that are present. As the temperature falls to 650° C, the meteorite transforms to 77% kamacite, and the schreibersite doubles its Ni content to 9.0 atomic %, while increasing its amount by one-half. As the temperature drops to 600° C, kamacite increases in volume, schreibersite increases in both amount and in Ni content, and taenite shrinks to 8%. The higher P content seems to be more consistent with the observed structure and could actually be a little low. The presence of taenite and high Ni schreibersite in the actual structure (see above) demonstrates that equilibrium cooling did not persist down to 550° C, and that nonequilibrium phase growth continued to lower temperatures. As in the case with Coahuila, however, the gross features of the structure are accounted for by equilibrium cooling of this particular composition (Figure 19).

TABLE 11.—Equilibrium cooling of compositions appropriate to the Ballinger meteorite (percentage of phases present at indicated temperatures with their Ni contents)

	0.7 Atomic % P, 6.2 Atomic % Ni					
°C	%α	%γ	%Ph	%Ni_{α}	%Ni_{γ}	%Ni_{Ph}
995		100			6.2	
975		100			6.2	
925		100			6.2	
875		100			6.2	
850		100			6.2	
750	15	85		3.7	6.6	
700	60	40		4.0	9.1	
650	78	22		4.9	11	
600	89	10	1	5.2	14	13
550	99		1	6.0		15

	1.4 Atomic % P, 6.2 Atomic % Ni					
°C	%α	%γ	%Ph	%Ni_{α}	%Ni_{γ}	%Ni_{Ph}
995		100			6.2	
975		100			6.2	
925		100			6.2	
875	5	95		3.9	6.3	
850	4	95	1	4.0	6.3	4.4
750	30	68	2	4.0	7.2	5.3
700	62	36	2	4.5	9.1	7.1
650	77	20	3	5.0	11	9.0
600	88	8	4	5.2	14	13
550	96		4	5.7		15

SANTA LUZIA.—The Santa Luzia meteorite structure is dominated by schreibersite and schreibersite-troilite inclusions surrounded by broad areas of swathing kamacite (Figure 7). The literature values for its bulk composition, 6.3 atomic % Ni and 1.6 atomic % P (6.6 weight % Ni and 0.9 weight % P, Table 1), are very close to those assumed for the high P Ballinger composition (Table 11), only a 0.1% increase in Ni and 0.2% in P. This apparently minor change, however, has important ramifications for the structural development process in Santa Luzia. In Ballinger the expected sequence of phases with falling temperature,

$$\gamma \rightarrow \alpha + \gamma \rightarrow \alpha + \gamma + \text{Ph},$$

is followed. In Santa Luzia this sequence is interrupted around 850° C, where over a range of temperature taenite is in equilibrium with schreibersite, the sequence of phases being

$$\gamma \rightarrow \alpha + \gamma \rightarrow \alpha + \gamma. + \text{Ph} \rightarrow \gamma + \text{Ph} \rightarrow \alpha + \gamma + \text{Ph}.$$

The growth of significant amounts of schreibersite within taenite subsequent to the disappearance of preexisting kamacite produced conditions that resulted in the development of large volumes of swathing kamacite and the unusual schreibersite morphology observed in the meteorite.

The actual bulk P value for Santa Luzia may be somewhat larger than the 1.6 atomic % value given in Table 1. The calculations summarized in Table 12 indicate, however, that the same sequence of phases would be expected whether 1.6 atomic % or 2.7 atomic % P is assumed. In either case, kamacite and taenite would have been in equilibrium at 925° C. It is reasonable to assume that this kamacite nucleated within taenite at the preexisting troilite-taenite grain boundaries, with kamacite lamellae radiating away from the troilite. Upon cooling to 875° C, the proportion of kamacite was markedly reduced at both P levels. This small amount of kamacite presumably remained localized near the troilite nodules. The taenite interfaces with troilite and the kamacite-taenite interfaces acted as nucleation sites for schreibersite upon further cooling, producing a skeletal structure that sets the pattern for subsequent schreibersite growth. Nearly half in one case, and more than half in the other, of the schreibersite that formed upon cooling the meteorite to 500° C

TABLE 12.—Equilibrium cooling of compositions appropriate to the Santa Luzia meteorite (percentage of phases present at indicated temperatures with their Ni contents)

	1.6 Atomic % P, 6.3 Atomic % Ni					
°C	%α	%γ	%Ph	%Ni_α	%Ni_γ	%Ni_{Ph}
995		100			6.3	
975		100			6.3	
925	10	90		4.5	6.4	
875	3	96	1	4.0	6.4	4.4
850		98	2		6.3	4.5
750	26	71	3	4.0	7.2	5.3
700	60	37	3	4.5	9.1	7.1
650	76	21	3	5.0	11	9.0
600	87	8	5	5.2	14	13
550	95		5	5.8		15
	2.7 Atomic % P, 6.2 Atomic % Ni					
°C	%α	%γ	%Ph	%Ni_α	%Ni_γ	%Ni_{Ph}
995	43	57		5.3	6.8	
975	50	50		5.4	7.1	
925	35	65		4.9	7.0	
875	4	90	6	4.0	6.4	4.4
850		93	7		6.3	4.5
750	27	66	7	4.0	7.2	5.3
700	60	32	8	4.5	9.1	7.1
650	76	16	8	5.0	11	9.0
600	88	3	9	5.2	14	13
550	91		9	5.4		14

formed at the relatively high temperature of 850° C. Upon further cooling Ni and P continued to diffuse into the central schreibersite areas, P contributing to additional growth and Ni contributing to both growth and Ni enrichment. As a consequence of this localized growth of schreibersite, a large surrounding volume of low Ni metal was produced, the swathing kamacite zone of the final structure. This proposed growth sequence explains the morphology of these large schreibersite structures without the necessity of invoking precipitation from the liquid, a process that would require a bulk composition of more than 4.9 atomic % P at high temperatures.

The broad swathing zone developed as the meteorite cooled from 850° C down into the 700° to 650° C range (Figure 7). This transformation takes place easily at these temperatures as only a relatively small amount of Ni movement is required for both schreibersite growth and enrichment, and for production of the taenite border at the outer edge of the zone. This expanding taenite border acts as a barrier to isolate the large central schreibersites from the bulk material beyond the swathing zone. As the temperature drops and diffusion becomes increasingly restricted, conditions are met for the nucleation of schreibersite at

this taenite border. By 550° C the taenite border has been transformed and replaced with a continuous grain boundary, approximately half of which is occupied by grain boundary schreibersite. This is amply supported by examination of Santa Luzia specimens. The swathing zone boundary contains a large amount of schreibersite and is, with a few minor exceptions, free of residual taenite. The swathing zone itself is also free of large schreibersites and residual taenite, with the exception of several small areas very close to the swathing zone border. These appear to have been small areas of residual taenite that became trapped within the swathing zone at a very late stage and may have been part of the taenite border system at higher temperatures. Competition for P from neighboring schreibersites appears to be the reason that these areas were not converted completely to schreibersite.

Schreibersite equilibration with taenite in the 850° C temperature range results in a redistribution of P in the meteorite leading to the development of areas of coarse Widmanstätten pattern (Figure 7). At these high temperatures P diffuses with ease, lowering its level even in the distant bulk metal to approximately 1.0 atomic %. Subsequent to this, the swathing zone development described above took place, resulting in the isolation of that part of the meteorite from the areas where the coarse Widmanstätten pattern formed. The areas beyond the swathing zones developed an effective bulk composition similar to that of the low P Ballinger case described above. Widmanstätten pattern nucleated in these areas at temperatures below 750° C, and grain boundary schreibersite probably began nucleating at kamacite-taenite interfaces around 600° C. The observed metallography of these areas is consistent with this explanation.

The bulk composition of Santa Luzia is plotted on the diagrams in Figure 19. As in the previous cases, it is obvious from the observations reported in the results section that bulk equilibrium was not maintained down to 550° C, and that phase modification persisted to considerably lower temperatures.

LEXINGTON COUNTY AND BAHJOI.—The bulk compositions of the Lexington County and Bahjoi meteorites appear to be poorly established (Table 1). They are structurally similar, carbon- and sulfur-rich members of Group I with intermediate

TABLE 13.—Equilibrium cooling of compositions appropriate to the Lexington County and Bahjoi meteorites (percentages of phases present at indicated temperatures with their Ni contents)

	0.5 Atomic % P, 7.1 Atomic % Ni					
°C	%α	%γ	%Ph	%Ni_α	%Ni_γ	%Ni_{Ph}
995		100			7.1	
975		100			7.1	
925		100			7.1	
875		100			7.1	
850		100			7.1	
750		100			7.1	
700	40	60		4.1	9.2	
650	70	30		4.9	12	
600	79	20	0.3	5.2	14	13
550	99		1	6.9		16

	1.8 Atomic % P, 7.1 Atomic % Ni					
°C	%α	%γ	%Ph	%Ni_α	%Ni_γ	%Ni_{Ph}
995		100			7.1	
975	5	95		5.5	7.2	
925	10	90	0.3	5.3	7.3	5.2
875		98	2		7.1	5.0
850		97	3		7.2	5.3
750	Tr	96	4	(4.2)	7.2	5.3
700	42	54	4	4.5	9.1	7.1
650	60	35	5	5.0	11	9.0
600	78	16	5	5.2	14	13
550	94		6	6.5		15

bulk Ni. The P values of Lexington County (0.5 atomic % P, 0.3 weight % P) are too low to be reconciled with the amount of schreibersite observed in prepared sections. The Lexington County bulk Ni value is also probably somewhat higher than 7.0 weight % Ni when the contribution of large schreibersites is taken into consideration. Much of the kamacite in this meteorite contains 7.0 weight % Ni, and some of it contains slightly more Ni. Bahjoi also contains isolated large schreibersites, requiring its effective bulk P to be greater than 0.3 weight % P. For these reasons, the equilibrium phase calculations in Table 13 were made at the intermediate Ni value of 7.1 atomic % (7.5 weight % Ni), and at 0.5 atomic % P and 1.8 atomic % P (1.0 weight % P). These calculations suggest that the actual P value probably lies between the two, probably greater than 1 atomic % P.

Structure development in the cooling meteorite does not start until below 750° C in the low P case (Table 13), taenite being the only phase present at higher temperatures. Schreibersite precipitation does not begin until below 650° C, a temperature at which more than 70% of the structure has transformed to kamacite. At 600° C, only 0.3%

schreibersite is present. Under these conditions schreibersite would have precipitated at kamacite-taenite interfaces throughout a well-established Widmanstätten pattern. P could not move through the Widmanstätten pattern to precipitate as schreibersite borders at isolated sulfide interfaces. Schreibersite in these meteorites must have precipitated initially prior to extensive Widmanstätten pattern development, requiring a greater bulk P content.

The 1.8 atomic % P value used in Table 13 is somewhat higher than necessary to account for the observed structure. With this amount of P in the system, kamacite would precipitate by 975° C and schreibersite would be present by 925° C. If the P content were reduced to 1.4 atomic %, neither kamacite nor schreibersite would be present in the system at 925° C or above. At 875° C, however, schreibersite would be present growing within taenite. Kamacite would not nucleate until below 750° C. The important consideration here is that within a reasonable range of P contents, schreibersite nucleates within taenite, undoubtedly at preexisting taenite interfaces with troilite or troilite-silicate-graphite inclusions if they are available. Major quantities of schreibersite grow under these conditions prior to kamacite nucleation and the onset of Widmanstätten pattern development. The 1.8 atomic % P value is used in Figure 19, and it can be seen there that reasonable reduction in the amount of P changes only the amounts of the phases present. Nucleation temperatures for both schreibersite and kamacite would be lowered somewhat, and smaller amounts of P would produce smaller quantities of schreibersite. Neither of these meteorites would appear to contain as much as 6% schreibersite, but certainly they both contain more than 1%.

The structural development sequence in Lexington County and Bahjoi is similar to that of Santa Luzia. With falling temperature a few massive schreibersites grow within taenite, followed by nucleation and growth of a swathing kamacite zone. The Ni values in these massive schreibersites (16 atomic % Ni for Bahjoi, 21 atomic % Ni for Lexington County) require that Ni enrichment continued to below 550° C. At some temperature below 650° C, however, massive schreibersite growth is stopped by precipitation of cohenite. Cohenite contains no detectable P and, therefore, isolates the massive schreibersite from a source of P for continued growth. Ni gradients within the cohenite borders (Figure 13) suggest that Ni may continue to be supplied to the schreibersite through the cohenite. Under these circumstances, a distinct swathing zone morphology is not developed, but the surrounding kamacite does retain a low Ni level and is comparatively free of later-stage schreibersite precipitation.

Within the bulk metal surrounding these eventual cohenite-schreibersite inclusions, initial Widmanstätten pattern development started above 700° C, following its normal sequence. Bulk Ni is low enough that a coarse-structured octahedrite pattern formed. Both of these meteorites have schreibersite morphologies and distributions similar to a meteorite like Ballinger, but they contain more grain boundary taenite and residual taenite-plessite areas, particularly Bahjoi.

Goose Lake and Balfour Downs.—The Goose Lake and Balfour Downs meteorites are two of the highest Ni members of Group I (Table 1), and they are meteorites that contain significant amounts of C and S. The analytical P values from the literature again appear to be too low to explain the observed metallography. A planometric estimate of 0.9 weight % P (1.6 atomic % P) for Goose Lake was given by Doan and Goldstein (1969), and this figure appears to be consistent with the observed structure. Phase calculations are given in Table 14 using a pair of compositions to represent the two meteorites, 7.9 atomic % Ni (8.3 weight % Ni), and 1.4 and 2.7 atomic % P (0.75 and 1.5 weight % P), bracketing what was undoubtedly their effective bulk compositions.

When 1.4 atomic % P is assumed (Table 14), schreibersite nucleates within taenite at a temperature above 850° C. If 2.7 atomic % P is assumed, schreibersite nucleates above 975° C in the presence of 20% kamacite. No structural evidence for initial precipitation at kamacite-taenite interfaces has been observed, supporting the suggestion that the actual P level was in the neighborhood of 1.6 atomic % P. This means that schreibersite nucleated around 900° C, undoubtedly at taenite-troilite boundaries, were they available. The result was growth of a large amount of schreibersite in taenite, with nucleation of a kamacite swathing zone following at a temperature somewhat above 700° C. As the temperature fell, a large supply of Ni was required to keep these massive schreibersites in equilibrium, a process that seems to have

TABLE 14.—Equilibrium cooling of compositions appropriate to the Goose Lake and Balfour Downs meteorites (percentage of phases present at indicated temperatures with their Ni contents)

	1.4 Atomic % P, 7.9 Atomic % Ni					
°C	%α	%γ	%Ph	%Ni_{α}	%Ni_{γ}	%Ni_{Ph}
995		100			7.9	
975		100			7.9	
925		100			7.9	
875		100			7.9	
850		99	1		7.9	6.6
750		98	2		8.0	7.0
700	25	72	3	4.5	9.1	7.1
650	47	50	3	5.0	11	9.0
600	70	26	4	5.2	14	13
550	92	4	4	7.1	18	16

	2.7 Atomic % P, 7.8 Atomic % Ni					
°C	%α	%γ	%Ph	%Ni_{α}	%Ni_{γ}	%Ni_{Ph}
995	20	80		6.2	8.2	
975	23	75	2	6.3	8.3	6.0
925		96	4		7.8	5.7
875		95	5		7.9	6.0
850		93	7		7.9	6.2
750		92	8		7.9	6.6
700	25	67	8	4.5	9.1	7.1
650	47	44	9	5.0	11	9.0
600	70	21	9	5.2	14	13
550	91		9	7.0		16

continued down to below 550° C (17 to 24 atomic % Ni in cohenite-enclosed massive schreibersite). The size of the massive schreibersites requires that the cohenite borders precipitated at temperatures below 750° C. Within this same 700° to 550° C temperature range, the bulk of the metal away from the large schreibersites transformed to normal Widmanstätten pattern. Grain boundary schreibersite, rhabdites, and taenite border schreibersites were formed during this part of the sequence.

In Figure 19 the 2.7 atomic % P value is used. It is obvious here that the same sequence of phases is obtained if the P value is somewhat reduced. The higher Ni is the significant structural development factor in this case.

BELLSBANK.—The Bellsbank meteorite is anomalous, unusually low in Ni and high in P. The gross segregation of schreibersite in its structure makes it unusually difficult to arrive at a satisfactory bulk P content. For this reason the literature values of 5.3 weight % Ni and 2 weight % P were bracketed in Table 15 by assumed compositions of 5.3 weight % Ni and both 1 and 3 weight % P (5.0 atomic % Ni and 1.8 and 3.6 atomic % P, and 4.9 atomic % Ni and 5.3 atomic % P). The intermediate P level proved to be the most reasonable in terms of explaining the observed structure and will be considered first.

For the composition 5.0 atomic % Ni and 3.6 atomic % P (Table 15), kamacite is the only equilibrium phase present from 1100° C to below 975° C. At a temperature somewhat below 975° C taenite nucleates, and a small amount of it is in equilibrium with kamacite at 925° C. By 875° C, taenite has grown to be nearly as abundant as kamacite and the structure contains 6% schreibersite, undoubtedly having nucleated at preexisting kamacite-taenite grain boundaries as well as around sulfide inclusions. At 700° C most of the taenite has disappeared, and at 650° C, 90% kamacite is in equilibrium with 10% schreibersite. The schreibersite continues to increase in Ni as it cools, reaching a value of 11 atomic % Ni at 600° C and below, with a Ni content in the kamacite of 4.2 atomic percent. Both of these Ni values are in general agreement with observed values, perhaps a little on the high side.

If the 1.8 atomic % P value is assumed, kamacite and taenite are the phases present in the equilibrium structure from 1100° C down to below 850° C. Schreibersite first appears somewhat above 750° C, and is present in the amount of 2% when that temperature is reached. Nucleation under these circumstances would be expected to distribute schreibersite along kamacite-taenite borders, these phases being present in approximately equal amounts. Taenite disappears from the structure below 700° C, and by 600° C, 3% schreibersite is in equilibrium with kamacite. The final Ni contents of both kamacite and schreibersite are somewhat higher than in the 3.6 atomic % P case, the higher P situation agreeing better with actual measurements on the meteorite.

When 5.3 atomic % P is assumed, the bulk composition lies within the kamacite + liquid field of the phase diagram from 1100° C to somewhat above 1010° C. At 995° C, 5% schreibersite is in equilibrium with kamacite, and this schreibersite remains constant in amount down to 925° C. During the next 50° drop in temperature one-third of the structure transforms to taenite and the amount of schreibersite more than doubles to 13%. The taenite decreases in volume with further cooling and disappears below 750° C. By 700° C the equilibrium phases are again kamacite and schreibersite,

TABLE 15.—Equilibrium cooling of compositions appropriate to the Bellsbank meteorite (percentage of phases present at indicated temperatures with their Ni contents)

	1.8 Atomic % P, 5.0 Atomic % Ni					
°C	%α	%γ	%Ph	$\%Ni_{\alpha}$	$\%Ni_{\gamma}$	$\%Ni_{Ph}$
995	10	90		4.0	5.1	
975	30	70		4.2	5.3	
925	30	70		3.8	5.5	
875	35	65		3.5	5.8	
850	55	45		4.0	6.3	
750	68	30	2	4.0	7.2	5.3
700	88	9	3	4.5	9.1	7.1
650	97		3	4.9		8.9
600	96		4	4.7		12
555	95		5	4.6		13
	3.6 Atomic % P, 5.0 Atomic % Ni					
°C	%α	%γ	%Ph	$\%Ni_{\alpha}$	$\%Ni_{\gamma}$	$\%Ni_{Ph}$
995	100			5.0		
975	100			5.0		
925	85	15		4.7	6.6	
875	53	41	6	4.0	6.4	4.4
850	50	42	8	4.0	6.3	4.4
750	63	28	9	4.0	7.2	5.3
700	85	5	10	4.5	9.1	7.1
650	90		10	4.6		8.0
600	88		12	4.2		11
550	88		12	4.2		11
	5.3 Atomic % P, 4.9 Atomic % Ni					
°C	%α	%γ	%Ph	$\%Ni_{\alpha}$	$\%Ni_{\gamma}$	$\%Ni_{Ph}$
995	95		5	4.8		6.4
975	95		5	4.8		6.0
925	95		5	4.8		5.2
875	52	35	13	4.0	6.4	4.4
850	49	36	15	4.0	6.3	4.4
750	62	22	16	4.0	7.2	5.3
700	83		17	4.4		7.0
650	83		17	4.4		7.5
600	81		19	3.8		10
550	80		20	3.8		10

schreibersite being present in the amount of 17%. With further cooling, schreibersite increases in quantity and in Ni content, with a rather marked decrease in kamacite Ni content. The final Ni content of the schreibersite is possibly slightly lower than the measured value, the quantity of schreibersite seems too high, and the kamacite Ni values too low. The 3.6 atomic % P figure, the one plotted in Figure 19, seems to be the best choice of the three. A somewhat higher P value, perhaps 4 atomic %, would probably be even better, however. This would mean that schreibersite would initially nucleate in the presence of less taenite, and that final massive schreibersite and kamacite would have slightly smaller Ni values. The observed low temperature schreibersite morphology suggests that an extensive Widmanstätten pattern was not present when schreibersite nucleated.

The phase growth calculations that have been discussed above account for the major structural features of the selected group of meteorites. Appropriate compositions cooled under equilibrium conditions to approximately 600° C would produce the observed proportion of phases and account for the general character of the structures. Coahuila is single crystal kamacite containing a few isolated moderate-size schreibersite inclusions. Ballinger has a coarse Widmanstätten pattern interrupted by large schreibersites that may be surrounded by cohenite. Santa Luzia contains massive schreibersite areas surrounded by giant swathing kamacite, separating areas of coarse Widmanstätten pattern. The higher Ni members of the group have a finer Widmanstätten pattern with massive schreibersite morphology explainable in terms of the amounts of P and C present. Bellsbank contains massive schreibersite and low Ni kamacite and has similarities to the giant swathing kamacite areas in Santa Luzia.

It is interesting at this point to summarize equilibrium data given above and compare it with what would be expected in terms of Widmanstätten pattern growth from the binary Fe-Ni system. Here Widmanstätten pattern growth is construed in its conventional usage of simply taenite transforming to kamacite, ignoring the presence of P either in solution or in schreibersite. The comparison is made in Table 16, where the first two columns give the compositions of the meteorites as plotted in Figure 19, the compositions that best fit the structural arguments given above. These columns are followed by sets of data for the ternary system and for the binary system (Figure 1). In each set the first column gives equilibrium temperatures at which Widmanstätten pattern development starts ($\gamma \rightarrow \alpha + \gamma$) if undercooling effects are ignored, probably a reasonable assumption when P is present. The second column gives the expected temperatures at which taenite would be completely transformed to kamacite ($\alpha + \gamma \rightarrow \alpha$) if equilibrium were maintained down to these low temperatures. The third column gives the expected temperature range for Widmanstätten pattern growth (ΔT_{WPG}). The last two columns show the effect of P on increasing the temperatures of kamacite nucleation ($T\alpha_{Nuc}$) and taenite disappearance ($T\gamma_{Dis}$) over what would be expected from the binary system.

TABLE 16.—Temperatures (° C) for Widmänstatten pattern development in the ternary system as compared to the binary system

Meteorite	Atomic %		Fe-Ni-P System			Fe-Ni System			ΔT due to P	
	Ni	P	$\gamma \rightarrow \alpha+\gamma$	$\alpha+\gamma \rightarrow \alpha$	ΔT_{WGP}	$\gamma \rightarrow \alpha+\gamma$	$\alpha+\gamma \rightarrow \alpha$	ΔT_{WGP}	$T_{\alpha Nuc}$	$T_{\gamma Dis}$
Bellsbank	5.0	3.6	(~930°)*	690°	240°	775°	610°	165°	(155°)**	80°
Coahuila	5.3	0.8	860°	610°	250°	765°	580°	185°	95°	30°
Ballinger	6.2	1.4	880°	580°	300°	755°	570°	185°	125°	10°
Santa Luzia	6.2	2.7	840°	580°	260°	755°	570°	185°	85°	10°
Lexington County & Bahjoi	7.1	1.8	750°	565°	185°	740°	480°	260°	10°	85°
Goose Lake & Balfour Downs ..	7.8	2.7	730°	555°	175°	725°	--	--	5°	--

* For this composition WPG starts with the reaction $\alpha \rightarrow \alpha+\gamma$.
** Nucleation of γ within α.

The presence of P in the coarsest structured meteorites, Bellsbank through Santa Luzia, significantly increases the temperature at which Widmanstätten pattern growth starts, increases the temperature at which transformation of taenite would be expected to be complete, and also significantly increases the temperature range over which growth takes place. These three factors all work in the direction of producing larger kamacite crystals than would be expected from the binary diagram for the same cooling rate. In the coarse-structured meteorites, Lexington County through Belfour Downs, those with a well-developed Widmanstätten pattern, the amount of P has a less dramatic effect. The important point here is that kamacite nucleation takes place at significantly lower temperatures than is the case for meteorites with less Ni. The nucleation temperature is also very close to that which would be expected from the binary diagram. This leads to much more restricted conditions for kamacite growth and the retention of larger amounts of taenite and plessite in the structure, thereby producing the finer and more regular Widmanstätten pattern that is observed in these meteorites.

Details of these various structures as given in the results section, however, are not explained satisfactorily by this discussion. Taenite and plessite are retained in significant amounts in most of these meteorites, demonstrating that equilibrium cooling did not extend to 550° C. Diffusion controlled growth, modifying the equilibrium structure in significant ways continued to lower temperatures. It is this aspect of meteorite structure that will be discussed below.

LOW TEMPERATURE PHASE GROWTH AND THE EQUILIBRIUM DIAGRAM

The preceding section has shown that the major structural features of the selected meteorites may be explained on the basis of nucleation and growth of phases in a system responding to changing equilibrium conditions with decreasing temperature. Bulk equilibrium may have pertained down to 550° C or below for Bellsbank and Coahuila, but the other six meteorites were not in complete equilibrium at that temperature (Figure 19). Had they been, their structures would consist only of kamacite and schreibersite, and the taenite that they contain would have transformed. All eight of the meteorites also contain Ni and P concentration gradients in kamacite adjacent to schreibersite (Tables 2-9), although the recent work of Randich (1975) suggests that these gradients formed at much lower temperatures. Some of the massive and all of the smaller schreibersites have Ni concentrations that are greatly in excess of those permitted for schreibersite in equilibrium with kamacite at 550° C (Figures 18, 25). These observations are explained by the fact that as temperature drops the atomic mobility necessary to maintain bulk equilibrium is lost. Elemental diffusion becomes slower and compositional changes take place over much shorter distances, resulting in composition gradients. Kinetic factors must now be considered as well as equilibrium states. Upon cooling under these restrictive conditions, schreibersite continues to grow in volume, may increase in Ni content, and late-formed schreibersites nucleate and grow. Taenite shrinks in volume and increases in Ni, while kamacite decreases in Ni.

Phase interfaces are still in equilibrium in the sense that interface compositions represent tie lines within the Fe-Ni-P system (see below). Schreibersite-kamacite interface measurements on meteorites, therefore, give equilibrium information relevant to the Fe-Ni-P systems at temperatures well below those that are available experimentally. Combining this low temperature equilibrium data with both an analysis of the kinetic record present in the form of diffusion gradients and a detailed knowledge of specimen petrography may be expected to provide new possibilities for the elucidation of the structures at hand.

With these ideas in mind, it will be helpful first to examine the Fe-Ni-P diagram asking what changes would be expected with decreasing temperature. Meteorite data (Reed 1965a, 1967, 1969, and Tables 2–9 above) indicate major changes in the diagram on cooling to low temperatures. The top part of Figure 20 may be used as a starting point for a discussion of this transition. It is a schematic isothermal section of the ternary system at a temperature slightly below 550° C. The scale on the Fe-P axis has been interrupted so that the lower part of the diagram could be enlarged for clarity. The low P concentrations that are observed in kamacite and taenite make it impossible to show the three fields along the Fe-Ni axis and the three schreibersite-containing fields using the same scale.

Compositional data on schreibersite-kamacite and schreibersite-taenite associations suggest the following trends in the ternary diagram with decreasing temperature. The constant P content of schreibersite requires that the schreibersite composition corner of the three-phase field (point D in Figure 20) lie on the 25 atomic % P line regardless of temperature. Ni values for schreibersite embedded in taenite borders, an association that approximates the schreibersite corner of the three-phase field, range from 41 to 45 atomic %. Point D, therefore, must move at least that far to the right with decreasing temperature. Higher Ni contents in schreibersite have been measured (Reed, 1972), but these represent compositions in the taenite-schreibersite field, while lower Ni contents represent compositions in the kamacite-schreibersite field. Because of the steepness of the Ni concentration gradients, no serious attempt has been made to obtain taenite-schreibersite interface compositions, but incidental measurements (Figures 9, 11) may be used to bracket the position of point C. The Ni value in taenite associated with schreibersite is less than the schreibersite Ni value, perhaps by about 5 atomic %. This suggestion is supported also by Reed's (1972) measurements on the Octibbeha County meteorite and by similar measurements by the authors on this meteorite (60 atomic % Ni in schreibersite in contact with 55 atomic % Ni in taenite). Point C moves to the right, but trails behind point D. The P values in taenite at these interfaces are also not accurately known, but sufficient data is available to say that they are a fraction of the P value in kamacite associate with the same schreibersite (see discussion below and Figure 22). The Ni and P contents for point B may be estimated from the kamacite-schreibersite interface values of these taenite-embedded schreibersites. They range from 5.7 to 6.2 atomic % Ni, with constant P values of 0.05 atomic %. In summary the diagram changes as follows with decreasing temperature: point D moves to the right to approximately 45 atomic % Ni with point C moving to approximately 40 atomic % Ni and to a P value that is much smaller than 0.05 atomic %. As a consequence the α + Ph and $\alpha + \gamma$ + Ph fields greatly expand in area mainly at the expense of the γ + Ph field. The three small fields along the Ni axis also lose a large proportion of their areas, but they still retain considerable importance for the interpretation of meteorite structures.

The preceding illustrates the direction and extent of change in the ternary system with decreasing temperature, but it says nothing about what that temperature range might be. Do meteorite structures continue to develop to very low temperatures or is growth effectively concluded at temperatures not far below 550° C? The bottom section of Figure 20 suggests an approach that may be useful here. We know that D′ lies on the 25 atomic % P line and can assume that it moves continuously to the right with decreasing temperature. The points on the Fe-Ni axis can be obtained from the estimated portion of the Goldstein and Ogilvie (1965) binary Fe-Ni diagram down to about 350° C. If A′, B′, and C′ could be estimated as a function of temperature, we would have much of the information needed for extrapolated isothermal sections.

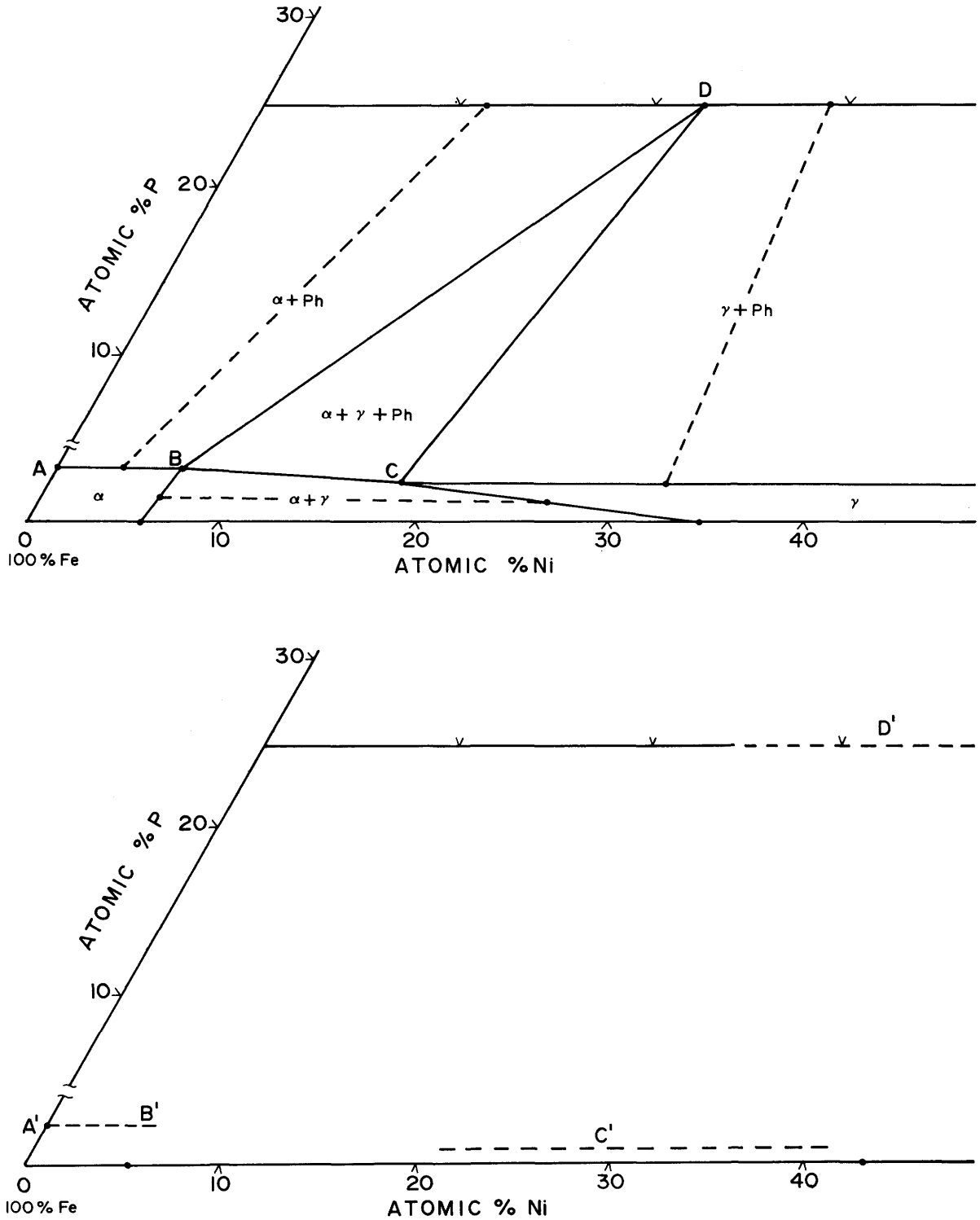

FIGURE 20.—Fe-Ni-P system below 550°C: top, schematic isothermal section; bottom, parameters of use in extrapolating to lower temperatures.

TABLE 17.—Experimental values of P concentration in kamacite and taenite in equilibrium with schreibersite

			Fe-P System*	Fe-Ni-P System**	
T°C	T°K	1/T (°Kx10^{-4})	Atomic % Pα	Atomic % Pα	Atomic % Pγ
1010	1283	7.79	4.8		
995	1268	7.89	4.1		
975	1248	8.01		4.1	1.9
925	1198	8.35		3.7	1.6
875	1148	8.71	2.9	3.0	1.3
850	1123	8.90		2.8	1.2
750	1023	9.78	1.7	1.8	0.68
700	973	10.3	1.3	1.2	0.49
650	923	10.8	0.99	0.9	0.27
600	873	11.5	0.59	0.57	0.22
550	823	12.1	0.45	0.47	0.15

* Doan and Goldstein (1970), table IV.
** Doan and Goldstein (1970), table III.

A′, B′, and C′ represent corners of composition fields, and these particular compositions are very dilute solutions of P in Fe or in Fe-Ni. Data for these points at a number of temperatures within the experimental range are given by Doan and Goldstein (1970), and their values converted to atomic % P are given in Table 17. This type of data is frequently used to extrapolate concentration-temperature relationships to lower temperatures and is plotted accordingly in Figures 21 and 22. Atomic % P on a logarithmic scale is plotted against 1/T. Figure 21 uses P saturated kamacite values from the Fe-P system, and Figure 22 uses both P saturated kamacite and taenite values from the Fe-Ni-P system. Straight lines were drawn with ease through the three sets of data, suggesting that the extrapolations may give useful low temperature composition estimates. The thermodynamic rationale for this procedure is given in "Appendix."

A particularly interesting observation based on Figures 21 and 22 is that the kamacite line in the plot of the Fe-Ni-P system data is identical to the kamacite line in the plot of Fe-P system. Therefore, both sets of data yield the same extrapolated P-temperature relationship for kamacite. This means that line A′B′ is parallel to the Fe-Ni axis, and that the saturation value of P in kamacite is independent of Ni concentration. Should this actually prove to be the case, it would have interesting consequences for the interpretation of meteorite structures. Kamacite-schreibersite interface values would not only represent tie lines in an α + Ph field of the ternary diagram, but the P value in kamacite at a specific interface would represent the temperature of the isothermal section to which

TABLE 18.—Temperature versus P saturation concentration in kamacite and taenite taken from Figure 22

T°C	Atomic % Pα	Atomic % Pγ	Weight % Pα
540	0.40	0.14	0.22
527	0.35	0.12	0.19
508	0.30	0.10	0.17
488	0.25	0.080	0.14
473	0.22	0.070	0.12
465	0.20	0.062	0.11
460	0.19	0.058	0.11
454	0.18	0.054	0.10
449	0.17	0.052	0.09
444	0.16	0.048	0.09
436	0.15	0.046	0.08
431	0.14	0.041	0.08
424	0.13	0.038	0.07
417	0.12	0.034	0.07
410	0.11	0.032	0.06
403	0.10	0.028	0.06
394	0.090	0.025	0.05
383	0.080	0.022	0.04
372	0.070	0.019	0.04
362	0.060	0.015	0.03
348	0.050	0.013	0.03
333	0.040	0.009	0.02
315	0.030	0.007	0.02
298	0.020	0.005	0.01
252	0.010	0.002	0.006

that tie line belonged. The implication of this would be that schreibersite growth effectively stopped over a sequence of temperatures within a given meteorite. Numerical values for P concentration variation with temperature for both kamacite and taenite were read from Figure 22 and are listed in Table 18.

Although a flat line A′B′ has several interesting implications, it is necessary to consider as an alternate possibility that it actually slopes downward from left to right. The experimental technique employed by Doan and Goldstein (1970) was stretched to its limit in obtaining the lower temperature data, resulting in the possibility of significant error for the problem at hand. There is also ambiguity in their paper concerning one critical value. The weight % P in kamacite value for the Fe-P system at 550° C taken from their table IV is 0.25 ± 0.03. The value used on the 550° C isothermal section (their figure 8) is 0.4 weight % P. This difference probably represents confusion as to which value is best rather than a simple misprint in the diagram, a difficulty that can best be resolved by more careful experimental work. If this 0.4 weight % P value had been used in the extrapolation, the line in Figure 21 would have lain to the right of the kamacite line in Figure 22. This would mean a sloping line A′B′ with P decreasing as Ni increases. This situation could imply that all schreibersite within a given meteorite grew down to the same final temperature. Before attempting

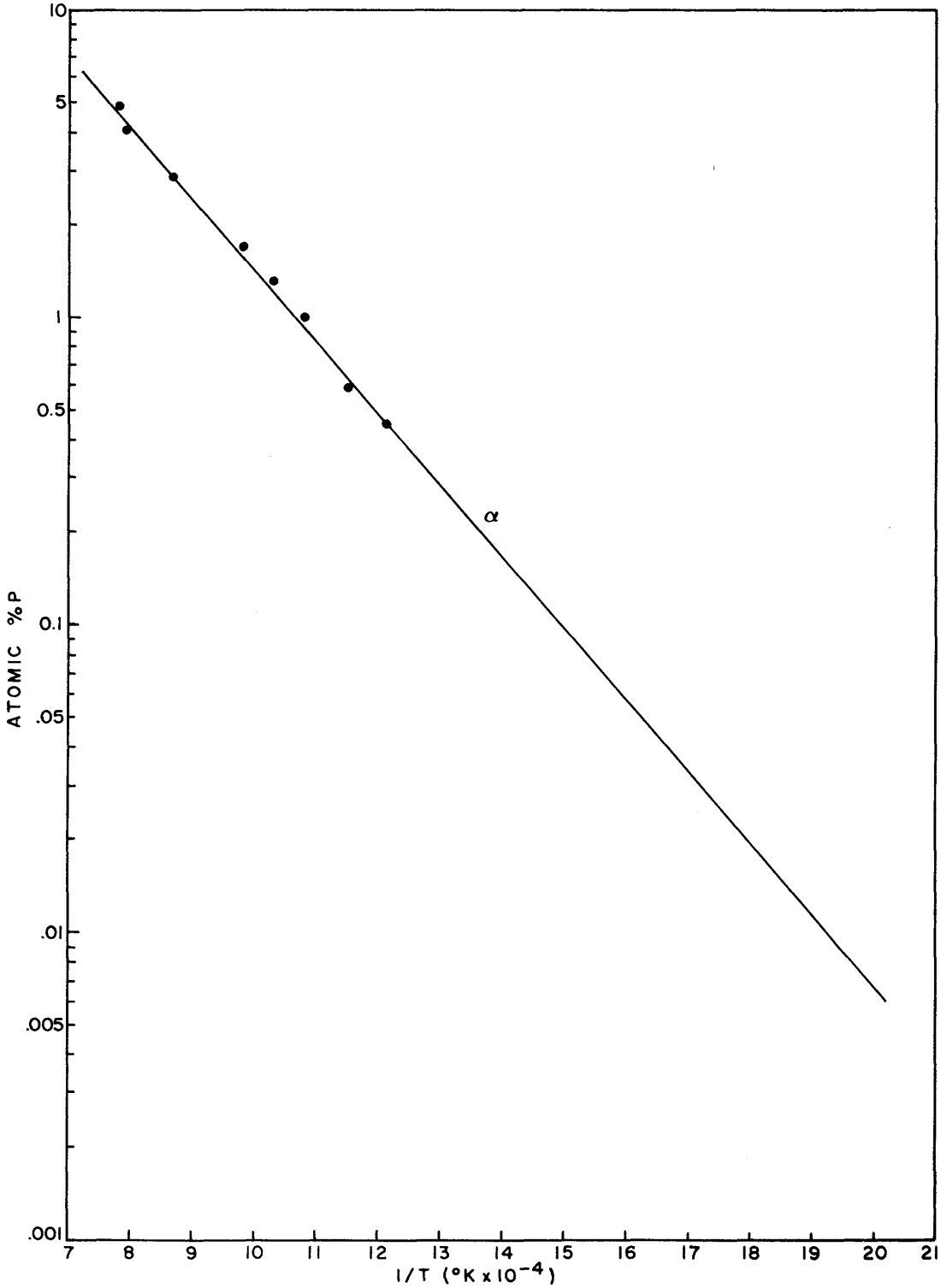

FIGURE 21.—Extrapolation of P saturation values in kamacite in Fe-P system to lower temperatures.

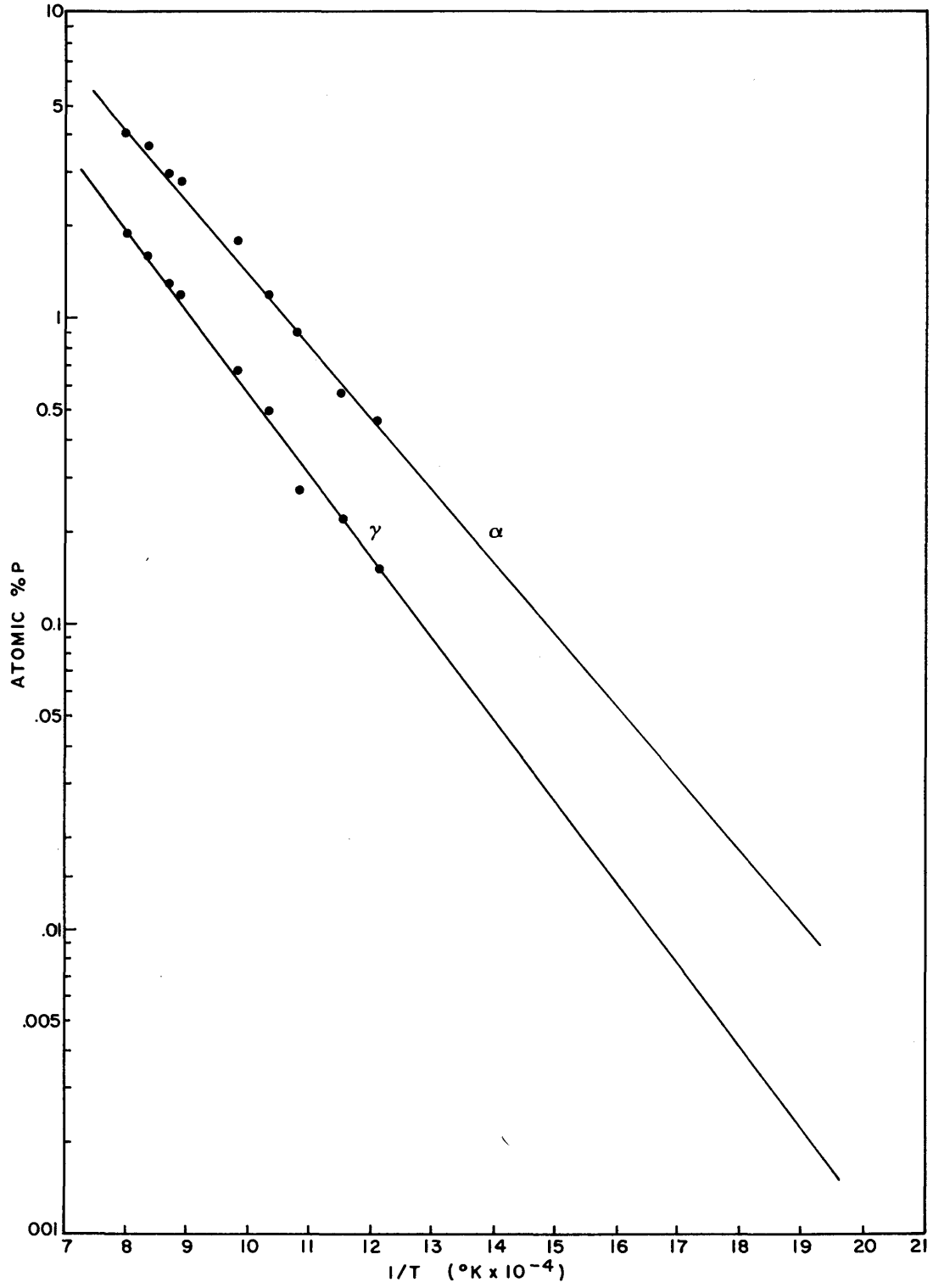

FIGURE 22.—Extrapolation of P saturation values in kamacite and taenite in Fe-Ni-P system to lower temperatures.

to resolve this and related problems in terms of meteorite measurements, however, it will be helpful if we first look at the diffusion process as it applies to schreibersite growth.

Diffusion-Controlled Schreibersite Growth

The data presented above on Ni and P gradients demonstrates that schreibersite grew by drawing these elements from increasingly restricted volumes of kamacite with decreasing temperature. Petrographic considerations combined with an understanding of the Fe-Ni-P system suggest the broad outlines of the nucleation and growth process. With this background in mind, a set of constraints and assumptions can be developed that allow the qualitative application of the nonisothermal diffusion-controlled growth theory for ternary systems recently developed by Randich and Goldstein (1975) to be applied to schreibersite growth in these meteorites (see also Randich, 1975).

Figure 23 may be used to relate schreibersite growth both to the Fe-Ni-P diagram and to growth equations. The top part of the diagram is a schematic isothermal section at some temperature below 550° C. The scale for P is broken so that very low levels of P can be indicated. The tie line represents schreibersite growing within kamacite. Its ends give interface P and Ni compositions for both kamacite (C'_P, C'_{Ni}) and schreibersite (C''_P, C''_{Ni}). The theory of Randich and Goldstein (1975) requires that equilibrium be maintained to the extent that Ni and P concentrations in the two phases are related by a tie line in the ternary system at the temperature that pertains. For diffusion-controlled conditions, this tie line need not be the equilibrium tie line (ETL), the one that passes through the bulk composition of the system.

The lower part of Figure 23 indicates kinetic factors that are important in the growth process. A schreibersite (Ph) of half width ξ_P^+ equal to ξ_{Ni}^+ is growing within kamacite in the X direction. The P and Ni values in schreibersite at the interface are C''_P and C''_{Ni}, and the equivalent values in kamacite are C'_P and C'_{Ni}. The P and Ni fluxes from kamacite into the growing schreibersite are $J^{\alpha}_{P,\xi}{}^{+}$ and $J^{\alpha}_{Ni,\xi}{}^{+}$, and the Ni flux from the interface into the schreibersite is $J^{Ph}_{Ni,\xi}{}^{-}$. The concentration gradients in P and Ni are $\partial C_P/\partial X$ and $\partial C_{Ni}/\partial X$.

The diffusion controlled growth process may be described by the mathematical treatment of Randich and Goldstein (1975). Diffusion in the Fe-Ni-P system may be described using an extension of Fick's first law. The P and Ni fluxes in terms of concentration gradients in kamacite and schreibersite are as follows.

$$J_P^{\alpha} = -D_{PP}^{Fe,\alpha}\frac{\partial C_P}{\partial X} - D_{PNi}^{Fe,\alpha}\frac{\partial C_{Ni}}{\partial X} \tag{1a}$$

$$J_{Ni}^{\alpha} = -D_{NiNi}^{Fe,\alpha}\frac{\partial C_{Ni}}{\partial X} - D_{NiP}^{Fe,\alpha}\frac{\partial C_P}{\partial X} \tag{1b}$$

$$J_{Ni}^{Ph} = -D_{NiNi}^{Fe,Ph}\frac{\partial C_{Ni}}{\partial X} - D_{NiP}^{Fe,Ph}\frac{\partial C_P}{\partial X} \tag{1c}$$

$$J_P^{Ph} = 0 \tag{1d}$$

Separate sets of equations are needed for each phase. The P flux in schreibersite is zero due to the constant atomic proportion of this element in schreibersite. The symbols $D_{PP}^{Fe,\alpha}$ and $D_{NiNi}^{Fe,\alpha}$ are diffusion coefficients, measures of the influence of the concentration gradients of these two elements on their own flux, where as $D_{PNi}^{Fe,\alpha}$ and $D_{NiP}^{Fe,\alpha}$ reflect cross effects usually referred to as the ternary diffusional interaction. The latter coefficients have been found to be so small in this system that the terms containing them may be dropped from the above equations (Heyward and Goldstein, 1973). These equations may then be simplified by neglecting the diffusional interaction terms and the P flux in schreibersite.

$$J_P^{\alpha} = -D_{PP}^{Fe,\alpha}\frac{\partial C_P}{\partial X} \tag{2a}$$

$$J_{Ni}^{\alpha} = -D_{NiNi}^{Fe,\alpha}\frac{\partial C_{Ni}}{\partial X} \tag{2b}$$

$$J_{Ni}^{Ph} = -D_{NiNi}^{Fe,Ph}\frac{\partial C_{Ni}}{\partial X} \tag{2c}$$

Fick's second law is applied in order to consider the time dependence of the fluxes. It is assumed that diffusion coefficients are independent of composition.

$$\frac{\partial C_P}{\partial t} = -\frac{\partial J_P^{\alpha}}{\partial X} = D_{PP}^{Fe,\alpha}\frac{\partial^2 C_P}{\partial X^2} \tag{3a}$$

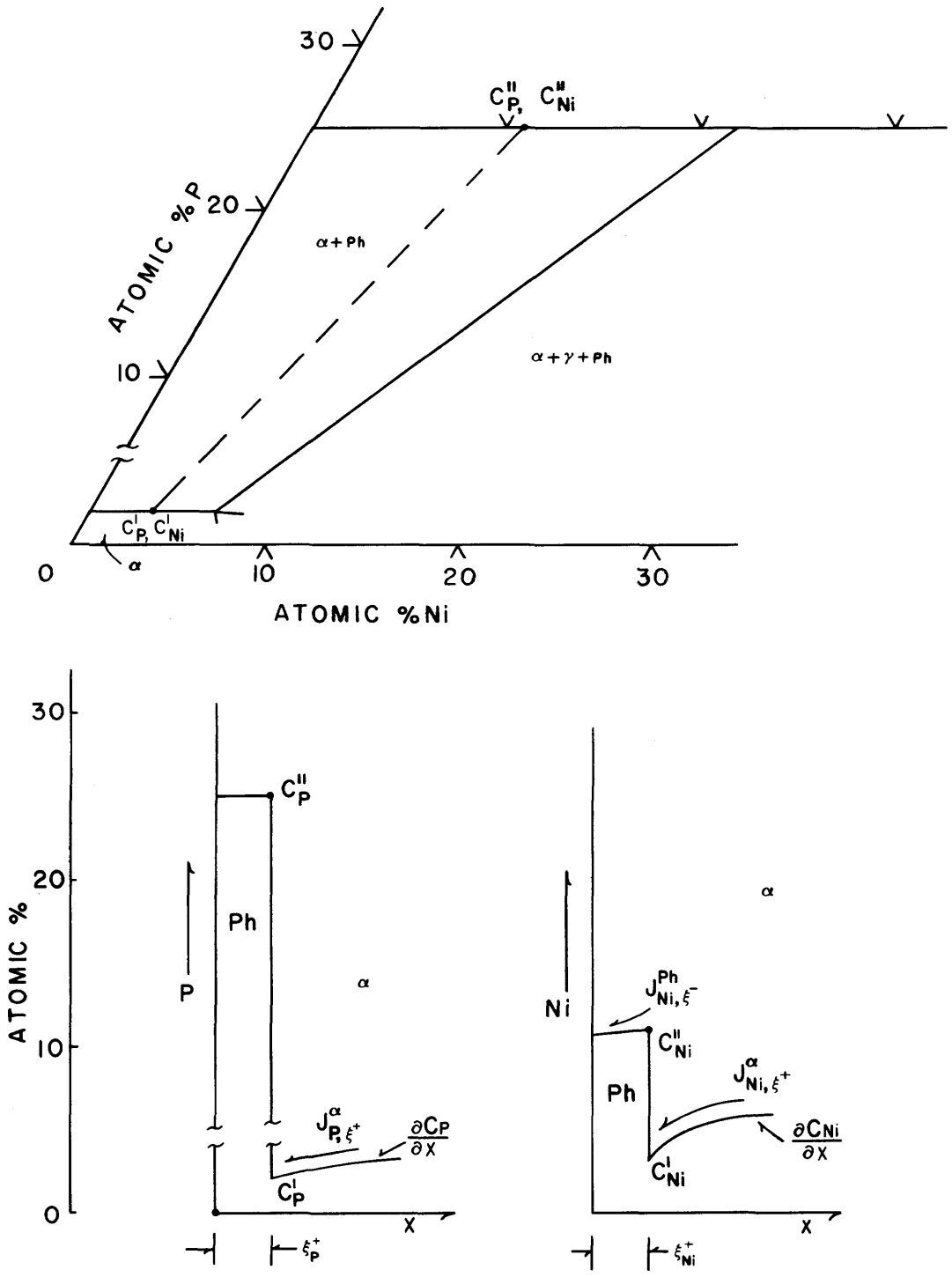

FIGURE 23.—Relation of schreibersite growth both to Fe-Ni-P diagram and to growth equations: top, schematic low temperature ternary with tie line indicating schreibersite growing in α + Ph field; bottom, α + Ph interface compositions, composition gradients, and associated P and Ni fluxes.

$$\frac{\partial C_{Ni}}{\partial t} = -\frac{\partial J^{\alpha}_{Ni}}{\partial X} = D^{Fe,\alpha}_{NiNi}\frac{\partial^2 C_{Ni}}{\partial X^2} \quad (3b)$$

$$\frac{\partial C_{Ni}}{\partial t} = -\frac{\partial J^{Ph}_{Ni}}{\partial X} = D^{Fe,Ph}_{NiNi}\frac{\partial^2 C_{Ni}}{\partial X^2} \quad (3c)$$

The resulting mass balance equations for P and Ni at a schreibersite-kamacite interface are as follows.

$$(C''_P - C'_P)\frac{d\xi_P}{dt} = -J^{\alpha}_{P,\xi}{}^{+} \quad (4a)$$

$$(C''_{Ni} - C'_{Ni})\frac{d\xi_{Ni}}{dt} = -(J^{\alpha}_{Ni,\xi}{}^{+} - J^{Ph}_{Ni,\xi}{}^{-}) \quad (4b)$$

The two mass balances are related to each other as the rate of movement of the interface, $d\xi/dt$, must be the same for both elements.

$$\frac{d\xi}{dt} = \frac{d\xi_P}{dt} = \frac{d\xi_{Ni}}{dt} \quad (5)$$

A schreibersite growth rate may then be expressed in terms of interface Ni and P concentrations, the flux of P in kamacite, and the fluxes of Ni in both kamacite and schreibersite.

$$\frac{d\xi}{dt} = \frac{1}{C''_P - C'_P}(-J^{\alpha}_{P,\xi}{}^{+}) \quad (6a)$$

$$\frac{d\xi}{dt} = \frac{1}{C''_{Ni} - C'_{Ni}}(-J^{\alpha}_{Ni,\xi}{}^{+} + J^{Ph}_{Ni,\xi}{}^{-}) \quad (6b)$$

It is beyond the scope of this study to attempt the difficult numerical analysis required to solve these growth equations. Randich (1975) has developed a model for this purpose and successfully applied it to the growth of schreibersite in hexahedrites. He compiled a computer program that treats diffusion controlled phase growth in ternary systems when the requisite portions of the phase diagram are known. The model accomodates ternary interactions, nonisothermal transformations (variable cooling rates), and impingement (overlapping diffusion fields). It is based on a one-dimensional space grid and is rigorous only for lamellar schreibersite growing within kamacite. The concepts that this model employs, however, are valid for meteorites more complex than the hexahedrites, and they will be used here in a qualitative interpretation of the data.

Equations 6a and 6b relate P and Ni interface concentrations to their gradients in kamacite and schreibersite for the final stages of growth. Cooling is assumed to be uninterrupted, with schreibersite growth continuing down to very low temperatures. Measurements with the electron microprobe, however, do not reveal changes that take place within less than 1 μm of an interface. Therefore, as a consequence of this limitation of the measurement technique, growth apparently stops when subsequent changes become unresolvable. Randich's (1975) calculations indicate a lower limit of 250° C for detectable change.

Equation 6a is a key to the understanding of schreibersite growth under the conditions that pertained in the meteorites under study. It demonstrates that the P flux controlled the schreibersite growth rate. The quantity C''_P in the equation is the P content of schreibersite at the interface (Figure 23), a constant at 25 atomic %. The quantity C'_P is the interface P content in kamacite. It is a small number, 0.2 to 0.05 atomic %, in the temperature range of formation of the observed interface relationships. The quantity $(C''_P - C'_P)$, therefore, may be considered to be independent of temperature even though C'_P is not. With this simplifying assumption, the rate of growth of a given interface, $d\xi/dt$, is seen to be dependent only on the P flux, $J^{\alpha}_{P,\xi}{}^{+}$. The P flux, however, will be dependent upon C'_P at any given temperature. The value of C'_P combines with the P level in the surrounding kamacite to establish the P gradient, $\partial C_P/\partial X$, the variable that determines the flux (equation 2a).

The system responds to the constraint of the P flux determining schreibersite growth rates by adjusting individual interface Ni concentrations so that the growth rate established by P (equation 6a) is matched by the growth rate due to Ni (equation 6b). This permits individual schreibersites containing markedly different Ni levels to continue to grow simultaneously within the cooling meteorite. Kamacite and schreibersite interface Ni and P concentrations must continue to be related by a tie line relationship, a requirement that is met by tie lines shifting from the equilibrium tie line. The nature of these tie line shifts and their effects on growth rates of individual schreibersites is illustrated in Figure 24.

Tie line shifts and their effects are illustrated using hypothetical ternary diagrams in Figure 24. The symbols for Ni and P are retained as a matter of convenience, although scale problems preclude

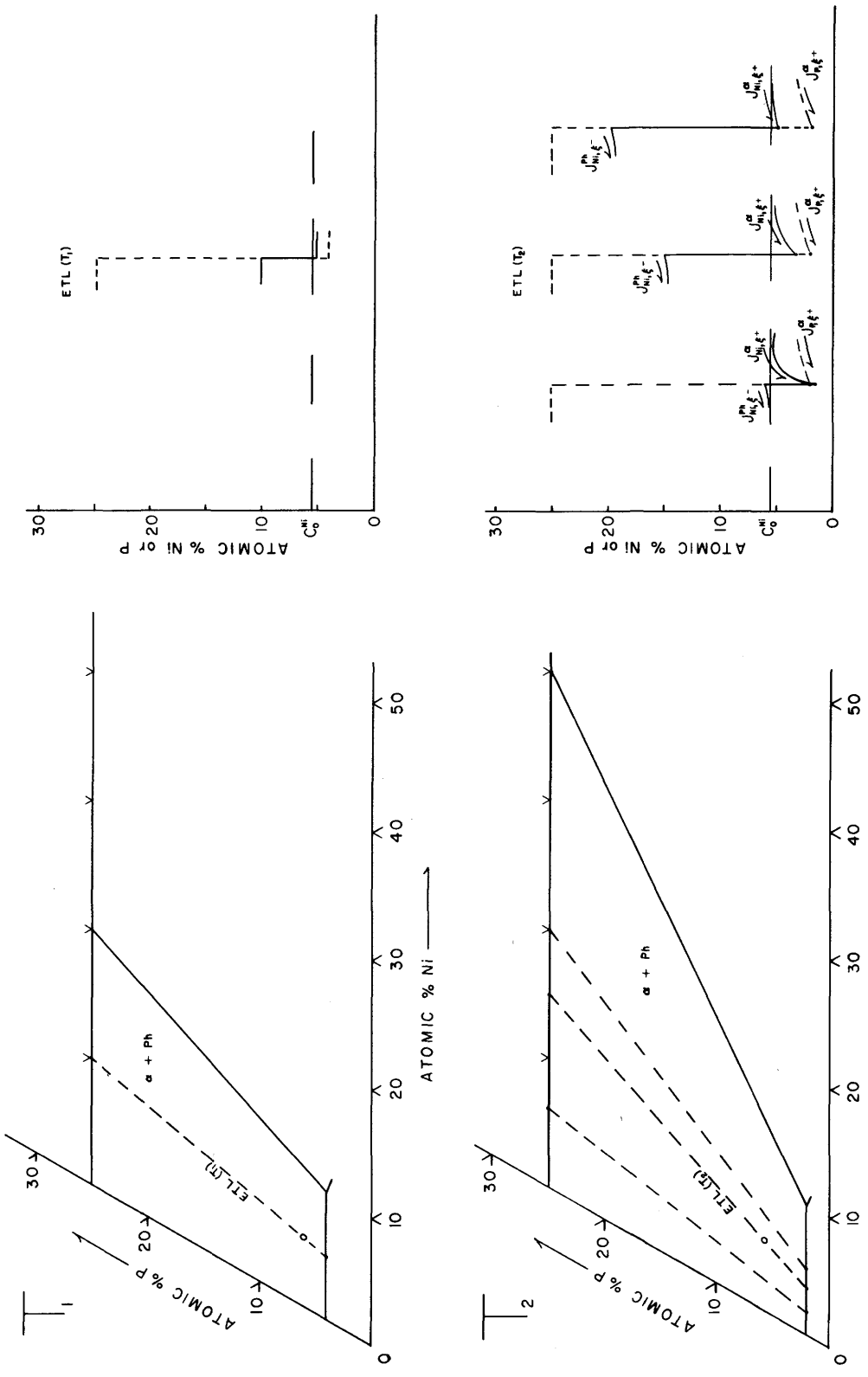

FIGURE 24.—Hypothetical isothermal sections at temperature T_1 and at lower temperature T_2 (tie lines indicated in α + Ph fields; diagrams at right indicate interface relationships for these tie lines).

use of actual values. The tie line indicated at the higher temperature T_1, ETL(T_1), is assumed to represent bulk equilibrium in the α + Ph region of the diagram. It passes through the bulk composition indicated by the small circle (5.5 atomic % Ni and 6.0 atomic % P). Upon cooling to temperature T_2 the α + Ph field expands along the α + Ph/Ph boundary, and the α/α + Ph boundary moves closer to the Fe-Ni axis. It is assumed that in this lower temperature range mass transfer is insufficient to achieve bulk equilibrium. Growth becomes diffusion controlled and gradients develop within the phases. Tie lines may therefore shift from the equilibrium tie line so that the Ni growth rate can match the P growth rate. Three possible tie lines are indicated at T_2, the equilibrium tie line for the same composition used above, ETL(T_2), and tie lines shifted to the right and to the left of ETL(T_2).

The interface relationships for these four tie lines are illustrated at the right in Figure 24. The upper diagram shows interface Ni and P compositions for ETL(T_1). The bulk Ni value for the system is indicated by C_0^{Ni}. The bulk P value is 0.5 atomic % higher and was omitted for clarity. Bulk equilibrium has been achieved at temperature T_1 as is indicated by the absence of compositional gradients in both kamacite and schreibersite.

Interface relationships for diffusion controlled growth at temperature T_2 are illustrated in the lower right side of Figure 24. The P interface values are assumed to be identical in the three interface situations shown. The consequence is similar P fluxes feeding schreibersite growth, $J^{\alpha}_{P,\xi}{}^{+}$, and the establishment of similar growth rates, $d\xi/dt$, for the interfaces through equation 6a. Tie line shifts from ETL(T_2) induced by conditions of limited mass transfer produce a continuously varying range of growth rates that permits Ni flow to match that required by P.

The equilibrium tie line at the lower temperature, ETL(T_2), passes through the bulk composition. Its interface Ni and P values are those that would be observed if the system were at complete equilibrium. The presence of compositional gradients in both kamacite and schreibersite, however, show that complete equilibrium has not been reached.

Shifting the tie line to the left results in an increase in the growth rate due to Ni (equation 6b). The quantity $1/(C''_{Ni} - C'_{Ni})$ and the Ni flux in kamacite, $J^{\alpha}_{Ni,\xi}{}^{+}$, become larger and the Ni flux in schreibersite, $J^{Ph}_{Ni,\xi}{}^{-}$, becomes smaller. All three of these changes increase the growth rate over that of ETL(T_2). Ni is supplied to the growing schreibersite in a way that size is increased at the expense of Ni enrichment.

Moving the tie line to the right of ETL(T_2) has the effect of slowing the growth rate due to Ni. The quantity $1/(C''_{Ni} - C'_{Ni})$ and the Ni flux in kamacite, $J^{\alpha}_{Ni,\xi}{}^{+}$, become smaller, and the Ni flux in schreibersite, $J^{Ph}_{Ni,\xi}{}^{-}$, becomes larger. All three of these changes decrease the growth rate over that for ETL(T_2). Ni is supplied to the growing schreibersite in a way that it becomes enriched in Ni rather than growing in size. A theoretically infinite range of growth rates may be obtained by these tie line shifts. One of these possible tie lines will give a unique growth rate that satisfies both equations 6a and 6b.

Cooling Rate Variations

Cooling rates of meteorite parent bodies are known to vary over several orders of magnitude (Goldstein and Short, 1967b). These variations will affect the growth of schreibersite, particularly in the lower temperature ranges. Compositions and associations we observe in meteorite specimens will depend in part on specific cooling histories. Measurements of schreibersite, therefore, would be expected to be interpretable in terms of cooling rates. Randich (1975) has recently demonstrated the validity of this assumption by calculating cooling rates for hexahedrites. In the course of his work important observations were made that will help in the interpretation of more complex meteorite structures. Several aspects of this work will be reviewed here.

Calculations using the Randich and Goldstein (1975) schreibersite growth model were made using a bulk composition of 2.1 weight % P, 4.1 weight % Ni, and 93.8 weight % Fe. Cooling rates of 5×10^{-3}, 5×10^{-4}, and 5×10^{-5}° C per second were employed over a cooling interval of 900° C to 685° C. Decreasing the cooling rate produced schreibersites of predicted greater widths and higher Ni contents. P gradients were predicted in kamacite and Ni gradients were predicted for both kamacite and schreibersite. The calculated Ni interface values were significantly lower than those for the equilibrium tie line for this composition.

Tie lines had shifted to the left to increase the growth rate for Ni. An experimental validation of these calculations was carried out using this same composition and the 5×10^{-4}° C per second (43.2° C per day) cooling rate. Calculated and observed compositions agreed within the limits of electron microprobe measurements.

Additional cooling rate calculations were made by Randich (1975) in a study of schreibersite nucleation temperatures. Cooling rates in the meteorite range of 1°, 10°, and 100° C per million years were used with the Coahuila bulk composition of 5.49 weight % Ni and 0.49 weight % P. The results were similar to those given above, the slower cooling rates producing slightly larger schreibersite containing slightly higher Ni values. The calculated Ni values were within the range of observed Ni values in hexahedrites, establishing the validity of the model at cooling rates within the meteoritic range. Ni gradients were predicted for the schreibersites, contrary to observations on meteorites. This is probably explained by the fact that the ternary diffusion constant for Ni in schreibersite is not known in this temperature range.

These calculations led to a conclusion that is significant for our purpose. It was shown that if nucleation occurs above 500° C the amount of undercooling prior to nucleation in unimportant. The kamacite-schreibersite assemblage at 500° C will be in equilibrium, assuming a diffusion field of 1000 μm or less. Randich (1975) also points out that this situation leads to the conclusion that Reed's (1965b) theory that lamellar schreibersite and rhabdite nucleated simultaneously must be correct. Had the plate schreibersite grown significantly prior to nucleation of rhabdite, the rhabdite would have been prevented from nucleating. Both types are observed together over very short distances, requiring that nucleation temperatures were very close. Under these circumstances, impingment of P and cooling rate are the two factors that control schreibersite growth for a given bulk composition.

Interface Data and Schreibersite Distribution

In a previous section we have seen that the main petrographic features of coarse-structured iron meteorites can be understood in terms of equilibrium cooling of specific compositions in the Fe-Ni-P system. This approach can be extended to much lower temperatures with the aid of concepts developed by Randich (1975) in his analysis of schreibersite growth in hexahedrites. The application of diffusion theory permits the interpretation of schreibersite-kamacite interface data in a way that yields a more detailed understanding of schreibersite distribution and composition than has been possible previously.

Phases and compositions resulting from equilibrium cooling of the meteorite compositions of interest have been summarized in Tables 10 through 15, and these same compositions have been plotted on the iron-rich corner of isothermal sections in Figure 19. At the top of Figure 25 these compositions have also been plotted on the 550°C isothermal section with their respective tie lines. This is the lowest temperature for which an experimentally based ternary section is available. Table 19 lists the equilibrium percentages of kamacite and schreibersite with their Ni contents as taken from Figure 25. This plot shows that had complete equilibrium been reached at this temperature for these compositions, taenite would have disappeared and the observed structures would consist of kamacite containing inclusions of schreibersite.

The bottom section of Figure 25 contains an estimated isothermal section at approximately 300° C. The schreibersite corner of the three phase field is plotted at 45 atomic % Ni, a value that is probably close to the real value. The kamacite corner of the three phase field is plotted at 5.5 atomic % Ni, and this value is considerably less certain. The compositions used above are again plotted with their tie lines. Although the diagram may not be accurate, it does tell us something of what would be expected if equilibrium cooling extended to this very low temperature. Proportions of phases and the expected compositions taken from this diagram are also listed in Table 19.

The bulk compositions plotted in the lower section of Figure 25 would also consist of kamacite and schreibersite only, and these two phases would be uniform in composition. The Bellsbank schreibersite would contain much more Ni than was observed for its massive schreibersite, and its kamacite would be considerably poorer in Ni than was observed. The massive schreibersite in Santa Luzia would be greatly enriched in Ni, its small schrei-

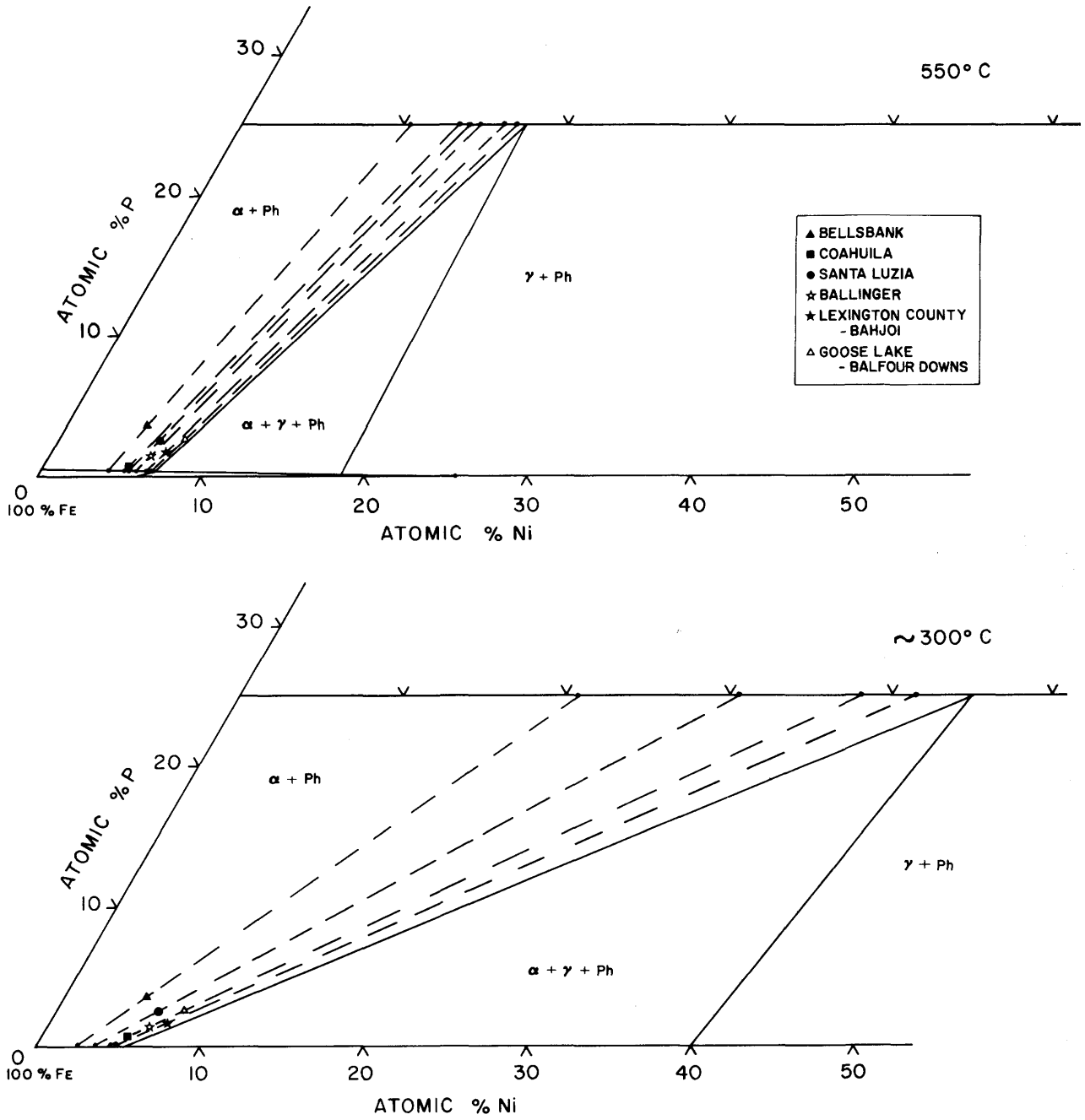

FIGURE 25.—Schreibersite compositions resulting from equilibrium cooling of meteorite compositions: top, 550° C isothermal section with meteorite compositions and their respective equilibrium tie lines; bottom, similar plot at approximately 300° C.

bersite would contain less Ni, and its kamacite would be poorer in Ni. The Coahulia, Ballinger, and Goose Lake-Balfour Downs compositions all lie on the same tie line, but would consist of different proportions of kamacite and schreibersite. The Lexington County-Bahjoi composition would produce the most Ni rich schreibersite. The structures suggested by this diagram, therefore, are markedly different than those actually observed in the meteorites under study. At what

TABLE 19.—Equilibrium compositions at 550° C and ~300° C taken from Figure 25

Meteorite	550°C % α	% Ph	% Ni_α	% Ni_{Ph}
Bellsbank	87.0	13.0	4.1	11.9
Coahuila	99.3	0.7	5.2	13.3
Santa Luzia	91.3	8.7	5.4	14.0
Ballinger	96.3	3.7	5.8	15.0
Lexington County & Bahjoi	94.8	5.2	6.6	16.2
Goose Lake & Balfour Downs	91.2	8.8	6.9	17.0

Meteorite	~300°C % α	% Ph	% Ni_α	% Ni_{Ph}
Bellsbank	86.4	13.6	2.5	20.8
Coahuila	97.2	2.8	4.3	38.0
Santa Luzia	90.2	9.8	3.6	30.5
Ballinger	94.5	5.5	4.3	38.0
Lexington County & Bahjoi	93.3	6.7	4.7	41.2
Goose Lake & Balfour Downs	90.0	10.0	4.3	38.0

temperatures do these observed differences become introduced into the structures?

Taenite is retained in the form of the Widmanstätten pattern in the six octahedrites studied. This shows that mass transfer required by the taenite-kamacite transformation is insufficient at somewhat above 550° C to achieve bulk equilibrium in the cooling rate range pertaining. The presence of the Widmanstätten pattern may also affect subsequent P movement through the structure. Randich's (1975) calculations show that mass transfer through 1000 μm diffusion fields in kamacite is sufficient for kamacite-schreibersite equilibrium to be maintained down to 500° C in the same range of cooling rates. Kamacite-taenite transformations become restricted at higher temperatures than kamacite-schreibersite transformations. Therefore, it is reasonable to assume that as temperatures drop below 600° C, localized compositional changes become increasingly more important and bulk compositional effects become increasingly less important. As mass flow becomes more restricted, individual structural units maintain interface equilibrium and respond to compositional gradients in increasingly small volumes of material. These processes are responsible for the interface and gradient data that have been reported above.

Tie lines representing interface data from the Coahuila, Santa Luzia, and Goose Lake meteorites (Tables 2, 5, and 8) are plotted on isothermal sections in Figures 26. Average values were used where more than one set of interface measurements gave similar values. Any given tie line, therefore, may represent more than one set of measurements. The scale used made it impossible to indicate the differing low P values in kamacite, so all of these compositions are indicated by points resting on the Fe-Ni axis. This treatment of the data may well be an over simplification as various tie lines within a given meteorite may actually belong on different isothermal sections. A range of temperatures may be involved, and this point will be returned to in a later section. The three meteorites selected are representative of the group of eight meteorites studied.

Typical tie lines for the Coahuila meteorite are given in the top section of Figure 26. They fan out through a narrow composition range of 3.2 to 4.7 atomic % Ni in kamacite and 20 to 30 atomic % Ni in schreibersite. Kamacite P values at the interfaces range from 0.14 to 0.09 atomic %, a significant point that will be dealt with later. The structural associations related to compositions have been discussed above, but it should be noted here that the tie line on the left represents early-formed structures (schreibersite bordering troilite-daubreelite inclusions and a large schreibersite), and the three on the right are later-formed structures (large rhabdites). The estimated bulk composition of Coahuila is indicated on the diagram as a large dot. The point apparently falls on the right-hand tie line. All the measured schreibersite compositions in Coahuila then appear to be to the left of the ETL or on it, as was to be expected on the basis of Randich's (1975) analysis. Reed (1965a) has reported Coahuila schreibersite with 34 atomic % Ni. It is not clear how this value would plot on Figure 26 as the necessary Ni value in kamacite is not available.

The relationship of the equilibrium tie line to observed meteorite tie lines is actually somewhat more complex then Randich (1975) has implied. This can be concluded from consideration of Coahuila measurements, and it will become clearer when measurements on the octahedrites are considered. At temperatures above the final growth stages represented by the Coahuila tie lines in Figure 26, mass transfer had become inhibited except for very short-range interactions. Schreibersite continues to grow as long as there is a P

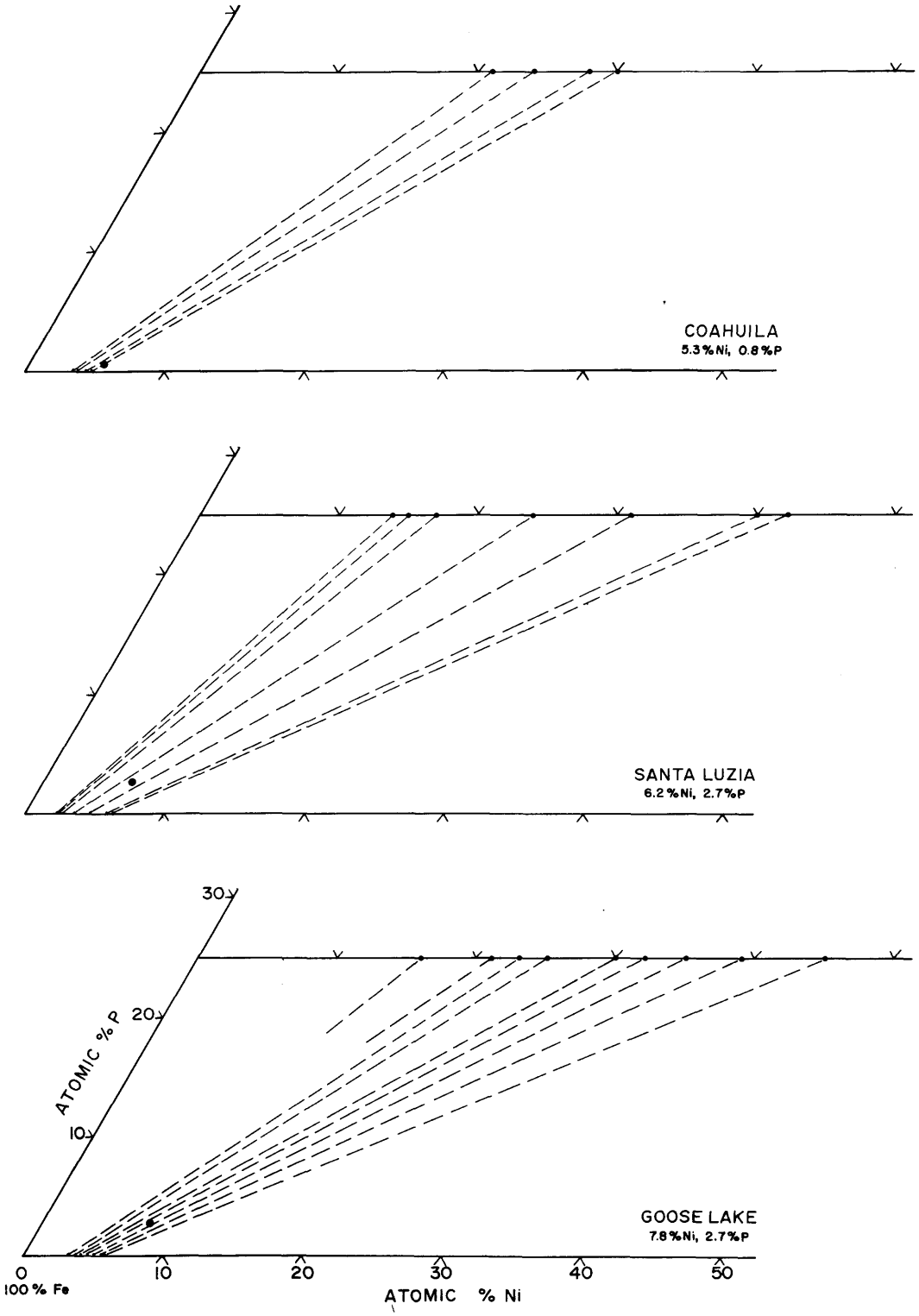

FIGURE 26.—Representative tie lines from Coahuila, Santa Luzia, and Goose Lake meteorites plotted on isothermal sections.

flow to the interface. Growth stops when P impingment reduces the P flux to zero, or, for our purpose, when we can no longer measure interface relationship changes. Although a theoretical possibility, there is no evidence that any of the schreibersites studied were in the process of dissolving. As the P flux decreases with decreasing temperature, a given interface tie line would be expected to shift to the right to conform to the change in shape of the α + Ph field of the phase diagram. It would also be expected to move farther to the right in order to slow the Ni growth rate as the P supply becomes more limited. The largest schreibersites undoubtedly nucleated first and have grown at comparatively high rates, drawing P from large volumes of metal. They have the lowest Ni concentrations. The smaller schreibersites that grew at slower rates due to a more limited P supply have higher Ni levels. The smallest schreibersites would be expected to approach a Ni content given by the tie line whose Ni value in kamacite equals the Ni value of the kamacite in which they are growing. Kamacite in the Coahuila meteorite has a higher Ni value than it would have had if complete equilibrium had been reached. It is therefore possible that microrhabdites in Coahuila contain more Ni than would be expected from the low temperature equilibrium tie line. Unfortunately, the necessary measurements needed to confirm this were beyond the capability of the techniques available.

Tie lines for the Santa Luzia meteorite are shown on a single temperature plot in the center section of Figure 26. Kamacite Ni values range from 2.2 to 6.2 atomic % with the corresponding Ni values in schreibersite of 14 to 42 atomic % covering a much broader range when compared to Coahuila. Kamacite P values at the interfaces range from 0.13 to 0.05 atomic %. The three tie lines at the left represent the early formed massive schreibersites, the three to their right are from grain boundary schreibersite, and the one on the extreme right is from a late-stage structure, a small schreibersite partially embedded in taenite. The Santa Luzia bulk composition lies in about the center of the spread of tie lines, demonstrating that interface tie lines depend upon local structure and may fall on either side of the ETL.

Had complete equilibrium been achieved for Santa Luzia at 550° C, kamacite would have contained 5.4 atomic % Ni and schreibersite 14 atomic % Ni. Equilibrium extending to the 300° C temperature range would have resulted in kamacite of 3.6 atomic % Ni and schreibersite of 31 atomic % Ni (Table 19, Figure 25). A very different situation is indicated by the tie lines in Figure 26. These represent interfaces from a range of schreibersite morphologies from massive schreibersite surrounded by large volumes of swathing kamacite to taenite border schreibersite.

The explanation of these differences lies in the fact that under conditions of diffusion-controlled growth, P can be drawn from much greater distances than Ni within a given time period. Complete equilibrium was not reached in the 600° to 500° C temperature range. Massive schreibersites had nucleated at much higher temperatures and grown to near their final size. This process had reduced the level of P in the complete volume of metal to near the equilibrium level. Even the volumes of metal most remote from the large schreibersites probably only contained about 0.6 atomic % P at 550° C (the equilibrium value is 0.4 atomic % P). Massive schreibersite growth may be viewed as a process that equalizes P levels in meteoritic metal in the 500° to 600° C temperature range regardless of initial P concentrations. Differences in initial P level are reflected in the amount of schreibersite produced.

While P diffusion in this temperature range resulted in a meteorite with a modest P gradient, the slower Ni diffusion resulted in an important segregation of this element. Ni could not be moved from a sufficiently large distance to maintain bulk equilibrium in the times available. The massive schreibersites had grown to near their final size, but their Ni contents had to have been significantly below the equilibrium value. Their interface tie lines, therefore, must have been to the left of the equilibrium tie line. The Ni gradient that probably already existed within the swathing kamacite zone became more pronounced. Beyond the swathing zone, however, sufficient Ni was maintained to yield the observed Wildmanstätten pattern. These areas of the meteorite have a higher average Ni content than the initial bulk Ni content of the meteorite. As a matter of fact, some areas of kamacite within the Widmanstätten pattern contain more Ni than the accepted bulk Ni value.

The consequence of massive schreibersite growth under these circumstances of composition and cooling is to establish two distinctly different

structural areas within the meteorite, swathing kamacite areas containing massive schreibersites and areas of Widmanstätten pattern (Figure 7). Both types of areas continue to change with decreasing temperature, but distances involved become increasingly more restricted. The massive schreibersites continue to grow, their growth rates being determined by the flux of P from the swathing kamacite. Interface Ni values shift to produce a tie line with a matching growth rate. The shift is undoubtedly to the right, resulting in a slower growth rate due to Ni and Ni enrichment of the schreibersite. The final Ni values of these schreibersites approximates the equilibrium value at 550° C.

The outer edge of the swathing zone develops as a kamacite-taenite boundary that recedes from the massive schreibersite with decreasing temperature. The final stage in this progression is the replacement of the boundary in part by grain boundary schreibersite. P is supplied to the boundary initially by the swathing kamacite, and the taenite boundary supplies the initial Ni. Nucleation of this type results in concentrations that are required by the three-phase field of the ternary diagram. The initial schreibersite-kamacite tie line will be the α + Ph/α + γ + Ph boundary for the given temperature. With decreasing temperature the taenite border is replaced with a grain boundary that contains grain boundary schreibersite over about half of its distance. Nucleation may take place over a range of temperatures as the taenite recedes along the forming grain boundary, resulting in different initial Ni contents in the schreibersite and different initial growth rates. As growth continues at the individual interfaces, Ni concentrations adjust to match the P controlled growth rate. The general tendency will be for tie lines to move to the right as the P supply dwindles.

Simultaneously with continued growth of the massive schreibersites and development of the exterior swathing zone grain boundary, Widmanstätten pattern development is continuing in the remaining areas of the meteorite. The Ni level is high enough in these areas so that a coarse Widmanstätten pattern forms, containing large kamacite lamellae and occasional plessite areas and grain boundary taenite. Grain boundaries contain occasional grain boundary schreibersite, and the kamacite lamellae contain rhabdites and microrhabdites. The rhabdites and grain boundary schreibersites develop analogously to the similar morphologies described above for Coahuila, reacting to specific local conditions to achieve appropriate interface values. Nucleation of grain boundary schreibersites under these circumstances may take place at lower temperatures, undoubtedly leading to smaller schreibersites with higher initial Ni content that continues to increase upon further cooling. Small rhabdites would also be expected to reach high Ni values because they are growing in a relatively Ni rich kamacite.

A final type of schreibersite morphology observed in Santa Luzia is represented by the tie line at the far right in Figure 26. It represents the taenite border schreibersite illustrated in Figures 10 and 11. Schreibersite of this type appears to nucleate within taenite at a taenite-kamacite interface at a very late stage in the structural development process. P is undoubtedly supplied mainly from the kamacite, with most of the Ni coming from the taenite. Associations of this type yield the highest Ni schreibersites to be observed in coarse octahedrites. The schreibersites may also contain a slight Ni gradient, undoubtedly due to the fact that they are associated with kamacite on one side and taenite on the other. If this type of schreibersite nucleates earlier or grows more rapidly due to a particularly high P gradient, it isolates itself from the enclosing taenite by converting it to kamacite.

Goose Lake meteorite tie lines are shown in the bottom isothermal section in Figure 26. Differences from the Santa Luzia pattern result from higher bulk concentrations of both carbon and Ni. Only the upper portions of the two tie lines on the left can be indicated. At some point in the development of these schreibersites, cohenite precipitated in the adjacent metal, transforming the interface to a cohenite-schreibersite interface and preventing further schreibersite growth. The partial range of Ni values in kamacite, therefore, is 3.2 to 5.7 atomic %, with Ni values in schreibersite ranging from 16 to 45 atomic %. The value of 45 atomic % Ni is the highest observed for a schreibersite in contact with kamacite. Kamacite P values at the interfaces cover the same range as observed in Santa Luzia, 0.13 to 0.05 atomic %. This range in P values may indicate that these tie lines do not all belong on the same isothermal section, a point

that will be discussed in a later section. The bulk composition again lies in the center of the spread of tie lines.

The general outline of the schreibersite growth process may be summarized on the basis of this discussion and that given in previous sections. In the meteorites under study schreibersite petrography has been strongly affected by sequential nucleation. Initial schreibersite nucleation is a function of temperature and bulk composition. It took place at greater than 850° C for all of the meteorites containing massive schreibersite. The low P Coahuila meteorite is the only exception. These massive schreibersites grew rapidly under equilibrium or near equilibrium conditions, at least as far as P is concerned, for most of their growth period. Randich (1975) has shown that meteorite cooling rates are sufficiently slow to allow this. It is important to note that massive schreibersite has achieved the major portion of its growth by the time it has cooled to 600° C. On subsequent cooling, Ni is enriched but size does not increase appreciably. The massive schreibersite growth process, therefore, has the effect of lowering the P level in the bulk metal and isolating it, as schreibersite enclosed in zones of swathing kamacite, from areas of developing Widmanstätten pattern.

By 600° C the Widmanstätten pattern is well established in these meteorites (Table 16). Kamacite lamellae have grown to near their final size, and taenite bands have shrunk to near theirs. Both taenite and kamacite will continue to increase in Ni with cooling, but compositional changes will take place over increasingly short distances. It is in this environment, one that contains P in kamacite at the 0.5 to 0.8 atomic % level, that rhabdite nucleation must take place. They nucleate homogeneously in kamacite within a narrow range of temperatures and grow under conditions of equilibrium combined with severe P impingment. It is the limited amount of P and the competition for it from closely spaced schreibersites that controls their growth rates and consequently their eventual size. The larger the volume of metal from which a schreibersite draws P, the faster it grows and the larger it becomes. Tie line shifts permit Ni levels to vary depending upon growth rates. The larger faster-grown rhabdites achieve lower Ni levels than the smaller slower-grown schreibersites.

A third major type of schreibersite is grain boundary schreibersite. Its petrography suggests that it replaces taenite at late stages in structural development. Heterogeneous nucleation probably takes place at kamacite-taenite interfaces, resulting in initial concentrations being controlled by the three-phase $\alpha + \gamma +$ Ph field of the ternary diagram. P is supplied to the nucleation site mainly from the bordering kamacite and Ni comes mainly from the taenite. Equation 6 does not describe initial growth rates but may well apply to kamacite-schreibersite interfaces after they become isolated from the influence of taenite. Nucleation temperatures probably depend upon specific local conditions and may extend to considerably lower temperatures than those appropriate for rhabdite formation.

There are three types of associations that may be included under the term grain boundary schreibersite. They appear to represent a sequence of stages in structural development. The first type is the isolated grain boundary schreibersite. These are elongated schreibersites that lie along kamacite-kamacite grain boundaries. They frequently occupy grain boundary junctions and branch accordingly. Their morphology suggests that they replaced residual taenite as it receded along the grain boundary. Their Ni values decrease with distance away from the nearest taenite ribbon or taenite-plessite area, suggesting that the lowest Ni grain boundary schreibersite nucleated first. An alternate possibility is essentially simultaneous nucleation with faster growth accounting for lower Ni. These schreibersites are frequently somewhat larger than the higher Ni ones closer to taenite. There is no obvious reason, however, why P impingment should be more critical at one site than at another.

The second type of grain boundary schreibersite is found in close association with taenite and taenite-plessite areas. It appears to have formed similarly to the isolated grain boundary schreibersites, but it either nucleated later or grew more slowly. It separated itself from taenite but was not able to completely absorb it. The final stage in this sequence is the formation of taenite boundary schreibersites. These are the small, highest Ni schreibersites that appear to be embedded in taenite at taenite-kamacite borders. These would seem to be the final schreibersites to form.

Interface Data and the α/α + Ph Boundary

In the earlier discussion of the extrapolation of experimental data to low temperatures the slope of the α/α + Ph boundary was mentioned. The extrapolation shows that the boundary moves toward the Fe-Ni axis with decreasing temperature and suggests that it is parallel to it (Figures 21, 22). This led to the simplifying assumption that P saturation values in kamacite are independent of Ni and Fe concentrations and may be equated to specific temperatures (Table 18). This in turn leads to a possible interpretation of the measured P in kamacite values at kamacite-schreibersite interfaces as being equivalent to a final growth temperature, a temperature below which subsequent interface changes would be undetectable by the technique employed.

Observed P interface values cover a range of concentrations from 0.16 to 0.05 atomic %. A factor of three is involved, indicating that small differences in measured concentrations may have more than trivial significance. The higher P values are associated with massive schreibersite at interfaces with low Ni kamacite, and the lower P values are associated with taenite border schreibersite at interfaces with high Ni kamacite. Assuming that these values represent solubility limits, we can equate them to a temperature range of 445° to 350° C (Table 18). Measurements on the Santa Luzia meteorite alone covered most of this range, 0.14 to 0.05 atomic % P, equivalent to a temperature difference of 430° to 350° C. Is it reasonable to assume that large schreibersites stopped detectable growth before the later formed schreibersites, or does the α/α + Ph boundary really have a downward slope with increasing Ni? Are there other factors that may make a clear choice between these two alternatives impossible on the basis of the available data?

The P and Ni kamacite interface data is summarized in Figure 27. The points represent individual interface Ni and P concentrations in kamacite and are plotted using the axes at the left and at the bottom of the diagram. The symbols indicate the meteorite from which the data were taken. There is a general trend of decreasing P concentration in kamacite with increasing Ni concentration. The relationship of these values to the estimated $\alpha/\alpha + \gamma$ boundary of the Fe-Ni binary diagram of Goldstein and Olgivie (1965) is also indicated. The scale to the right of the diagram is the temperature equivalent to the P concentration at the left, using the data from Table 18. The dashed line is the $\alpha/\alpha + \gamma$ boundary plotted in relation to temperature and Ni concentration. It is obvious that interface values for individual meteorites, as is the case for the group as a whole, cover a range of both P and Ni levels. A meteorite has interface values at several P levels, and a range of Ni values may be covered at any given P level. All of the interface values are to the left of the $\alpha/\alpha + \gamma$ boundary, the higher Ni values being closest to it.

There are at least three factors that must be considered as possible contributors to the observed distribution in Figure 27. These are (1) cooling rates, (2) the possibility of a slopping α/α + Ph boundary, and (3) the possibility of low temperature nucleation at α/γ boundaries and subsequent grain boundary diffusion playing a role in the growth of grain boundary and taenite border schreibersite. The available data is insufficient to sort out these influences in a quantitative way, but their expected effects can be outlined and suggestive observations mentioned.

Cooling rates have only been reported for four of the meteorites under consideration here. Values of 2° C per million years for Lexington County and Goose Lake and 3.5° C per million years for Bahjoi were given by Goldstein and Short (1967b). The recent measurements of Randich (1975) gave a somewhat higher value of 5° C per million years for Coahuila, and there is no reported value for Bellsbank. Kamacite band widths for the other three meteorites were taken from Buchwald (1976), and cooling rates were estimated using the Goldstein and Short (1967b) cooling rate curves. Ballinger and Balfour Downs gave cooling rates of 2° C per million years and Santa Luzia gave an estimated 0.8° C per million years. These numbers indicate that cooling rate values for this group of meteorites cluster in a rather narrow range centering around 2° C per million years.

The effect of cooling rate variations on schreibersite-kamacite interface values has been discussed above. It is to be expected that slower cooling rates would produce lower detectable interface values of P in kamacite and lower levels of P in kamacite generally. This would be equivalent to detectable growth continuing to lower temperatures. This type of variation may be present on a minor scale in the data considered here. Coahuila

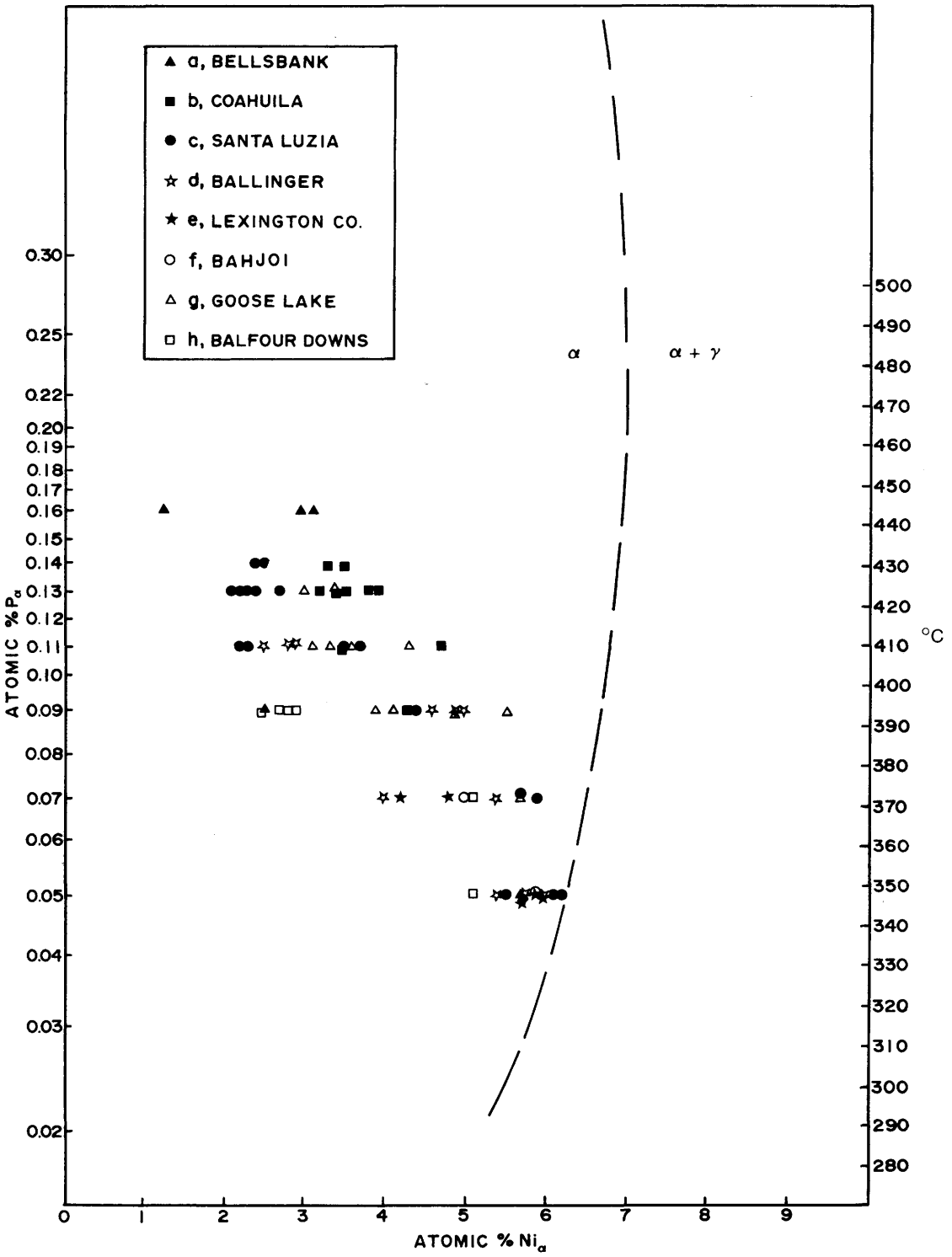

FIGURE 27.—P in kamacite at kamacite-schreibersite interfaces plotted against Ni in kamacite (temperature scale at right relates P saturation values to $\alpha/\alpha + \gamma$ boundary of Fe-Ni system).

does have the highest reported cooling rate of 5° C per million years, and its interface P values and P levels in kamacite do seem to be somewhat higher than for some of the other meteorites studied. Bellsbank also seems to have unusually high levels of P in kamacite, and this could be the consequence of a comparatively high cooling rate. The points representing both Coahuila and Bellsbank interfaces are in the upper part of Figure 27, perhaps meaning that detectable change ceased at higher temperatures for these two meteorites due to higher cooling rates.

An α/α + Ph boundary (AB in Figure 20) that slopes downward from the Fe-P axis toward the Fe-Ni axis would contribute to the type of data distribution observed in Figure 27. At any given temperature lower Ni schreibersites would have a higher P interface value in kamacite than higher Ni schreibersites. The range of the data, however, seems to require much too steep a slope to be reasonable in terms of the extrapolation given above. An Fe-P axis intercept value of approximately 0.2 atomic % would be indicated. This would mean either an unreasonably high P saturation temperature in the neighborhood of 465° C (Table 18), or that the actual curve bends sharply to the right of the indicated extrapolation (Figure 21). It also seems unlikely that error in locating the data points is a major factor. It was pointed out above that reproducibility of P determinations was ±0.005 weight % and for Ni was ±0.1 weight %. This means that the P levels shown are distinguishable from their nearest neighbors with reasonable certainty and that the Ni variations are meaningful. Ni variations at a given P level range from 0.8 to 3.0 atomic %. Variations for a specific meteorite at a given P level are not so wide, but they do range up to 1.5 atomic %. This range in Ni values for a single meteorite at a given P level suggests that factors other than simply a sloping α/α + Ph boundary are involved. The boundary may well have a gentle slope, but other factors must also contribute to the observed distribution.

Tie lines representing three of the P levels in Figure 27 are plotted on isothermal sections in Figure 28. The symbols used in Figure 27 are used at the schreibersite ends of the tie lines to identify the meteorite represented. Tie lines actually belonging to a given isothermal section will fan out across the field without overlap. When overlap occurs it implies either error in the data or plotting on the wrong isothermal section. We saw in Figure 26 that all of the measured tie lines for three of the meteorites can be plotted without obvious cases of overlap. This could mean they all belong to the same isothermal section, but it could also be fortuitous. If interface data for all of the meteorites could be plotted as tie lines on a single intelligible drawing, several cases of overlap would be observed. When tie lines are separated on the basis of P level as in Figure 28, no serious cases of overlap are encountered. The two tie lines at the left on the 0.09 atomic % P section do overlap slightly, but a small shift in Ni values could do away with it. The surprising point is how little overlap is seen when the data are taken directly from the tables given earlier and plotted in this way.

Had all of the tie lines in Figure 28 been plotted on a single isothermal section, there would have been several cases of overlap. The most serious offender would be a Bellsbank tie line, the second one from the left on the 0.09 atomic % P isothermal section. If it were plotted on the top section of Figure 28, there would have been obvious overlap with another Bellsbank tie line. All three of the tie lines in this top isothermal section are from the Bellsbank meteorite, and there is additional evidence to be discussed below that suggests that two temperatures are involved.

Plotting tie lines as has been done in Figure 28 supports the idea that a temperature effect is real. That is to say that late formed schreibersites continued significant growth to temperatures below those of early formed schreibersites. Unfortunately, these meteorites do not supply us with a full range of tie lines at any one temperature. More work will be required before the slope of the α/α + Ph boundary within this low temperature range can be established with certainty.

A third possibly complicating process that could be of importance here has been discussed by Comerford (1969). He pointed out that grain boundary diffusion might play an important role in the development of grain boundary schreibersites. He suggested that grain boundary diffusion would supply Ni to schreibersites growing at low temperatures more readily than lattice diffusion. The discussion above has pointed out that P is the controlling element rather than Ni, but his suggestion would be equally valid for P.

The measurements on grain boundary schrei-

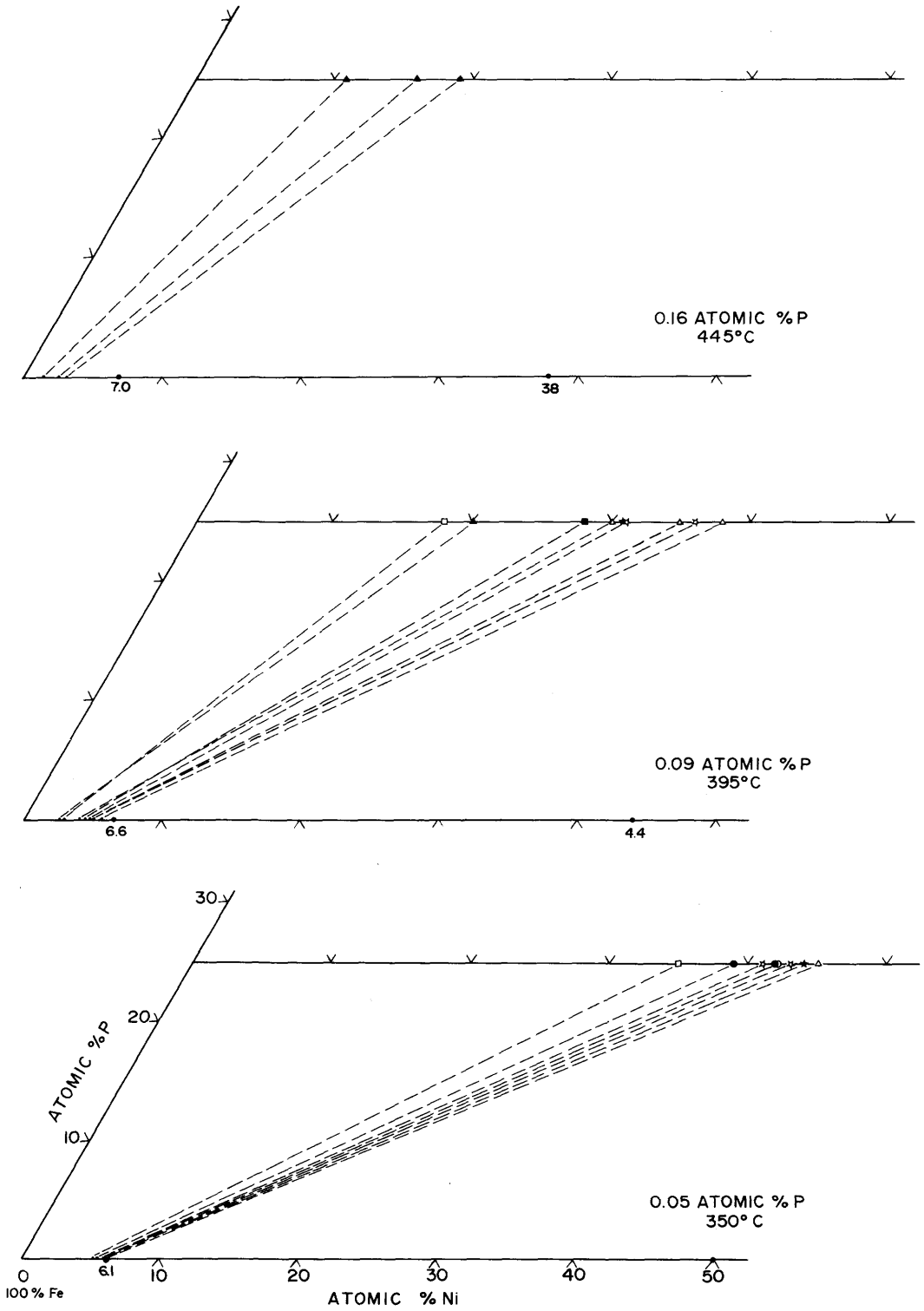

FIGURE 28.—Tie lines from various meteorites separated according to interface P saturation values in kamacite for plotting on isothermal sections.

bersite in the Santa Luzia meteorite are representative of many such measurements reported above (Figures 10, 11). Petrographic relationships suggest that this type of schreibersite nucleated at kamacite-taenite interfaces absorbing residual taenite. Nucleation temperatures were probably low compared to those for homogeneously nucleated rhabdite, but the data does not allow a closer temperature estimate. It would also appear that nucleation occurred over a range of temperature, nucleation of the lowest Ni schreibersite farthest along the grain boundary away from taenite having taken place first (Figure 11, traverse 11). The Ni concentration of schreibersite nucleated at a kamacite-taenite border is that of the schreibersite corner of the three-phase field at the nucleation temperature. The presence of the phase boundary probably serves both as a site for nucleation and as a source of P through the process of grain boundary diffusion. As the schreibersite becomes larger, however, the contribution of grain boundary diffusion becomes increasingly less important. The schreibersite grows rapidly, with its Ni level increasing only slightly. Its interface with kamacite represents a tie line that probably tends to shift to the left with decreasing temperature, as P is drawn from a relatively large diffusion field.

Along the grain boundary at a location closer to the final residual taenite a second grain boundary schreibersite nucleates at a lower temperature (Figure 11, traverse 12). Its initial Ni is higher, and the P diffusion rate is lower. Grain boundary diffusion again makes an important contribution during initial growth, but it probably becomes increasingly less important as the schreibersite increases in size.

The observed taenite border schreibersite undoubtedly nucleated at a still lower temperature (Figure 11, traverse 13). It formed at the taenite-kamacite border and had a high initial Ni concentration. Growth was insufficient to separate the schreibersite completely from taenite. A small schreibersite that has a Ni gradient due to the fact that it is in contact with kamacite at one end and taenite at the other resulted. This type of schreibersite has both the highest observed Ni concentrations and the lowest observed P interface values in kamacite. A reasonable explanation of these observations is that grain boundary diffusion plays an increasingly important role both with small schreibersite size and lower temperature of growth.

Grain boundary diffusion may also help explain the Bellsbank interface measurements summarized in Figure 5. Four of the seven interfaces shown have a P level in kamacite of 0.09 weight % P (0.16 atomic %), and the other three are at 0.05 weight % P (0.09 atomic %). The schreibersite interface illustrated at the top of the diagram is a typical one for massive schreibersite. The schreibersite illustrated at the lower left is a large rhabdite (Table 3, traverse 6) surrounded by clear kamacite within an area of microrhabdites. There were no grain boundaries or subgrain boundaries observed. The schreibersite illustrated at the lower right is another large elongated rhabdite (Table 3, traverses 4 and 5) that was observed to be along a definite subgrain boundary. Both of these rhabdites have extremely large P gradients, and their P interface values differ by 0.04 weight % P (0.07 atomic %). The center schreibersite in the lower section of the diagram is a large rhabdite (Table 3, traverses 2 and 3) along a subgrain boundary with different P and Ni interface values in kamacite on its opposite sides. Tie lines representing these interfaces are given in Figure 28. The three high P tie lines are in the top isothermal section and the fourth, representing the low P interfaces, is at the left in the middle section. A possible rationale for these observations is that Bellsbank cooled more rapidly than the other meteorites studied. As a result, growth apparently stopped at higher temperatures than has been the case for other rhabdite-containing meteorites. The presence of grain boundaries, however, permitted P flow to continue to significantly lower temperatures for the two schreibersites with the lower interface levels. A faster type of diffusion permitted detectable interface changes to extend to lower temperatures. It would be interesting to find similar situations in other meteorites.

Schreibersite with Cohenite Borders

A prominent feature of the meteorites selected for study is the presence of 100-to-200-μm-wide cohenite borders separating massive schreibersite from kamacite. It is a feature that can be recognized with the unaided eye on many well-prepared exhibit sections of Group I meteorites, but it has

been little noted in the literature until relatively recently. Cohenite borders may partially or completely enclose schreibersite bordering troilite inclusions or massive schreibersite isolated within kamacite. This type of association has been reported above for the Ballinger (Figure 6), Lexington County (Figure 12), Bahjoi (Figure 13), Goose Lake, and Balfour Downs (Figures 15, 16, 17) meteorites. The Ni concentrations in these cohenite enclosed schreibersites range from 16 to 21 atomic %, comparable to those observed for similar unenclosed schreibersites within the same meteorite or within similar meteorites. The cohenite borders contain small amounts of Ni and no detected P. Their Ni profiles show a gradient varying from as much as 1.7 weight % Ni at the cohenite-kamacite interface to as low as 0.8 weight % Ni at the cohenite-schreibersite interface (Figures 13, 17).

Similar Ni gradients in cohenite borders have been reported previously by Drake (1970) and Scott (1971a). Drake (1970) noted that Ni diffuses through cohenite, increasing the Ni content of enclosed kamacite and taenite grains with decreasing temperature, but he felt that cohenite shells around schreibersite prevented equilibration of schreibersite with the enclosing metal. Scott (1971a) interpreted the presence of Ni gradients in cohenite borders as implying equilibration of Ni to low temperatures. The observed Ni concentrations in cohenite-enclosed schreibersite supports Scott's interpretation.

Massive schreibersite growth is apparently blocked by enclosure in cohenite. The absence of detectable P in these cohenites indicates that P solubility is very low. It seems reasonable to assume, therefore, that cohenite borders isolate schreibersite from a source of additional P. The situation with Ni, however, is different. The cohenite borders contain appreciable Ni, and the measured Ni gradients suggest a flow of Ni to the cohenite-schreibersite interfaces. Under these circumstances the size of the schreibersite indicates the maximum temperature at which cohenite could have nucleated. The temperature must have been low enough to permit schreibersite to reach its full size. At this maximum temperature, or at some lower temperature, cohenite encases the schreibersite. Growth is stopped but Ni enrichment continues with decreasing temperature. The minimum temperature at which cohenite could have formed is at or below the temperature at which the schreibersite achieved its final Ni concentration. According to the Fe-Ni-P diagram this would be at 550° C or below. In this low temperature range schreibersite would be surrounded by large volumes of kamacite. Is kamacite a reasonable source for the large amount of carbon required for cohenite growth? The work of Brett (1967) and A. D. Romig, Jr. (1977, pers. comm.) on the Fe-Ni-C system seems to require an alternate explanation.

Consideration of the Goose Lake meteorite structure in terms of both its cooling history within the Fe-Ni-P system (Table 14) and Romig's Fe-Ni-C diagram may be instructive at this point. Goose Lake is a meteorite that has large amounts of massive schreibersite. Surface areas totaling more than 1000 cm^2 were examined and found to contain more than 20 areas of clustered massive schreibersites. All of these schreibersites appeared to be enclosed in cohenite, although poor condition of surfaces left some ambiguity in one or two cases. In any event, the ubiquitous nature of cohenite bordering massive schreibersite in Goose Lake was established. This suggested that Goose Lake might be expected to yield a more straight-forward interpretation of cohenite border growth than would be possible using meteorites where the association was more sporadic.

Equilibrium compositions of phases derived from the Fe-Ni-P system for a range of decreasing temperatures are given in the lower section of Table 14 for the assumed Goose Lake meteorite bulk composition. At 925° C schreibersite is in equilibrium with 96% taenite. On cooling to 750° C the schreibersite doubles in amount to 8% and increases in Ni from 5.7 to 6.6 atomic %. Taenite is slightly reduced in volume during this process, but its Ni concentration remains essentially constant at 7.9 atomic %. Cooling through this 175° C range has resulted primarily in the localization of P. Massive schreibersites have grown within taenite and have achieved most of their eventual size.

In the 750° to 650° C temperature range major structural changes take place. Taenite increases in Ni from 7.9 to 11 atomic % and decreases in volume by one-half. Schreibersite increases in Ni from 6.6 to 9.0 atomic % and increases in volume by approximately 10%. The shrinking taenite is

converted to kamacite of 5.0 atomic % Ni, which makes up nearly half the structure at 650° C. With further decreasing temperature, kamacite expands in volume, taenite shrinks, and schreibersite holds its own. All three phases continue to increase in Ni.

What happens if carbon is also present in the system? Romig's Fe-Ni-C phase diagram gives carbon saturation values for taenite in equilibrium with cohenite. These are given in Table 20 for selected taenite compositions for the range of temperatures covered. The taenite Ni values given are those of taenite in equilibrium with schreibersite at the indicated temperature and the Goose Lake bulk composition using the Fe-Ni-P system (Table 14). Carbon has appreciable solubility in taenite throughout this temperature range, but its solubility in kamacite is negligible. This solubility of carbon in taenite means that a meteorite such as Goose Lake with a structure consisting of 92% taenite at 750° C might well contain enough dissolved carbon to produce significant amounts of cohenite on subsequent cooling. The important factor is that the amount of taenite present is drastically reduced with decreasing temperature. This results in carbon concentration increasing in the ever decreasing amount of taenite. Supersaturation must result at some temperature if sufficient carbon were present to start with.

Brett (1967) assumed that P could be neglected in his discussion of cohenite formation in meteorites. That may be true for some types of cohenite associations, but it may well not hold for cohenite bordering massive schreibersite. It is difficult to understand these associations using the Fe-Ni-C system alone. Brett (1967) shows that in this system cohenite grows by the following reaction:

$$\gamma = \text{cohenite} + \alpha.$$

He also points out that when the Ni content is high, kamacite and graphite form with falling temperature. Cohenite is what we see, however, not significant amounts of graphite in kamacite.

If we assume that carbon is present in taenite, then we are actually dealing with the Fe-Ni-P-C system. The more complex system permits the postulation of the following sequence of events to account for massive schreibersite with cohenite borders. Massive schreibersite nucleates at high temperature and grows upon cooling to near its final size, perhaps in the 650° to 700° C temperature range, assuming the Goose Lake bulk composition. These schreibersites are in contact with taenite that has become saturated in carbon. With further cooling both taenite and schreibersite require more Ni, and taenite requires a repository for its carbon. Under these circumstances it is reasonable to assume the following nucleation reaction taking place at taenite-schreibersite interfaces:

$$\gamma(C_{sat}) + \text{Ph} = \gamma + \text{cohenite} + \text{Ph}.$$

A cohenite border at the preexisting taenite-schreibersite interface results. Cohenite becomes a repository for carbon and the Ni that previously resided there is absorbed by taenite and/or schreibersite. As the structure develops, a dynamic equilibrium involving two interfaces is established; carbon saturated taenite-cohenite and cohenite-schreibersite. Cohenite grows as long as carbon saturated taenite is present. Taenite shrinks in volume, cohenite fills in behind the receding taenite, and schreibersite becomes enriched in Ni. At some point kamacite precipitates at the cohenite-taenite interface and then kamacite becomes the source of Ni for transport to schreibersite. The cohenite border is established and subsequent changes involve diffusion of Ni and Fe only.

The postulated reaction sequence would permit cohenite to grow over a broader temperature range than was suggested by Brett (1967). The maximum temperature can be estimated from the size of the cohenite-enclosed schreibersite. What is the highest temperature that could have produced schreibersite of the observed size starting with a given bulk composition? In a meteorite like Goose Lake the temperature might be as high as 750° C. The minimum temperature of nucleation

TABLE 20.—Carbon saturation values for taenite in equilibrium with cohenite from the Fe-Ni-C diagram of A. D. Romig, Jr. (taenite Ni values are equilibrium values using the Goose Lake bulk composition, Table 14).

°C	Weight % C_γ	Atomic % Ni_γ
730	0.75	~8.2
650	0.45	11
600	0.36	14
500	0.18	~25

would be established by the disappearance of sufficient taenite to supply the required carbon supersaturation. It seems unlikely for the meteorites that have been studied here that this would be below 600° C. This postulated growth sequence could extend Brett's (1967) temperature range of 610° to 650° C upward, but it is unlikely that it would be lowered appreciably. If Brett's (1967) estimated rates of cohenite decomposition with temperature are correct, nucleation within the lower part of the possible temperature range would favor preservation of cohenite. Confirmation of this proposed sequence of events will have to await the results of detailed experimentation.

Summary and Conclusions

The role that schreibersite growth played in the structural development process in coarse-structured iron meteorites has been examined. The availability to the writer of many large meteorite surfaces and an extensive collection of metallographic sections made it possible to undertake a comprehensive survey of schreibersite petrography. This study was the basis for the selection of samples for detailed electron microprobe analysis. Samples containing representative structures from eight chemical Groups I and IIAB meteorites were selected. All of these meteorites contain schreibersite, ranging in amount from easily detectable to abundant, and they contain additional P in solution in kamacite and taenite. Their detailed metallography indicates that they are comparatively free of secondary effects such as shock and reheating that might mask or distort relationships of interest. The range of bulk compositions covered is one where small changes in P-Ni concentration relationships may be more important to the structural development process than would be the case at higher Ni levels.

Lengthy electron microprobe traverses were made across structures representative of the observed range of schreibersite associations, with the exception of microrhabdites. Particular emphasis was placed on schreibersite-kamacite interface compositions. Ni and P interface concentrations in kamacite and Ni interface values in schreibersite were determined, along with associated Ni and P concentration gradients in kamacite and Ni gradients in schreibersite. An analysis of these data has led to a more comprehensive description of the structural development process in these individual meteorites than has been available previously.

Massive schreibersite, one of the four major types of schreibersite encountered, may be accounted for by equilibrium considerations. The Fe-Ni-P equilibrium diagram and estimated bulk compositions for individual meteorites were used to explain the basic structures present. Subsolidus nucleation and growth with slow cooling from temperatures at least as high as 850° C, and probably much higher, explain the phase relationships that one sees in meteorite specimens. No need was found to invoke eutectic liquids to account for any of the observed massive schreibersite morphologies. After nucleation, schreibersite and kamacite grew in volume and increased in Ni content while taenite receded and increased in Ni content under equilibrium or near equilibrium conditions into the 600° C temperature range. The retention of taenite in the octahedrites establishes that bulk equilibrium did not extend as low as 550° C. Schreibersite undoubtedly continued in equilibrium with its enclosing kamacite to lower temperatures. The growth of massive schreibersite from high temperatures into the 600° C temperature range served both to localize P by reducing its level throughout the bulk metal and to produce the large swathing kamacite zones that are observed.

The second type of schreibersite to form is homogeneously nucleated rhabdite. It nucleated in kamacite in the 600° C temperature range, either as a consequence of low initial P level or after local P supersaturation developed following massive schreibersite growth. Growth of these schreibersites was also under equilibrium conditions to below 500° C. They drew their source of P from limited diffusion fields when compared to the massive schreibersites.

The third type of schreibersite is grain boundary and taenite border schreibersite. It formed at kamacite-taenite interfaces, absorbing residual taenite. Nucleation took place successively along grain boundaries over a range of temperatures starting as high as 500° C or perhaps slightly higher. With decreasing temperature taenite receded and became richer in Ni and the schreibersite that nucleated at these interfaces had higher Ni. The

highest Ni schreibersites are the small ones that nucleated at low temperatures and are observed still in contact with taenite. Grain boundary diffusion probably became an increasingly important factor in the growth of these schreibersites with decreasing temperature.

The fourth type of schreibersite is microrhabdite. These schreibersites nucleated homogeneously in supersaturated kamacite at temperatures in the 400° C range or below.

P diffusion controlled the growth rate of schreibersite. The Ni flux to a growing interface had to produce a growth rate equal to that established by the P flux. This was accomplished by tie line shifts that permitted a broad range of Ni growth rates and accounts for the observed range of Ni concentrations in schreibersite. Interface measurements on meteoritic schreibersites, therefore, yield a range of tie lines in the low temperature Fe-Ni-P system. Equilibrium conditions pertained at growth interfaces to temperatures far below those available experimentally. Kinetic factors, however, restricted mass transfer to increasingly small volumes of material with decreasing temperature.

Schreibersite with cohenite borders is a common occurrence in many meteorites. It is suggested that it formed as a reaction in the Fe-Ni-P-C system in the 750° to 600° C temperature range. Carbon saturated taenite reacted with schreibersite to form cohenite. Cohenite then grew in equilibrium with both taenite and schreibersite.

Berzelius' prescient comment of 1832 on the role of P in the development of the Widmanstätten pattern has been confirmed and expanded upon.

Appendix

In the discussion of the low-temperature ternary diagram, experimental values for P saturation concentrations in kamacite and taenite were extrapolated to lower temperatures (Table 17, Figures 21, 22). This is a commonly used procedure when dealing with dilute solutions and is a variation on a method used for the determination of partial molal properties of substances. It is applicable to solid state transformations in dilute metallic systems and may be justified by the following thermodynamic reasoning adapted from Swalin (1972:168–171).

At a given temperature (T_1) the end points of a kamacite-schreibersite tie line in the kamacite-schreibersite field of the equilibrium diagram represent equilibrium concentrations of the two phases. The relationship between P-saturated kamacite ($\alpha_{P(sat)}$) and schreibersite (Ph) may be expressed as follows:

$$\alpha_{P(sat)} \rightleftarrows Ph + \alpha \qquad \Delta G = 0.$$

Since the reaction represents equilibrium the change in the Gibbs free energy (ΔG) is zero. Therefore, the chemical potentials (μ) of P in the two phases are equal,

$$\mu_P^{\bullet Ph} = \mu_{P(sat)}^{\alpha}$$

as are their activities (a),

$$a_P^{\bullet Ph} = a_{P(sat)}^{\alpha}.$$

Since schreibersite is a pure substance with respect to P

$$a_P^{\bullet Ph} = 1$$

requiring that

$$a_{P(sat)}^{\alpha} = 1.$$

If the saturation concentration of P in kamacite is sufficiently small, P may be assumed to follow Henry's law and the activity coefficient of P in kamacite, γ_P°, may be evaluated.

$$a_{P(sat)}^{\alpha} = 1 = \gamma_P^{\circ\alpha} X_{P(sat)}^{\alpha}$$

$$\gamma_{P\alpha}^{\circ} = \frac{1}{X_{P(sat)}^{\alpha}}$$

In order to derive a relationship for the solvus line (kamacite saturated with P) as a function of temperature (T), we must consider a situation where ΔG for the reaction is not zero. This may be done by assuming a P concentration in kamacite, X_P^{α}, such that X_P^{α} is within the kamacite field of the equilibrium diagram

$$X_P^{\alpha} < X_{P(sat)}^{\alpha}.$$

Kamacite of this concentration would react with schreibersite to form P-saturated kamacite,

$$\alpha_P + Ph \rightleftarrows \alpha_{P(sat)} \qquad \Delta G_1.$$

The following equation may be written relating the Gibbs free energy (ΔG_1) for the above reaction, the chemical potentials of the reacting species, and the activities of these species,

$$\Delta G_1 = \mu_P^{\alpha} - \mu_P^{\circ Ph} = RT \ln \frac{a_P^{\alpha}}{a_{Ph}^{\circ}}.$$

for a pure substance,

$$a_{Ph}^{\circ} = 1$$

for a dilute solution following Henry's law

$$a_P^{\alpha} = \gamma_P^{\circ\alpha}(X_P^{\alpha})$$

and from equation given above

$$a_P^{\alpha} = \frac{1}{X_{P(sat)}^{\alpha}}(X_P^{\alpha}) = \frac{X_P^{\alpha}}{X_{P(sat)}^{\alpha}}.$$

Substituting these values of a_{Ph}° and a_P^{α} in the expression for ΔG_1 given above we obtain

$$\mu_P^{\alpha} - \mu_P^{\circ Ph} = RT \ln X_P^{\alpha} - RT \ln X_{P(sat)}^{\alpha} - RT \ln (1).$$

We know that the enthalpy of a component i, H_i, is related to the temperature and chemical potential by

$$\frac{\partial(\mu_i/T)}{\partial(1/T)} = H_i.$$

Substituting, we obtain

$$\frac{\partial(\mu_P^g/T)}{\partial(1/T)} - \frac{\partial(\mu_{Ph}^\circ/T)}{\partial(1/T)} = \bar{H}_P\alpha - H_{Ph}^\circ$$

$$= \frac{\partial(RT \ln X_P^g/T)}{\partial(1/T)} - \frac{\partial(RT \ln X_{P(sat)}^\alpha/T)}{\partial(1/T)} - \frac{\partial(RT \ln (1)/T)}{\partial(1/T)}$$

X_P^g and (1) are constants, dropping out these two terms,

$$\bar{H}_P\alpha - H_{Ph}^\circ = -R\frac{\partial(\ln X_{P(sat)})}{\partial(1/T)}$$

$$\partial(1/T)\frac{\Delta H_P}{R} = -\partial(\ln X_{P(sat)}^\alpha)$$

$$\ln X_{P(sat)}^\alpha = \frac{-\Delta\bar{H}_P}{R}(1/T).$$

Therefore, when $X_{P(sat)}^\alpha$ is plotted on a log scale against 1/T, a straight line with slope $-\Delta H_P/R$ should result. Straight lines with negative slopes are observed in our case, and it is reasonable to assume on the basis of experience in other systems that $\Delta\bar{H}_P\alpha$ is independent of temperature over a reasonable temperature range. It would seem then that an extrapolation over a reasonable temperature range is justified. A similar treatment would apply to P-saturated taenite data.

Literature Cited

Adler, I., and E. J. Dwornik
1961. Electronprobe Analysis of Schreibersite (Rhabdite) in the Canyon Diablo Meteorite. *U.S. Geological Survey Professional Papers*, 424B(112):B263–B265.

Agrell, S. O., J. V. P. Long, and R. E. Ogilvie
1963. Nickel Content of Kamacite Near the Interface with Taenite in Iron Meteorites. *Nature*, 198:749–750.

Anders, Edward
1962. Meteorite Ages. *Reviews of Modern Physics*, 34:287–325.
1971. Meteorites and the Early Solar System. *Annual Review of Astronomy and Astrophysics*, 9:1–34.

Axon, H. J., and J. Boustead
1967. Kamacite-Taenite Relationships in Iron Meteorites. *Nature*, 213:166–167.

Axon, H. J., and D. Faulkner
1970. A Metallographic and Microprobe Study of the Barranca Blanca Meteorite. *Mineralogical Magazine*, 37:898–904.

Axon, H. J., and J. I. Goldstein
1972. Temperature-Time Relationships from Lunar Two Phase Metallic Particles (14310, 14163, 14003). *Earth and Planetary Science Letters*, 16:439–447.
1973. Metallic Particles of High Cobalt Content in Apollo 15 Soil Samples. *Earth and Planetary Science Letters*, 18:173–190.

Axon, H. J., and P. L. Smith
1972. A Metallographic Study of Some Iron Meteorites of High Nickel Content. *Mineralogical Magazine*, 38:736–755.

Axon, H. J., and C. V. Waine
1971. A Metallographic Study of the Angra dos Reis (Iron) Meteorite. *Mineralogical Magazine*, 38:94–101.
1972. A Metallographic Study of Some Hexahedrites. *Mineralogical Magazine*, 38:725–735.

Belaiew, N. T.
1924. On the Genesis of Widmanstätten Structure in Meteorites and in Iron-Nickel and Iron-Carbon Alloys. *Mineralogical Magazine*, 20:173–185.

Benedicks, Carl
1910. Synthèse du fer météorique. *Nova Acta Reglae Societatis Scientiarum Upsaliensis*, series IV, 2(10):1–26.

Berwerth, Frederick
1907. Steel and Meteoritic Iron. *Journal of the Iron and Steel Institute*, 75(3):37–51.

Berzelius, J. J.
1832a. Undersökning af en vid Bohumiliz i Böhmen funnen jernmassa. *Kongelige Svenska Vetenskaps-Academiens Handlingar*, pages 106–119.
1832b. Untersuchung der Bohumulitzer Eisenmasse. *Zeitschrift für Physik und Mathematik, Wein*, 1:289–297.
1833. Untersuchung einer bie Bohumiliz in Böhmen gefundenen Masse. *Annalen der Physik und Chemie*, 27:118–132.
1834a. Om Meteorstenar. *Kongelige Svenska Vetenskaps-Academiens Handlingar*, pages 115–183.
1834b. Ueber Meteorsteinen, V: Pallas-Eisen und Pallas-Olivin, VI: Meteoreisen von Elbogen. *Annalen der Physik und Chemie*, 33:123–137.

Bild, Richard W.
1974. New Occurrences of Phosphates in Iron Meteorites. *Contributions to Mineralogy and Petrology*, 45:91–98.

Brett, Robin
1967. Cohenite: Its Occurrence and a Proposed Origin. *Geochimica et Cosmochimica Acta*, 31:143–159.

Brezina, Aristides
1906. Zur Frage der Bildungsweise Eutropischer Gemenge. *Denkschriften der Kaiserlichen Akademie der Wissenschaften, Wein*, 78:635–643.

Brown, G. M., A. Peckett, R. Phillips, and C. H. Emeleus
1973. Mineral-Chemical Variations in the Apollo 16 Magnesio-Feldspathic Highland Rocks. *In* Proceedings of the Fourth Lunar Science Conference. *Geochimica et Cosmochimica Acta*, supplement 4, 1:505–518.

Buchwald, V. F.
1966. The Iron-Nickel-Phosphorous System and the Structure of Iron Meteorites. *Acta Polytechnica Scandinavica*, 51: 45 pages.
1976. *Handbook of Iron Meteorites*. Volumes I–III, 1418 pages. Tempe: Center for Meteorite Studies, Arizona State University; Berkeley: University of California Press.

Buchwald, V. F., and S. Munck
1965. Catalogue of Meteorite in the Mineralogical Museum of the University, Copenhagen. *Analecta Geologica*, 1: 81 pages.

Buseck, Peter R.
1969. Phosphide from Meteorites: Barringerite, a New Iron-Nickel Mineral. *Science*, 165:169–171.

Carter, J. L., and E. Padovani
1973. Genetic Implications of Some Unusual Particles in Apollo 16 Less Than 1 mm Fines 68841,11 and 69941,13. *In* Proceedings of the Fourth Lunar Science Conference. *Geochimica et Cosmochimica Acta*, supplement 4, 1:323–333.

Clarke, Roy S., Jr.
1969. Comments on Cohenite and Schreibersite in Iron Meteorites (Abstract). *Meteoritics*, 4:161.

Cohen E.
1894. Meteoreisen-Studien III: Rhabdit. *Annalen des K.K. Naturhistorischen Hofmuseums*, IX:97–118.

Comerford, M. F.
1969. Phosphide and Carbide Inclusions in Iron Meteorites. Pages 780–795 *in* P. M. Millman, editor, *Meteorite Research*. 940 pages. Dordrecht: D. Reidel Publishing Company.

Daubrée, M. A.
1868. *Expériences synthetiques relatives aux météorites*. 65 pages. Paris: Dunod.

De Laeter, J. R., G.J.H. McCall, and S.J.B. Reed
1973. The Redfields Meteorite—A Unique Iron from Western Australia. *Mineralogical Magazine*, 39:30–35.

Derge, G., and A. R. Kommel
1937. The Structure of Meteoric Irons. *American Journal of Science*, 34:203–214.

Doan, A. S., Jr., and J. I. Goldstein
1969. The Formation of Phosphides in Iron Meteorites. Pages 763–779 *in* P. M. Millman, editor, *Meteorite Research*. 940 pages. Dordrecht: D. Reidel Publishing Company.
1970. The Ternary Phase Diagram, Fe-Ni-P. *Metallurgical Transactions*, 1:1759–1767.

Drake, John C.
1970. Mineralogical Relationships in Seymour, a Course Octahedrite. *Meteoritics*, 5:19–31.

El Goresy, Ahmed
1965. Mineralbestand und Strukturen der Graphit- und Sulfideinschlüsse in Eisenmeteoriten. *Geochimica et Cosmochimica Acta*, 29:1131–1151.

El Gorsey, A., P. Ramdohr, and O. Medenback
1973. Lunar Samples from Descartes Site: Opaque Mineralogy and Geochemistry. *In* Proceedings of the Fourth Lunar Science Conference. *Geochimica et Cosmochimica Acta*, supplement 4, 1:733–750.

Farrington, Oliver C.
1915. *Meteorites, Their Structure, Composition, and Terrestrial Relations*. 225 pages. Chicago: Published by the author.

Fricker, P. E., J. I. Goldstein, and A. L. Summers
1970. Cooling Rates and Thermal Histories of Iron and Stony-iron Meteorites. *Geochimica et Cosmochimica Acta*, 34:475–491.

Fuchs, Louis H.
1969. The Phosphate Mineralogy of Meteorites. Pages 681–695 *in* P. M. Millman, editor, *Meteorite Research*. 940 pages. Dordrecht: D. Reidel Publishing Company.

Goldberg, E., A. Uchiyama, and H. Brown
1951. The Distribution of Nickel, Cobalt, Gallium, Palladium, and Gold in Iron Meteorites. *Geochimica et Cosmochimica Acta*, 2:1–25.

Goldstein, J. I.
1965. The Formation of the Kamacite Phase in Metallic Meteorites. *Journal of Geophysical Research*, 70:6223–6232.
1969. The Classification of Iron Meteorites. Pages 721–737 *in* P. M. Millman, editor, *Meteorite Research*. 940 pages. Dordrecht: D. Reidel Publishing Company.

Goldstein, J. I., and H. J. Axon
1973. The Widmanstätten Figure in Iron Meteorites. *Naturwissenschaften*, 60:313–321.

Goldstein, J. I., H. J. Axon, and C. F. Yen
1972. Metallic Particles in the Apollo 14 Lunar Soil. *In* Proceedings of the Third Lunar Science Conference. *Geochimica et Cosmochimica Acta*, supplement 3, 1:1037–1064.

Goldstein, J. I., and A. S. Doan, Jr.
1972. The Effects of Phosphorus on the Formation of the Widmanstätten Pattern of Iron Meteorites. *Geochimica et Cosmochimica Acta*, 36:51–69.

Goldstein, J. I., E. P., Henderson, and H. Yakowitz
1970. Investigation of Lunar Metal Particles. *In* Proceedings of the Apollo 11 Lunar Science Conference. *Geochimica et Cosmichimica Acta*, supplement 1, 1:499–512.

Goldstein, J. I., and R. E. Ogilvie
1963. Electron Microanalysis of Metallic Meteorites, Part 1: Phosphides and Sulfides. *Geochimica et Cosmochimica Acta*, 27:623–637.
1965a. A Re-evaluation of the Iron-Rich Portion of the Fe-Ni System. *Transactions of the Metallurgical Society of AIME*, 233:2083–2087.
1965b. The Growth of the Widmanstätten Pattern in Metallic Meteorites. *Geochimica et Cosmochimica Acta*, 29:893–920.

Goldstein, J. I., and J. M. Short
1967a. Cooling Rates of 27 Iron and Stony-iron Meteorites. *Geochimica et Cosmochimica Acta*, 31:1001–1023.
1967b. The Iron Meteorites, Their Thermal History and Parent Bodies. *Geochimica et Cosmochimica Acta*, 31:1733–1770.

Goldstein, J. I., and H. Yakowitz
1971. Metallic Inclusions and Metal Particles in the Apollo 12 Lunar Soil. *In* Proceedings of the Second Lunar Science Conference. *Geochimica et Cosmochimica Acta*, supplement 2, 1:177–191.

Goode, George Brown
1877. *The Smithsonian Institution 1846–1896*. 856 pages. Washington: The Smithsonian Institution.

Gooley, R. C., R. Brett, and J. L. Warner
1973. Crystallization History of Metal Particles in Apollo 16 Rake Samples. *In* Proceedings of the Fourth Lunar Science Conference. *Geochimica et Cosmochimica Acta*, supplement 4, 1:799–810.

Grossman, L., and J. W. Larimer
1974. Early Chemical History of the Solar System. *Reviews of Geophysics and Space Physics*, 12:71–101.

Haidinger, Wilhelm
1847. Versammlung, am 16, Juli. *Berichte über die Mitteilungen von Freunden der Naturwissenschaften in Wien*, 3:69–71.

Heyward, T. R., and J. I. Goldstein
1973. Ternary Diffusion in the α and γ Phases of the Fe-Ni-P System. *Metallurgical Transactions*, 4:2335–2342.

Henderson, Edward P.
1965. Hexahedrites. *Smithsonian Miscellaneous Collections*, 148(5): 41 pages.

Henderson, E. P., and S. H. Perry
1958. Studies of Seven Siderites. *Proceedings of the United States National Museum*, 107:339–403.

Hornbogen, E., and H. Kreye
1970. The Microstructure of Two Iron Meteorites. *Zeitschrift für Metallkunde*, 61:914–923.

Lovering, J. F., W. Nichiporuk, A. Chodos, and H. Brown
1957. The Distribution of Gallium, Germanium, Cobalt, Chromium, and Copper in Iron and Stony-Iron Meteorites in Relation to Nickel Content and Structure. *Geochimica et Cosmochimica Acta*, 11:263–278.

Malissa, H. jun
1974. Electron Microprobe Analysis of Some Minor- and

Accessory Components in Mesosiderites. *TMPM Tschermaks Mineralogische und Petrographische Mitteilungen*, 21:233–245.

Massalski, T. B., and F. R. Park
1962. A Quantitative Metallographic Study of Five Octahedrite Meteorites. *Journal of Geophysical Research*, 67:2925–2934.

McKay, G. A., S. J. Kridelbaugh, and D. F. Weill
1973. The Occurrence and Origin of Schreibersite-Kamacite Intergrowths in Microbreccia 66055. *In* Proceedings of the Fourth Lunar Science Conference. *Geochimica et Cosmochimica Acta*, supplement 4, 1:811–818.

Mehl, R. F., and G. Derge
1937. Studies Upon the Widmanstätten Structure, VIII: The Gamma-Alpha Transformation in Iron-Nickel Alloys. *Transactions of the American Institute of Mining and Metallurgical Engineers, Iron and Steel Division*, 125:482–500.

Meunier, Stanislas
1880. Imitation synthétique des fers nickelés meteoritiques. *Bulletin de la Société Mineralogique de France*, 3:153–155.

Moore, C. B., C. F. Lewis, and D. Nava
1969. Superior Analyses of Iron Meteorites. Pages 738–748 *in* P. M. Millman, editor, *Meteorite Research*. 940 pages. Dordrecht: D. Reidel Publishing Company.

Olsen, E., and K. Fredriksson
1966. Phosphates in Iron and Pallasite Meteorites. *Geochimica et Cosmochimica Acta*, 30:459–470.

Olsen, E., and L. H. Fuchs
1967. The State of Oxidation of Some Iron Meteorites. *Icarus*, 6:242–253.

Osmond, F., and G. Cartaud
1904. Sur les fers météoriques. *Revue de Métallurgie* (Paris), 1:69–79.

Owen, E. A.
1938. Formation of Widmanstätten Figures in Meteorites. *Nature*, 142:999–1000.

Owen, E. A., and Y. H. Liu
1949. Further X-Ray Study of the Equilibrium Diagram of the Iron-Nickel System. *Journal of the Iron and Steel Institute*, 163:132–137.

Owen, E. A., and A. H. Sully
1939. The Equilibrium Diagram of Iron-Nickel Alloys. *Philosophical Magazine*, 7th series, 27:614–636.

Palache, C., H. Berman, and C. Frondel
1944. *The System of Mineralogy*. 7th edition, volume I, 834 pages. New York: John Wiley & Sons, Inc.

Paneth, F. A.
1960. The Discovery and Earliest Reproduction of the Widmanstätten Figures. *Geochimica et Cosmochimica Acta*, 18:176–182.

Pauly, Hans
1969. White Cast Iron with Cohenite, Schreibersite, and Sulfides from Tertiary Basalts on Disko, Greenland. *Bulletin of the Geological Society of Denmark*, 19:8–26.

Perry, Stuart H.
1944. The Metallography of Meteoric Iron. *United States National Museum Bulletin*, 184: 206 pages.

Phillips, J. P.
1965. J. Lawrence Smith, Pioneer of American Analytical Chemistry. *Journal of Chemical Education*, 42:390–391.

Powell, Benjamin N.
1971. Petrology and Chemistry of Mesosiderites, II: Silicate Textures and Compositions and Metal-Silicate Relationships. *Geochimica et Cosmochimica Acta*, 35:5–34.

Ramdohr, Paul
1973. *The Opaque Minerals in Stony Meteorites*. 245 pages. New York: Elsevier Publishing Company.

Randich, E.
1975. *Non-Isothermal Diffusion Controlled Phase Growth in Ternary Systems and Its Application to Iron Meteorites*. 125 pages. Ph. D. dissentation, Lehigh University.

Randich, E., and J. I. Goldstein
1975. Non-Isothermal Finite Diffusion-Controlled Growth in Ternary Systems. *Metallurgical Transactions*, 6A:1553–1560.

Reed, S.J.B.
1965a. Electron-Probe Microanalysis of Schreibersite and Rhabdite in Iron Meteorites. *Geochimica et Cosmochimica Acta*, 29:513–534.
1965b. Electron-Probe Microanalysis of the Metallic Phases in Iron Meteorites. *Geochimica et Cosmochimica Acta*, 29:535–549.
1967. The Distribution of Phosphorus in the Mount Edith Octahedrite. *Geochimica et Cosmochimica Acta*, 31:1969–1974.
1969. Phosphorus in Meteoritic Nickel-Iron. Pages 749–762 *in* P. M. Millman, editor, *Meteorite Research*. 940 pages. Dordrecht: D. Reidel Publishing Company.
1972. The Oktibbeha County Iron Meteorite. *Mineralogical Magazine*, 38:623–626.

Rose, Gustav
1865. Systematische Eintheilung der Meteoriten. *Annalen der Physik und Chemie*, 124:193–213.

Schreibers, C. Von
1820. *Beyträge zur Geschichte und Kenntniss meteorischer Stein und Metallmassen, und der Erscheinungen, welche deren Neiderfall zu begleiten pflegen (als Nachtrag zu Herrn Chladni's neuestem Werke über Feuer-Meteore)*. 97 pages. Vienna: J. G. Heubner.

Scott, Edward R. D.
1971a. *Studies of the Structure and Composition of Iron Meteorites*. 179 pages. Ph. D. dissertation, University of Cambridge, Cambridge, England.
1971b. New Carbide, $(Fe,Ni)_{23}C_6$, Found in Iron Meteorites. *Nature Physical Science*, 229:61–62.

Scott, E.R.D., and J. T. Wasson
1975. Classification and Properties of Iron Meteorites. *Reviews of Geophysics and Space Physics*, 13:527–546.
1976. Chemical Classification of Iron Meteorites, VIII: Groups IC, IIE, IIIF, and 97 Other Irons. *Geochimica et Cosmochimica Acta*, 40:103–115.

Shepard, Charles Upham
1846. Report on Meteorites. *American Journal of Science*, series 2, 2:377–392.
1853. Notice of the Meteoric Iron Found Near Seneca River, Cayuga County, N.Y. *American Journal of Science*, series 2, 15:363–366.

Short, J. M., and C. A. Anderson
1965. Electron Microprobe Analyses of the Widmanstätten Structure of Nine Iron Meteorites. *Journal of Geophys-*

ical Research, 70:3745–3759.

Short, J. M., and J. I. Goldstein
1967. Rapid Method for Determining Cooling Rates of Iron and Stony-iron Meteorites. *Science*, 156:59–61.

Silliman, Benjamin
1886. Memoir of John Lawrence Smith 1818–1883. *National Academy of Science Biographical Memoirs*, 2:217–248.

Smith, Cyril Stanley
1960. *A History of Metallography*. 293 pages. Chicago: University of Chicago Press.
1962. Note on the History of the Widmanstätten Structure. *Geochimica et Cosmochimica Acta*, 26:971–972.

Smith, J. Lawrence
1855. Meteoritic Iron from Tazewell County, East Tennessee. *American Journal of Science*, series 2, 19:153–159.

Smith, S.W.J., and J. Young
1938. Formation of Widmanstätten Figures in Meteorites. *Nature*, 142:1162.
1939. The Widmanstätten Structure of Octahedral Meteoric Iron. *Nature*, 143:384–385.

Sorby, H. C.
1877. On the Structure and Origin of Meteorites. *Nature*, 15:495–498.
1887. On the Microscopical Structure of Iron and Steel. *Journal of the Iron and Steel Institute*, 1:255–288.

Spencer, L. J.
1916. Crystals of Iron Phosphide (Rhabdite) from a Blast-furnace. *Mineralogical Magazine*, 17:340–343.

Stodart, J., and M. Faraday
1820. Experiments on the Alloys of Steel, Made with a View to Its Improvement. *Quarterly Journal of Science*, 9(18):319–330.

Swalin, R. A.
1972. *Thermodynamics of Solids*. 2nd edition, 387 pages. New York: John Wiley and Sons.

Thomson, G.
1804. On the Malleable Iron, etc: Essai sur le fer malléable trouvé en Sibérie par le Prof. Pallas. *Bibliothèque Britannique*, 27(2, October 1804): 135–154, plate opposite page 184; (3, November 1804): 209–229.
1808. Sur ferro malleabile trovato da Pallas in Siberie. *Atti Accademia delle Scienze di Siena*, 9:37–57.

Vogel, Rudolf
1927. Über die Strukturformen des Meteoreisens und Ihre Spezielle Beeinflussung durch Umwendlung und Beigemengten Phosphor. *Abhandlunger der Gesellschaft der Wissenschaften zu Göttingen, Mathematisch-physikalische Klasse*, 12(2): 51 pages.
1928. Ueber die Strukturformen des Meteoreisen. *Archiv für das Eisenhüttenwesen*, 1:605–611.
1932. Eine umfassendere Deutung der Gefügeerscheinungen des Meteoreisens durch das Zustandsdiagramm des ternären Systems Eisen-Nickel-Phosphor. *Abhandlungen der Gesellschaft der Wissenschaften zu Göttingen, Mathematisch-physikalische Klasse*, 3(6): 31 pages.
1951. Die Gefügeformen des Meteoreisen und ihre Erklärung auf Grund des Zustandsdiagrammes des Systems Eisen-Nickel-Phosphor. *Neues Jahrbuch für Mineralogie, Abhandlungun*, 83:23–52.
1952. Über Rhabdit und Schreibersite. *Neues Jahrbuch für Mineralogie, Abhandlungen*, 84:327–349.
1957. Über Metabolite und ihre Kennzeichnung durch das Gefüge. *Chemie der Erde*, 19:147–169.
1964. Über die Entstehung des Wickelkamazit. *Neues Jahrbuch für Mineralogie, Monatshefte*, 2:57–63.

Vogel, R., and H. Baur
1931. Ueber das ternäre System Eisen-Nickel-Phosphor. *Archiv für das Eisenhüttenwesen*, 5:269–278.

von Reichenbach, C.
1861. Ueber die nähern Bestandtheile des Meteoreisens. *Annalen der Physik und Chemie*, 114:477–491.

Wai, C. M.
1974. Geochemical Affinities of Cobalt and Germanium toward Metal, Silicate, and Sulfide Phases at High Temperature. *Geochimica et Cosmochimica Acta*, 38:1821–1825.

Wasson, J. T.
1974. *Meteorites*. 316 pages. New York: Springer-Verlag.

Waterston, Charles D.
1965. William Thomson (1761–1806) a Forgotten Benefactor. *University of Edinburgh Journal* (autumn 1965), pages 122–134.

Wood, John A.
1964. The Cooling Rates and Parent Planets of Several Iron Meteorites. *Icarus*, 3:429–459.

Young, J.
1926. The Crystal Structure of Meteoric Iron as Determined by X-Ray Analysis. *Proceedings of the Royal Society* (London), A112:630–641.

Ziebold, Thomas O.
1967. Precision and Sensitivity in Electron Microprobe Analysis. *Analytical Chemistry*, 39:858–861.